Optimizing Drinking Water Disinfection: Balancing Corrosion, Byproduct Formation, and Pathogen Removal

by

Margaret M. Reuter

A dissertation submitted in partial fulfillment
of the requirements for the degree of
Doctor of Philosophy
(Environmental Engineering)
in the University of Michigan
2019

Doctoral Committee:

Associate Professor Christian M. Lastoskie, Chair
Assistant Professor Brian R. Ellis
Professor Emeritus Rudy J. Richardson
Associate Professor Krista Rule Wigginton

Margaret M. Reuter

mmreuter@umich.edu

ORCID iD: 0000-0001-9329-6944

Dedication

To my family. For your unwavering love and support of me and science.

Acknowledgements

This dissertation was funded by the University of Michigan Mcubed grant, the Rackham Graduate School Summer Award, and the Civil and Environmental Engineering Department at the University of Michigan.

Without the mentorship, help, and support of many people, I could never have finished this dissertation. Firstly, I thank my adviser, Dr. Christian Lastoskie for his guidance. I am grateful for the freedom you gave me to explore projects atypical for our field and for all the feedback that has made me a better researcher and presenter. I also thank you for supporting me as a person outside of research.

I would like to thank my committee members Dr. Rudy Richardson, Dr. Brian Ellis, and Dr. Krista Wigginton. I am grateful to Dr. Richardson for all the time spent teaching me molecular modeling and how generous you have always been with your time and mentorship. In particular, finding a way to model the curious molecule that is chlorine dioxide. Thank you to Dr. Ellis for welcoming me into your research group and having an open door to all my questions, whether they were research, teaching, or career related. Thank you to Dr. Wigginton for supporting my virus modeling work, encouraging my conversations and experiments with Dr. Yinyin Ye, and being an inspiring teaching mentor while I was your GSI.

I would like to thank the Lastoskie and Ellis research groups, especially Dr. Sahithya Reddivari, Anne Menefee, and Ellen Thompson. Your feedback, support, and friendship have been incredibly generous and has helped me feel both intellectually and emotionally grounded. A

special thanks to Dr. Christina Reynolds for being my friend, my role model, my cheerleader, and the best lab group member anyone could ask for.

I would also like to thank Dr. Jeremy Semrau for your teaching mentorship but also for all the generous advice you have given me outside the classroom. Thank you to Tom Yavaraski for your crucial support with all the analytical equipment and laboratory set up. Thank you to Dr. Yinyin Ye for your incredible help with all the virus modeling work and for all the inspiring and invigorating research conversations. Thank you to all the undergraduate and graduate students who made my teaching experiences exciting and rewarding

Deep thanks to all my friends I found in graduate school. For all the times I needed help someone was there for me, especially through a frustrating year of knee surgery and recovery. To Brett Wagner, Enrique Rodriguez, and Katie Lagenfeld for being the best office mates and true friends. To Maddy Wax and Tim Fairley for all our adventures living together. To Dr. Heather Goetsch for the incredible emotional support you have given me over the years. To Dr. Caroline Van Steendam and Andrea McFarland for being my biggest cheerleaders and best adventurers. To Nicole Rockey and David Barron for all the intellectual debates in odd places and for being the sources of both fun and support. To Ernesto Martínez for all the times I needed a break and you were there to listen and relax. To Kate Dowdell for all the party hats but more importantly for your incredible generosity. To Joey Dickens, Dr. Amanda Leone, Dr. Alyssa Miller, Dr. John Wiltshire-Gordon, Dr. Mike Newman, Dr. Wenbing Hu, Kate Blessing-Kawamura, John Kawamura, and Dr. Gabe Friedan for your friendship and love of volleyball. To Dr. Leigh Korey and Matt Vedrin for being my stabilizing forces in graduate school and always being there when I needed you.

My final thanks to my incredible family, who have supported and loved me through every doubt, setback, frustration, and triumph.

Table of Contents

List of Tables

List of Figures

List of Appendices

Abstract

The oxidants used in water treatment to inactivate pathogens are powerful and, consequently, react with other constituents they encounter, notably organic matter and pipe corrosion scale. Moreover, the complex relationships between said reactions remains poorly understood. Reactions with organic matter produce disinfection byproducts, many of which are regulated by the United States Environmental Protection Agency (EPA) due to their toxicity. To remove these byproducts and meet EPA standards, water treatment facilities add chemicals that can exacerbate corrosion and increase the concentration of dissolved metals in drinking water.

Chlorine dioxide, the focus of this dissertation, has been used as an alternative to free chlorine, the most commonly used disinfectant, because it does not produce organic disinfection byproducts. Additionally, chlorine dioxide has a disinfecting power equal to or higher than that of free chlorine, its disinfection capabilities are independent of pH, and it can be used as either a primary or secondary disinfectant. From a corrosion standpoint, chlorine dioxide has a high oxidation-reduction potential, which promotes the formation of passivating scale layers on metal pipe surfaces, thereby preventing dissolution of heavy metals into drinking water. Chlorine dioxide does, however, produce two toxic inorganic byproducts, chlorite and chlorate.

Despite the drawbacks associated with inorganic byproduct formation, chlorine dioxide is a disinfectant worthy of investigation with regards to three reactions: pathogen disinfection mechanisms; drinking water pipe corrosion; and formation of inorganic byproducts. The first part of this dissertation addresses the inactivation of the H1N1 influenza virus using computational models. Both computational and experimental methods identified tryptophan 153, an amino acid

residue key in the binding of H1N1 to its human host cell, as the primary target of chlorine dioxide oxidation.

Part two of this work shows results from batch reactor experiments of chlorine dioxide with lead and copper minerals commonly found in corrosion scale layers. Decay of chlorine dioxide in the presence of lead oxide and lead carbonate was significantly faster and produced different byproducts than decay in the presence of cupric oxide. It was further revealed that the relationship between pH and reaction rate is likely dependent upon surface charge for lead oxide but not for cupric oxide.

These findings were the impetus for the third and final part of this dissertation which employed computational methods to model the subtle differences between surface adsorption on cupric oxide and lead oxide, of either the chlorine dioxide monomer or dimer, in the presence or absence of hydroxide. The results of the calculations suggest that the chlorine dioxide degradation pathway on the cupric oxide surface favors dimerization of chlorine dioxide and its ensuing disproportionation into chlorite and chlorate, whereas the lead oxide surface favors direct electron transfer and formation of chlorite.

These findings add to the body of knowledge on the alternative disinfectant, chlorine dioxide, and its chemical interactions with pathogens and corrosion scale. The results suggest that chlorine dioxide may have highly specific mechanisms of virus inactivation and computational methods could be valuable tools for elucidating these mechanisms. Further conclusions suggest that chlorine dioxide decay caused by mineral scales in lead-containing water supply networks may be more pronounced than in those assembled from copper pipes.

Chapter 1. Introduction

1.1 DISINFECTION

Disinfection reduces the number of viable waterborne and airborne pathogens to protect the public from disease, yet knowledge gaps persist in how disinfectants kill these pathogens. The disinfection process is a fundamental part of drinking water treatment systems as viral infections, including gastroenteritis, meningitis, and hepatitis, are often a result of exposure to improperly treated water.[1] Gaseous disinfection is also used in the food industry to inactivate pathogens on fruits and vegetables and in the medical industry to sterilize medical equipment and surfaces.[2–4] Historically, the most common chemical oxidant used for disinfection has been chlorine gas due to its low cost.[5] In the past two decades, water utilities, food industries, and medical facilities have begun using alternative disinfectants including: liquid free chlorine, chlorine dioxide, chloramines, ozone, and ultraviolet irradiation (UV).[2,5–9] The alternatives to free chlorine will be further discussed to explain their use in drinking water treatment and what is known of their inactivation mechanisms. Gaps in understanding of inactivation mechanisms of both free chlorine and its alternatives remain, especially for unculturable viruses. These gaps must be filled to maintain disinfectant efficacy and thereby safe drinking water.

1.1.1 Disinfection in drinking water treatment

Drinking water facilities in the United States commonly add a residual chemical, during secondary disinfection, to protect against pathogens in the distribution system. Of the alternative disinfectants, ozone can only be use for primary disinfection, while chloramines can only be used

for secondary disinfection. Free chlorine and chlorine dioxide can be used in both primary and secondary disinfection. Compared to chlorine dioxide, free chlorine and chloramines require larger concentrations and longer contact times, and their effectiveness can vary with pH, including within common drinking water pH regimes.[10,11] Free chlorine, chlorine dioxide, and ozone all have much greater disinfection power than chloramines, which is needed for primary disinfection. Thus chloramines are suitable only for secondary disinfection.[12]

Disinfection via ozone, UV, and chlorine dioxide is used by a small percentage of treatment systems in the United States, but all have increased in popularity over the years.[13] Chlorine dioxide and ozone are both powerful oxidants that inactivate viral pathogens through chemical reactions with either the outer protein or inner genetic material.[14,15] UV primarily attacks the inner genetic material of pathogens, causing inactivation, but it can also target capsid proteins causing backbone cleavage and general damage.[16,17] Chlorine dioxide and ozone require special equipment for on-site generation, storing, and byproduct control. UV systems also require the installation of special equipment and monitoring technology for application. While chlorine dioxide, ozone, and UV can be more complex to handle than free chlorine, they offer advantages such as fewer disinfection byproducts, higher inactivation efficiencies, and little or no sensitivity to pH.[5,18]

The characteristics of each oxidant need to be weighed when selecting a disinfectant for water treatment. While utilities have been implementing all types of oxidants in water treatment, the complexity of their effects on pathogen disinfection, corrosion, and byproduct formation and how these reactions affect each other are not well understood.

1.1.2 Virus Inactivation

Inactivation mechanisms are highly dependent on the type of disinfectant used. The variability comes from targeting virus proteins versus genomes. In general, damage to proteins causes the virus to lose the ability to recognize and bind to host cells, while damage to the genome prevents viral replication. Typically, free chlorine, the most common disinfection oxidant, destroys both viral protein and genome.[14,15] Chlorine dioxide, in contrast, tends to exclusively target viral proteins.[14,15] More specific mechanisms of inactivation are still unclear and seem to also depend on the virus type.[14,15,19] Previous studies on bacteriophage MS2 show free chlorine damage causes loss of replication and injection but not binding ability despite widespread protein damage.[14] Chlorine dioxide in the same study exclusively damaged the bacteriophage MS2 protein and had no influence on replication ability.[14] This is in agreement with a narrower study attributing chlorine dioxide inactivation of the H1N1 influenza A virus to oxidation of tryptophan 153 in the hemagglutinin protein, which ruined the virus's ability to bind to host cells.[20]

To effectively inactivate dangerous pathogens, disinfectants must have high reactivities. Powerful oxidants, however, will readily react with water constituents other than pathogens. Thus, inactivation is only one type of reaction that occurs during treatment. Other reactions include reactions with organic material, forming potentially hazardous disinfection byproducts, and reactions with metals in the distribution system, forming corrosion scales and potentially dissolving hazardous amounts of heavy metals into drinking water. The interplay and complexity of these reactions, for chlorine dioxide, is poorly understood.

1.2 DISINFECTION BYPRODUCTS

Disinfection reduces the risk of waterborne illness, but in the process, it can increase the risk of exposure to dangerous compounds formed during unwanted reactions with water constituents. Moreover, the relationships between these unwanted reactions and how they impact water quality is not well understood. The oxidants used during treatment react with natural organic matter (NOM), bromide, and iodide, which are naturally present in most source water.[21,22] Despite the risks associated with these compounds, adequate disinfection for microbial control is essential. In 1993, 400,000 people were infected by cryptosporidiosis in Milwaukee, Wisconsin and more than 100 people died, due to improperly disinfected water.[23,24] Accordingly, disinfection remains a critical part of water treatment, but must be balanced with disinfection byproduct (DBP) control.

The proliferation of DBPs could be attributed to the need for high concentrations of disinfectants added to drinking water to safeguard against unculturable viruses, whose inactivation kinetics are unmeasurable. Despite having employed the same disinfection methods for decades, the exact mechanisms by which they cause inactivation are poorly understood, as are the differences in efficacy for specific pathogens.[14,15,19] The susceptibility of dangerous unculturable viruses to these disinfection methods is also unknown due to an inability to perform experiments on such viruses *in vitro.*[15] Because of this knowledge gap, water treatment systems routinely administer disinfectants, specifically free chlorine, at higher concentrations than needed in order to achieve pathogen inactivation. This in turn leads to a proliferation of reactions with NOM rather than pathogens. Gaps in understanding of how formation and mitigation of DBPs influences corrosion of water treatment distribution systems and vice versa also persist. For chlorine dioxide there remains gaps in knowledge for chlorite and chlorate formation, especially in the presence of lead-based

corrosion scale. The state of knowledge on formation, regulation, and mitigation of these DBPs will be discussed herein.

1.2.1 Formation of DBPs

While many reactions between disinfectants and NOM create harmless byproducts, others form hazardous halogenated compounds called disinfection byproducts (DBPs), which can cause liver, kidney, heart, and neurological impairments; birth defects; and pregnancy risks even at relatively low concentrations.[5,21,25] The most common disinfectants used in water treatment, free chlorine, chlorine dioxide, chloramines, and ozone, all produce their own, sometimes overlapping, sets of DBPs.[21] As there are no DBP-free oxidants, a delicate balance that needs to be struck between byproduct formation and pathogen inactivation to maintain public health standards and create appropriate regulations that mitigate risk.[26] This can only be achieved through a comprehensive understanding of DBP formation. Currently, more work needs to be done for chlorine alternatives, including chlorine dioxide, which create different sets of byproducts. It is not well understood what system parameters influence the production of chlorine dioxide byproducts or how these byproducts are formed in the presence of metal or organic matter catalysts.

DBP formation is especially prevalent in systems that use free chlorine. Free chlorine has been shown to produce trihalomethanes (THMs) and haloacetic acids (HAAs), the two most regulated groups of DBPs.[6,27,28] The discovery of THMs in the 1970s catalyzed research focused on mitigating public health issues related to DBPs.[29,30] Since the first detection of THMs approximately 600 DBPs have been identified, including chloral hydrate, chloropicrin, haloketones, iodo- and bromo-compounds, MX, halonitromethanes, N-nitrosodimethylamine, and others.[5,31] Concentrations of these newer compounds, in drinking water, can be comparatively low ranging

from nanograms per liter to 100 micrograms per liter but can still be hazardous due to their high toxicity.[32] Both concentration and potency therefore play a role in public health risk as highly toxic compounds can pose serious human health concerns. Work on DBP formation continues to reveal new byproducts, especially nitrogenated compounds, which are formed when chloramines are used as a disinfectant and are posited to be more toxic than THMs and HAAs.[33] Due to the toxicity of DBPs, regulatory agencies have put measures in place to protect the public from ingesting high doses of DBPs in their drinking water.

1.2.2 Regulation of toxic DBPs

US Environmental Protection Agency (EPA) Regulations are based on total THM and HAA concentrations which include four distinct THMs and five distinct HAAs under the Stage 1 Disinfectants/Disinfection Byproducts Rule (Table 1.1 and Table 1.2). These compounds form from reactions between disinfectants and NOM, where chlorine is substituted into the organic molecule. Also regulated by the EPA are the disinfectants themselves (Table 1.1), chlorite (a DBP associated with chlorine dioxide, Table 1.2), and bromate (associated with ozone and free chlorine if bromide is present in the treated water, Table 1.2).

Table 1.1 EPA Disinfectant Rules adapted from the EPA.[34] Maximum residual disinfection level (MRDL).

Contaminant (as Cl_2)	**MRDL (mg/L)**	**Potential Health Effects from Long-Term Exposure Above the MRDL**	**Sources of Contaminant in Drinking Water**
Chloramines	4.0	Eye/nose irritation; stomach discomfort, anemia	Water additive used to control microbes
Chlorine	4.0	Eye/nose irritation; stomach discomfort	Water additive used to control microbes
Chlorine dioxide	0.8	Anemia; infants and young children: nervous system effects	Water additive used to control microbes

Table 1.2. EPA Disinfection Byproducts Rules adapted from the EPA.[34] Maximum contaminant level (MCL).

Contaminant	MCL (mg/L)	Potential Health Effects from Long-Term Exposure Above the MCL	Sources of Contaminant in Drinking Water
Bromate	0.01	Increased risk of cancer	Byproduct of drinking water disinfection
Chlorite	1	Anemia; infants and young children: nervous system effects	Byproduct of drinking water disinfection
Haloacetic acids (HAA)	0.06	Increased risk of cancer	Byproduct of drinking water disinfection
Total Trihalomethanes (TTHMs)	0.08	Liver, kidney or central nervous system problems; increased risk of cancer	Byproduct of drinking water disinfection

To meet the standards set by the EPA, utilities originally focused on reducing the organic precursors to DBPs by coagulation,[22] however, the methods used for the reduction of DBPs have had unintended consequences on corrosion and heavy metal dissolution in water distribution systems. Knowledge gaps remain how the formation and mitigation of DBPs influences corrosion and disinfection kinetics, especially with regards to chlorine alternatives such as chlorine dioxide.

Early research showed coagulation methods resulted in successful reduction of total organic carbon, and were easily implemented in existing treatment systems.[22] However, the mechanisms behind NOM removal by coagulation are still poorly understood, leading to excessive application of chemicals that cause unwanted corrosion effects. Commonly used coagulants containing chloride, such as ferric chloride and polyaluminum chloride, exacerbate corrosion in distribution systems by increasing the ratio of chloride to sulfate, which has been shown to create an environment conducive to high galvanic currents.[35,36] Connections between copper and lead are highly susceptible to galvanic corrosion and are made more vulnerable by a high chloride to sulfate

mass ratio.[36,37] While mitigating health risks associated with DBPs, chloride-based coagulants can inadvertently increase risks associated with heavy metal exposure. It has therefore been of interest to utilities to investigate disinfectants such as chloramines, ozone, UV and chlorine dioxide, which produce fewer THMs and HAAs than free chlorine without the use of coagulation. This dissertation aims to fill the gaps in knowledge of chlorine dioxide byproduct production and said byproducts' influence on lead and copper corrosion and disinfection kinetics.

1.2.3 Mitigation of DBPs

The two strategies employed by utilities to reduce DBPs are: remove as much organic matter as possible before disinfection and avoid free chlorine as a disinfectant. Removal of organic matter can sometimes cause problems with corrosion and requires additional chemicals to be added during the treatment process. The literature has primarily focused on the mechanisms of free chlorine reaction with precursor NOM. It is of interest, however, to look at alternative disinfectants and the mechanisms they favor in forming DBPs as utilities continue to replace free chlorine with these alternatives.

As an alternative to reducing NOM prior to disinfection, treatment plants have adopted alternative oxidants to chlorine to meet EPA regulations. Chloramines, chlorine dioxide, ozone, and UV are all alternatives to free chlorine with lower propensities to form DBPs.[5] While they can reduce or eliminate THM and HAA formation, alternative disinfectants can produce alternative DBPs, especially in bromated waters. Ozone produces bromate,[38] a carcinogen regulated by the EPA, while chloramines and free chlorine can form brominated organic compounds, which are demonstrably more toxic than chlorinated equivalents.[39] Chloramines increase the occurrence of highly toxic nitrogenated compounds, such as nitrosodimethylamine (NDMA),[7] and produced higher levels of

other priority DBPs such as iodinated THMs, especially when used in conjunction with ozonation.[39] Some of these compounds have much higher toxicities and associated risks than THMs or HAAs.[7,40] Chlorine dioxide readily forms chlorite and to a lesser degree chlorate[41] but no iodinated, bromated, or nitrogenated DBPs.[21]

1.3 CORROSION SCALE

Alongside reactions with NOM, disinfectants react with drinking water distribution infrastructure producing corrosion byproducts. These reactions occur with iron and copper plumbing, but recent water crises in Flint, Michigan and Washington DC have prompted increased interest in reactions with lead. Corrosion reactions cause serious public health concerns, as well as erosion of system materials, thereby influencing the cost of clean water, and affecting public perception of safe practices.[37,42] Due to the complexity of drinking water chemistry, corrosion reactions are still poorly understood, as is apparent from the recent Flint, MI and Washington DC water crises. Additionally, the relationships between corrosion, byproduct formation and removal, and disinfection efficacy have not been well studied, especially for free chlorine alternatives.

The costs associated with corrosion can be huge. Regulations established in 1986 prohibit the use of lead pipes in new construction, but a glut of older structures still contain original lead infrastructure. The EPA estimated $335 billion would be needed to repair corrosion related issues over the next 20 years for 70,000 water systems.[43] Often these problems go overlooked until a public health crisis exposes dying infrastructure, as in the case of the Flint Water Crisis in Michigan beginning in 2014 and the Washington D.C. lead contamination from 2001 to 2004. Both events resulted in widespread public health problems, mistrust of government agencies, and costs to repair systems that should have already been upgraded.

The two primary metals that are regulated in the United States are copper and lead, whose concentrations have been subject to the EPA Lead Copper Rule since 1991.[44] This dissertation focuses on the issue of lead corrosion. The main sources of lead exposure are normally through lead paint, dust containing lead paint, and leaded gas.[6,45] There is no safe blood lead level in children according to the Center for Disease Control and Prevention. Lead is stored in the skeletal system and accumulates in the body over time, primarily affecting the nervous system and slowing mental and physical growth in children.[46] In adults, lead toxicity affects the growth of red blood cells, metabolism, and sperm production, and causes anemia, kidney damage, miscarriages, and high blood pressure.[34] As sources of lead exposure were reduced, such as the ban of leaded gasoline, there has been more of a focus on lead infrastructure as a route of exposure.[47] The Lead Copper Rule requires drinking water systems to notify the public and/or reduce the corrosivity of the water if lead levels in more than 10% of the sampled consumer taps are over 15ppb.[44] Lead infrastructure is the source of 50-75% of the total lead in drinking water.[48] Because of the dissolved oxygen content, untreated water will corrode lead pipes and cause the EPA Action Level in the Lead Copper Rule to be exceeded.[49,50] Disinfectant residuals, i.e. free chlorine, chloramines, or chlorine dioxide will also cause lead corrosion and produce mineral scales on the inside of lead plumbing.[37] The following will discuss the formation, dissolution, and control of these mineral scales.

This dissertation aims to address some of how these mineral scales affect byproduct formation and pathogen removal when chlorine dioxide is used as a disinfectant. Previous work has investigated chlorine dioxide reactions with copper, nickel, and iron scales,[51] but there is little work on chlorine dioxide reactions with lead scales.

1.3.1 Formation of lead corrosion scale

To control lead leaching into drinking water, the reactions between disinfectants and lead-containing pipes and the affect these reactions have on byproduct mitigation must be better understood. The type of scales, layers of mineral deposits that form on distribution system plumbing, that develop on lead pipes depend on the chemistry of the system water. Metallic lead is too thermodynamically unstable and will immediately be oxidized to corrosion products where lead is in a divalent or tetravalent form.[37] Lead can be found in lead (II) carbonates, lead (II) oxides, and lead (IV) oxides when phosphate inhibitors are absent from the system.[52–54]

In drinking water systems, the oxidation-reduction potential (ORP) is the primary indicator of what the oxidation state of the corrosion products will be and therefore what type of scale will develop.[55] ORP or redox potential is a measure of the water's propensity to reduce or oxidize material and is based on the availability of free electrons.[55] In drinking water systems, distribution plumbing is commonly made of iron, lead, or copper, metals which lose their electrons to oxidants in the water such as residual disinfectants (free chlorine, chloramines, chlorine dioxide), dissolved oxygen, and organic matter.[55]

Free chlorine creates a high ORP and drives the system toward lead (IV) in the passivating form of lead oxide (PbO_2), whereas oxygen or chloramines create lower ORPs that favor lead (II) (Table 1.3).[53] The mechanism from metallic lead to tetravalent lead is not completely understood, but it is proposed that lead (II) minerals are formed as precursors to lead (IV) oxides [52,53]. Both plattnerite (β- PbO_2) and scrutinyite (α- PbO_2) develop in the long term presence of free chlorine.[53] Formation of the lead oxide scale takes time to develop and can only occur in high ORP waters; thus, lead (II) compounds, hydrocerussite and cerussite, can also coexist with lead (IV) oxide

depending on alkalinity and/or pH of the water.[53] It has been assumed that chlorine dioxide will also create a high ORP conducive to lead (IV) scale development (Table 1.3) [55].

Table 1.3. Maximum E_H values (Volts) as a function of pH and oxidant type.[55]

Oxidant	pH 7	pH 8	pH 9
Oxygen	0.582	0.552	0.508
Monochloramine	0.806	0.716	0.660
Chlorine dioxide	0.980	0.943	0.912
Free chlorine	1.020	0.922	0.769

Systems that use chloramines do not develop ORPs high enough to oxidize lead to the (IV) state. Instead, lead (II) minerals, hydrocerussite ($Pb_3(CO_3)_2(OH)_2$) and to a lesser extent cerussite ($PbCO_3$), are the primary corrosion products.[56,57] Litharge (PbO) and plumbonacrite ($Pb_5O(CO_3)_3(OH)_2$ have also been found in pipe scales but are much less common than hydrocerussite or cerussite.[57] Lead (II) solids are more soluble than lead (IV) oxides, which can increase levels of dissolved lead in plumbing that contains lead (II) scale.[48] Previous studies showed chloraminated waters to have lead concentrations ten times that of chlorinated waters.[37,47] Chloramines also react with brass, cause galvanic corrosion, and promote the growth of nitrifying bacteria which all may further aggravate lead release.[37,47]

1.3.2 Lead scale dissolution

To prevent leaching of lead into drinking water, it is preferable to maintain a high ORP and thus a stable lead (IV) oxide passivating layer. Lead solubility is high when a bare pipe first comes into contact with a disinfectant or other natural oxidants,[51] and as free chlorine or another

disinfectant of high ORP is consumed lead is oxidized from lead (0), to lead (II), to lead (IV).[53] Concentration of dissolved lead steadies when lead (II), which forms more soluble compounds, develops into lead (IV) scale, relatively insoluble.[58] Once the oxidant has been completely consumed, dissolved lead concentration increases dramatically due to the dissolution of the scale.[58] Free chlorine prevents the dissolution of lead into drinking water [37,58,59].

Within distribution systems, it should be noted that water is not in contact long enough with pipe scales to reach equilibrium; even equilibrium in stagnant waters can take hours.[60] The concentration of dissolved lead is therefore controlled by dissolution rates and the scale type rather than a controlling solid.[60,61] Water in the plumbing system can have periods of stagnation and varying velocities which also influence lead leaching and prevent the system from reaching equilibrium.[58]

High concentrations of lead in drinking water can also be attributed to the destabilization of any of the previously discussed corrosion scales. Stability of the scale depends on the chemical characteristics of the water, specifically pH, alkalinity, anions present, organic matter concentration, disinfectant concentration, and ORP.[51,58] A switch from free chlorine to chloramine residual in Washington, D.C. in the early 2000s resulted in huge spikes in drinking water lead concentrations and public blood lead levels.[37] The cause of this dramatic increase was the abrupt change in ORP of the system which resulted in the dissolution of the lead oxide scale previously formed by long term free chlorine use.[37,47] Understanding the factors influencing the oxidation state of lead is essential in understanding and controlling corrosion chemistry.

1.3.3 Control of corrosion scale

Disinfectants, corrosion control anions, pH and the presence of NOM are the main factors that influence corrosion chemistry. The relationships between these factors are vital in the mitigation of dissolved lead in tap water. Also crucial are the relationships between these factors, byproduct formation, and disinfection efficacy. While there are many studies on free chlorine and chloramine effects on corrosion, less work has been done on chlorine dioxide, especially in the context of lead dissolution.

To control the release of lead, drinking water plants have monitored and maintained a high pH.[54] More recently, corrosion inhibitors have become common additions to create passivating layers on metallic infrastructure. Phosphates have been added in the following forms: phosphoric acid, a combination of orthophosphoric acid and zinc orthophosphate, polyphosphates, and blends of orthophosphoric acid and polyphosphates.[62] From 1992 to 1994, there was a significant increase in phosphate inhibitors as a result of the Lead Copper Rule, instituted in 1991.[63] In the case of lead corrosion, orthophosphates, added as $Na_3PO_4 \cdot H_2O$, are the most effective and decrease soluble lead over a range of water chemistries, whereas polyphosphates can increase soluble lead.[62]

Orthophosphate prevents the formation of both divalent and tetravalent lead corrosion products.[61] Instead of a lead oxide or lead carbonate scale, orthophosphate facilitates the formation of hydroxypyromorphite, tertiary lead orthophosphate, and chloropyromorphite, all of which are insoluble, hydroxypyromorphite being the most prevalent.[52] Phosphate inhibitors can passivate lead surfaces in systems that use both chloramines and free chlorine. If there is no orthophosphate present hydrocerussite forms and, if the water ORP is high enough, there is a subsequent shift to plattnerite and scrutinyite.[53]

In drinking water systems, NOM also plays a role in both the stability and the dissolution of lead corrosion scales. In the absence of a high ORP disinfectant, lead (IV) oxide scale will be reduced by NOM from lead (IV) to lead (II) thereby increasing soluble lead.[59] NOM will also react directly with disinfectants to form DBPs, as discussed in 1.2 Disinfection byproducts. The interaction of NOM and disinfectants can also impact corrosion by influencing the system ORP. NOM and oxidants readily react, which can decrease the ORP of the system and promote the dissolution of corrosion scales.[48]

Understanding the chemistry of corrosion is essential for regulating and avoiding lead release in tap water, and for chlorine dioxide, this chemistry is understudied. There are three major components to consider for distribution systems: the strength of the oxidant used for disinfection residual i.e. ORP; formation and destabilization of lead scales; and the presence of anions, primarily orthophosphate, and/or NOM. Corrosion chemistry is just one piece of the complex reactions that occur during disinfection. To avoid lead release, water treatment systems also need to consider byproduct formation and mitigation as well as the effect on disinfectant efficacy. The key knowledge gaps are in these relationships between corrosion scale, DBPs, and pathogens.

1.4 THE CASE FOR CHLORINE DIOXIDE

Since the implementation of the Disinfectant Byproduct Rule by the EPA, utilities have been searching for alternate disinfectants that produce controllable DBPs (or none at all) while still maintaining safe water quality. One oxidant that could meet these criteria is chlorine dioxide. Numerous European countries including Italy, Germany, France and Switzerland have already employed chlorine dioxide as a secondary disinfectant.[12] In the United States, chlorine dioxide use has increased in recent decades but is still used only by a small percentage of drinking water

treatment plants, typically for pre-oxidation purposes.[64] Despite some implementation of chlorine dioxide as a disinfectant, its effect on corrosion scale and inorganic byproduct formation are key gaps in knowledge this dissertation aims to investigate.

Chlorine dioxide has many benefits as a disinfectant when compared to free chlorine and chloramines. It has been shown to have greater disinfection efficiency than that of free chlorine or chloramines.[12] Unlike chloramines and free chlorine, it has the oxidizing capacity to inactivate viruses, bacteria, and protozoa including *Giardia* and *Cryptosporidium.*[10,65] Chloramines have also been shown to increase nitrification in distribution networks [66] and produce toxic nitrogenous DBPs.[29] Free chlorine is susceptible to changes in pH and produces halogenate DBPs, primarily THMs and HAAs. Chlorine dioxide is pH resistant and does not produce THMs, HAAs, or nitrogenated DBPs.

Free chlorine and chlorine dioxide have also been shown to have a similar ORP, which could facilitate a transition to chlorine dioxide without disrupting the passivating layers already in place in the distribution system. In Washington D.C., the switch from free chlorine to chloramines as a secondary disinfectant resulted in dangerously high levels of dissolved lead in the water system. It was concluded that the change in ORP due to the switch in oxidant upset the passivating layers on piping, resulting in lead dissolution.[37] At high ORPs, chlorine dioxide and free chlorine should both form similar insoluble passivating layers on lead surfaces and thus lead dissolution due to change in disinfectant could be a nonissue but requires further investigation.

Chlorine dioxide does produce inorganic byproducts chlorite and chlorate. Both have associated health risks including anemia and nervous system effects. Chlorite is regulated by the EPA with a maximum contaminant level of 1.0 mg/L whereas chlorate is unregulated.[67] Chlorine dioxide does not produce either THMs or HAAs like free chlorine, carcinogenic bromate like

ozone, or nitrogenated compounds like chloramines.[5,23,68] Chloramines, a more common secondary disinfectant in the US, can produce haloacetonitriles and iodoacetic acids that are potentially more toxic than currently regulated compounds.[33] Chlorine dioxide could be used as a primary disinfectant for water rich in bromide (e.g. coastal waters) instead of ozone as it readily forms bromate when bromide is present whereas chlorine dioxide does not.[69] Furthermore, ozone is also not a viable option for secondary disinfection due to its high reactivity.

Despite producing inorganic DBPs, chlorine dioxide can still be used as a disinfectant in treatment systems. Adjustments to both pre-oxidation and coagulant application processes can greatly reduce chlorine dioxide consumption and chlorite formation.[70] There are also specific removal techniques to control chlorite/chlorate formation and make chlorine dioxide a viable disinfectant for full scale implementation. Chlorite can be removed by chemical reduction via sulfate ions, granular activated carbon, or ferrous ions.[71] Ferrous ions are the most effective form of removal and can be added in exiting coagulation/flocculation tanks and removed during sedimentation and/or filtration.[72,73] Further work should be done to establish relationship between these chemicals and corrosion, especially with regards to the chloride sulfate ratio.

Utilities that keep chlorine dioxide concentrations under 1.25mg/L have no problems meeting the chlorine dioxide Maximum Residual Disinfectant Level (MRDL) or chlorite Maximum Contaminant Level (MCL).[74] A treatment plant in Roanoke County, VA successfully employed chlorine dioxide under these regulations; at a water demand of 2.3 to 3.7 mgd, chlorine dioxide demand was 0.19 mg/L and exceeded 0.3 mg/L only on four occasions.[74]

Chlorine dioxide is a more powerful disinfectant than both free chlorine and chloramines, as manifested in the CT values for certain targets like cryptosporidium, while only producing inorganic DBPs that can be removed post disinfection. Free chlorine is susceptible to changes in

pH and produces carcinogenic, heavily regulated DBPs. Chloramines are ineffective against certain pathogens due to low disinfectant power, they can produce extremely toxic nitrogenated DBPs, and can nitrify water in distribution infrastructure. Ozone cannot be used as a residual and produces toxic brominated DBPs. With a similar ORP to free chlorine, chlorine dioxide could a more easily deployable alternative disinfectant than chloramines, which have a much lower ORP and thus the potential to disrupt passivating layers on metallic distribution system. Chlorine dioxide reactions with lead-based pipe corrosion and the byproducts produced during these reactions have yet to be investigated. All these factors make chlorine dioxide worth investigating as an alternative to free chlorine in drinking water treatment.

Drinking water treatment plants have not more broadly adopted chlorine dioxide for a few key drawbacks associated with its implementation. While there are examples of chlorine dioxide usage on treatment plant scales, the EPA regulations on chlorite are strict and difficult to maintain. Additionally, chlorine dioxide is a highly explosive and volatile chemical. Great care must be taken when manufacturing and storing the chlorine dioxide solution, therefore treatment plants are wary of investing in and training staff to safely manage its production. Although all powerful oxidants used in water treatment pose safety risks for operators, and chlorine dioxide is no different in this regard. Due to its volatility, chlorine dioxide must also be produced on site and can only be store for a limited amount of time. Nevertheless, its many and previously discussed advantages as a disinfectant do make it a potential option for drinking water treatment plants, especially if more is known about its pathogen disinfection mechanisms, inorganic byproducts, and reactions with corrosion on distribution pipes. Insight into these complex reactions could reveal further advantages over free chlorine for drinking water treatment.

1.5 MOLECULAR MODELING METHODS

Molecular scale interactions inherently govern all the macroscale properties of disinfection previously discussed. Computational techniques offer a way to examine molecular interactions and thereby explain results that experiments cannot. Background on the computational methods used in this dissertation is presented below.

1.5.1 Molecular Docking

Molecular docking methods use computations to predict the binding conformations and affinities of smaller molecules to macromolecules, termed ligands and receptors respectively.[75,76] Currently, the most common application of docking is for drug development, and it has never been applied to disinfectant docking. Using crystallographic structures of protein receptors and drug molecule ligands, docking calculates the free energy of binding and the preferred orientation of the ligand on the receptor pocket.[77] An example of one such calculation is shown in Figure 1.1, the binding of sialic acid to a virus protein. One of the most popular molecular docking programs is the AutoDock suite, which contains AutoDock Vina and AutoDock. AutoDock Vina relies on a scoring function to calculate chemical potentials whereas AutoDock relies on classical force fields to calculate free energy.[77] AutoDock Vina is much faster but has more limited applicability to atypical systems than AutoDock. Both programs were used in Chapter 2 of this dissertation.

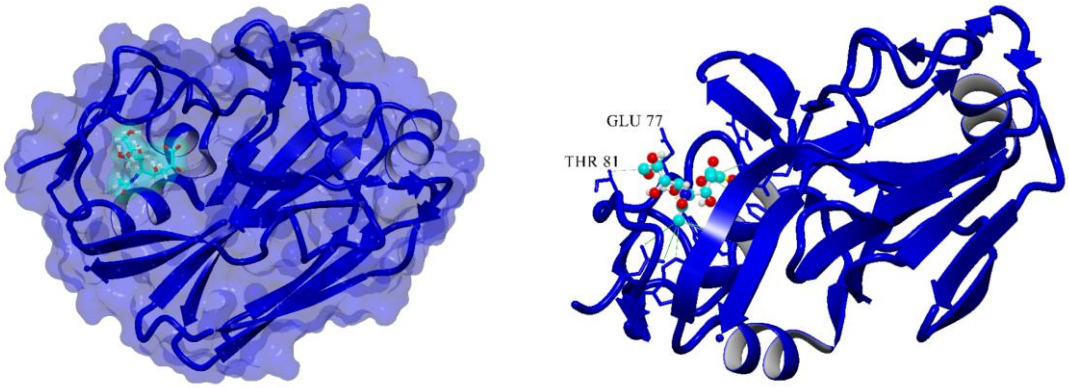

Figure 1.1 Image of a sialic acid residue (ligand) bound to the H1N1 influenza virus hemagglutinin protein (receptor). The left image shows the molecular surface of both ligand and receptor. The right image labels two amino acids that have an affinity for the sialic acid residue. Calculations were done using Auto Dock Vina.

1.5.2 Density Functional Theory

Ab-initio methods use quantum chemistry to solve the Schrödinger equation, the central equation describing the behavior of atoms in a system. Quantum methods are transferable and produce highly accurate results compared to classical or semi-classical methods, but at high computational cost, limiting both size and time scales of the system.[78] Classical and semi-classical methods treat electrons implicitly, which restricts their transferability and accuracy with regards to bond breaking or altering.[78,79] To converge to an exact solution of the Schrödinger equation, ab-initio methods treat electrons explicitly and the complexity of the calculations increases exponentially with the quantity of electrons considered in the simulated system.[80] A number of methods have been established to mitigate the limitations of ab-initio methods, the most popular and widespread being density functional theory (DFT).[78] DFT is primarily based on electronic ground state structure, which is determined via electron density distributions.[80] Other quantum mechanical methods such as Hartree and Hartree-Fock use wave functions rather than electron density distribution. The DFT calculations are based on the Hohenberg and Kohn theorems for

solving the Schrödinger equation.[80] DFT energy calculations can provide an understanding for any system that contains nuclei and electrons from molecules to clusters to solids.[81] DFT can also determine a variety of molecular properties such as vibrational frequencies, formation energies, activation energy barriers, minimum energy structures, reaction paths, magnetic properties, etc.[82]

Computational methods have grown popular in the field of organic chemistry as a way to understand structures and properties of compounds and to use this data to determine formation pathways.[82] Using DFT and other ab-initio methods, potential energy surfaces of reaction pathways can be calculated from geometric and electronic properties of reactants, products, intermediates, and transition-state structures.[82–84] A computational study of the Wacker process, which has been debated due to controversy in experimental studies, used ab-initio and classical methods to compared computed free energy barriers to experimentally measured kinetic parameters.[85] A study by Yuan et. al. ruled out three proposed pathways and pinpointed the true mechanism for aromatic C-H oxidation by calculating transition states and energy barriers.[86]

Computational calculations have also been used to study adsorption energies, conformations, and adsorbed transitions structures on crystal surfaces.[87] Most studies focus on rutile crystal structures which common materials for catalysts.[87–90] Of interest in the literature has been the diffusion or dissociation of a water molecule adsorbed to a rutile surface.[87,90] DFT has been employed to analyze adsorption geometries and reaction pathways to explain macroscale catalytic properties.[87] Chapter 4 of this dissertation aims to applies these methods to chlorine dioxide adsorption onto cupric and lead oxide surfaces.

Understanding the complexity of pathogen disinfection, corrosion, and byproduct formation has been limited by experimental methods. While there has been computational work

done in the area of pathogen inactivation, computational docking and DFT adsorption methods have yet to be used to study disinfection.

1.6 DISSERTATION CHAPTERS

This dissertation intends to contribute to the body of knowledge surrounding disinfectant reactions including inactivation, byproduct formation, and corrosion. The aims focus on the alternative disinfectant, chlorine dioxide, as it has potential to replace free chlorine in drinking water systems. Chlorine dioxide was thus evaluated based on inactivation mechanisms to use computational tools in a new way to better predict and understand chlorine dioxide disinfection efficacy (Chapter 2); byproduct formation and corrosion to fill the gaps in knowledge associated with chlorine dioxide reactions with lead-base corrosion scale and the inorganic DBPs it might produce during these reactions (Chapters 3 and 4).

Chapter 2 was motivated by the question: what components of a virus are susceptible to attack by a disinfectant? Chlorine dioxide appeared to have a highly specific mechanism for inactivation of the H1N1 influenza A virus, and because of this specificity H1N1 was chosen as a more easily testable starting point for evaluating the ability of docking methods to predict oxidation sites. It was shown this location could be predicted by molecular docking methods. Tryptophan 153 was identified by both the docking calculations and the mass spectrometry measurements as a primary target of chlorine dioxide oxidation. Additional docking calculations revealed free chlorine to have a more random docking pattern, and N-bromosuccinimide, a larger ligand known to selectively oxidize tryptophan residues, to dock near said residues including tryptophan 153.

Chapter 3 was motivated by the relationship between corrosion and toxic byproduct formation: what byproducts does chlorine dioxide produce when it interacts with corrosion scale minerals? The presence of lead-based minerals accelerates chlorine dioxide decay to a single inorganic byproduct, chlorite, whereas copper, nickel, and iron minerals catalyze reactions resulting in both chlorite and chlorate. The maximum rate of chlorine dioxide decay occurs at the zero-point pH for lead oxide.

Chapter 4 attempts to address the questions resulting from the findings of Chapter 3 concerning the differences in kinetics, byproduct formation, and dependence on pH between lead and copper oxides by using computational methods to determine adsorption energies and conformations. The adsorption of a single chlorine dioxide molecule and a chlorine dioxide dimer on the surface of lead oxide and cupric oxide, with hydroxide anion present, was investigated. It was found that cupric oxide favors the dimerization of chlorine dioxide. Lead oxide favors neither the chlorine dioxide monomer nor dimer but does have a weaker adsorption energy than cupric oxide, which could explain the kinetic rate disparity between the two metals.

Overall this work provides insights into computational methods for determining inactivation mechanisms, byproduct formation and variation in the context of corrosion, and the influence of metallic oxide structure on disinfectant decay reactions.

Chapter 2. Molecular Docking Predicts Tryptophan 153 in the Hemagglutinin Protein of H1N1 Influenza Virus as the Primary Target of Chlorine Dioxide Oxidation

2.1 INTRODUCTION

The influenza virus has long beleaguered human society,[91,92] most recently causing a pandemic that killed more than 18,000 people in 2009.[93] Epidemics of influenza A viruses annually infect individuals in a growing number of countries.[94] Chlorine dioxide, a powerful oxidant, has been used in various disinfection methods as it is effective against bacteria, protozoa, and viruses, including influenza A.[10,65] Chlorine dioxide is an alternative water disinfectant, and though H1N1 is not waterborne, there have been concerns over H1N1 inactivation in water, as viral shedding occurs in infected patients' stools.[95,96] Gaseous ClO_2 can be used to safely inactivate airborne viruses including H1N1 in mice and rats at low concentrations.[97,98] Sodium hypochlorite has been recommended by the World Health Organization for the disinfection of medical equipment and countertops/table surfaces to reduce the risk of H1N1; gaseous ClO_2 can serve as an alternative.[2,3] Starting in 1998, the Food and Drug Administration approved the use of ClO_2 for the disinfection of fruits and vegetables.[4] Given the viability of ClO_2 as a disinfectant for H1N1 risk reduction, its inactivation mechanism is worthy of further investigation.

One might expect ClO_2 to stochastically dock to the protein sheath of a pathogenic virus and indiscriminately attack its transmembrane proteins.[14] However, it has been proposed that ClO_2 has a highly specific inactivation mechanism for the H1N1 strain of the influenza virus that targets the HA tryptophan 153 (W153) residue, and that the oxidation of this amino acid is responsible for

the inactivation of H1N1.[20] W153, is in the HA spike protein of H1N1, which binds the virus to sialic acid residues on the cell. The HA protein and the amino acids that make up the receptor-binding region are indicative of the pathogenicity of an influenza virus strain.[94,99] The reported highly specific interaction of ClO_2 with the W153 oxidation target in the HA receptor-binding pocket makes the H1N1 virus a logical starting point for computational investigation of ClO_2 disinfection mechanisms.

Although mass spectrometry has proven an effective tool to probe the oxidation of virus proteins by chemical disinfectants,[20,100] the application of this experimental approach is limited to viruses that are both culturable and can be propagated to high concentrations. H1N1 was chosen as a model virus because previous studies noted the specificity of ClO_2 oxidation of the H1N1 HA protein. Therefore, the objectives of the present study were twofold: first, to assess the capability of molecular docking studies to predict ClO_2 oxidation targets on the HA protein of the H1N1 influenza virus, and second, to test the computational predictions using Orbitrap mass spectrometry to analyze the oxidation of H1N1 HA protein exposed to ClO_2.

2.2 METHODS

2.2.1 Reagents and HA protein.

H1N1 recombinant hemagglutinin (HA) protein, the A/New Caledonia/20/99 strain, was obtained from Protein Sciences. The concentration of HA was measured using a Qubit Fluorometer 2.0, which quantifies proteins via fluorescence-based assays using standards provided in the protein kit (ThermoFisher Scientific). ClO_2 stock solution was prepared by mixing aqueous solutions of 0.15 M potassium peroxodisulfate ($K_2S_2O_8$) and 0.88 M sodium chlorite ($NaClO_2$) purchased from Sigma Aldrich.[51] The solution was scrubbed with 0.11 M $NaClO_2$ solution before

storage to remove any chlorite from the ClO_2 stock. The stock solution was stored at 4 °C in amber bottles and its concentration was determined by spectrophotometry at 359 nm (ε_{359nm} = 1230 M^{-1} cm^{-1}).[101] Trypsin was purchased from Worthington.

2.2.2 Computational docking: receptor and ligand models.

YASARA-Structure 15.9.6,[102] a computational molecular modeling suite, was used as a platform to run AutoDock and AutoDock Vina.[75,103] The protein crystal structure file (PDB ID: 3MLH, A/Mexico/4603/2009) for the HA domain of the 2009 H1N1 influenza virus was obtained from the RCSB Protein Data Bank and was selected for crystallographic resolution (2.09 Å) and location on the transmembrane proteins, specifically the receptor-binding region.[104] Free energies of binding (ΔG) were calculated using the AMBER03 force field[105] with 3MLH as the receptor and the disinfectant compounds as the ligands. Clusters were determined by a cutoff of 2 Å as the root-mean square deviation of atomic positions. Global docking of the receptor in YASARA set the simulation cell automatically to extend beyond the geometric center of the receptor by 5 Å (x, y, z = 67.19, 55.34, 44.69 Å). Before docking, the receptor pdb file was edited to add hydrogens and remove solvent molecules.

Docking studies were conducted for hypochlorous acid (HOCl) and ClO_2, two chlorinated disinfectants. N-bromosuccinimide (NBS) was also modeled to analyze the effect of ligand size and type on ΔG. NBS is a significantly larger molecule than either ClO_2 or HOCl, and it has been shown to selectively oxidize tryptophan residues in proteins.[106,107] Ligand structures were imported from ChemSpyder into MarvinSketch, and the molecules were energy-minimized using the Merck Molecular Force Field provided by MarvinSketch 15.2.2.0 as a first step before more stringent minimization using AMBER03 in YASARA.[108]

Due to the unusual +4 oxidation state of chlorine in ClO_2, the ClO_2 molecule could not initially be modeled in YASARA. To enable this ligand to be modeled, a new topology file was created for YASARA to properly account for the +4-oxidation state and corresponding ClO_2 bond lengths and angles.

2.2.3 HA treatment with ClO_2 and digestion

Stock ClO_2 solution was diluted with 10 mM phosphate buffer (130 mM NaCl, pH 7.0). The reaction mixture was 95 μL and contained 26 μM ClO_2 and 173 mg/L HA protein of A/New Caledonia/20/99 strain in a chlorine demand-free glass vial. No quenching agent was used because $Na_2S_2O_3$ may partially reduce the oxidized proteins, as reported previously.[15] Instead, the reaction time was set for 6 hours to ensure that the ClO_2 was completely consumed. After ClO_2 treatment, the reaction mixture was washed with 50 mM Tris-HCl buffer at pH 8 and 37°C in a 100-kDa Amicon ultra-0.5 filter (Millipore), and digested with trypsin at 37°C overnight in accordance with a previously published protocol.[14]

2.2.4 Peptide analysis and identification

Digested HA peptides were subjected to liquid chromatography-tandem mass spectrometry (LC-MS/MS) to identify peptide degradation and oxidation reactions taking place on HA. Specifically, 20 μL of the HA peptides were separated with a reverse-phase column (Accucore aQ, 50 × 2.1 mm, 2.6 μm particle size, ThermoFisher Scientific), using mobile phase A (LC-MS grade water, 0.1% formic acid v/v) and mobile phase B (LC-MS grade methanol, 0.1% formic acid v/v) for peptide separation. The mobile phase gradient began at 6% B for 3 min, climbed linearly to 80% B over 30 min, maintained at 80% B for 5 min, and then equilibrated at 6% B for 5 min.

Eluted peptides from the column were directly sent to a QExactive Orbitrap high-resolution mass spectrometer (ThermoFisher Scientific). At the electrospray ionization source, the sheath gas flow rate was set as 24 AU, the spray voltage at 3 kV, and the auxiliary gas heater temperature at 275 °C. The full mass spectrum was scanned between 400-1800 m/z with an automatic gain control (AGC) target of 500,000 and mass resolution of 70,000.

For tandem MS scans, the top twenty most abundant peptides were selected and collided at 30 normalized collision energy (NCE), with the AGC target set at 200,000, mass resolution of 35,000, and isolation window of 1.6 Da. Raw MS and MS/MS data were analyzed using MASCOT Distiller (2.6.2.0) and searched against a customized database, including the HA sequence of the A/New Caledonia/20/99 strain, and human keratin contaminants. During the peptide searching, cysteine carbamidomethylation was set as a fixed modification and methionine oxidations as variable modifications. A 10 ppm mass tolerance for MS scans and a 0.3 Da mass tolerance for MS/MS scans yielded a false discovery rate of less than 1%.

2.2.5 Statistical analysis

One-way ANOVA and post-hoc Tukey's test for multiple comparisons were performed on docking clusters to assess the significance between cluster means. For one-way ANOVA and a P-value of less than 0.05, the null hypothesis, that ΔG means for each cluster were the same, was rejected. Rejection of the ANOVA null hypothesis preceded Tukey's test. The null hypothesis of Tukey's test was defined as any possible pairs of clusters having equivalent ΔG means and was rejected for a P-value less than 0.05. The analyses were completed in GraphPad Prism 8 for Windows.

2.3 **RESULTS**

2.3.1 Protein receptor-binding domain with ClO_2

Receptor-binding, the event at the onset of virus infection, is mediated by the HA protein in the influenza virus.[93,109,110] For H1 strains of influenza, two conserved amino acids in the HA protein, Asp 190 and Asp 225, are responsible for binding with human receptors.[94] Thus, damage to the amino acids in this region could lead to inactivation of H1N1. Experimental work has revealed that disinfectants oxidize residues in this region,[20] and so docking studies were conducted to determine if computational modeling identified the same HA regions as susceptible to oxidation.

As shown in Figure 2.1, nine distinct energetically favorable binding locations for ClO_2 were found from global docking analysis of the H1N1 HA receptor-binding domain (one-way ANOVA, P-value <0.0001). Statistical analyses were performed to test the variance in the means of ΔG between clusters. The null hypothesis was accepted at $P > 0.05$, which occurred between C1 and C2 (P-value 0.120), and C5 and C7 (P-value 0.934). Cluster member number was then assessed to distinguish between C1 and C2.

Although the top four clusters C1 through C4 had ΔG values within 2.5% of one another, cluster C1 contained four members, whereas clusters C2 through C4 contained two or fewer members. For binding locations with two or more members in the cluster, indistinct conformations were weighted to calculate an average ΔG. To qualify as distinct, the root-mean-square deviation of the atomic positions of two conformations had to be greater than 2 Å. The uncertainty in the reported ΔG is based on the standard deviations obtained from 500 separate docking calculations, with each docking run yielding one of the nine conformations shown in Figure 2.1. The ΔG values for the three- or four-membered clusters C1, C5, and C8 were obtained from averaging of the indistinct conformations for these clusters. The higher member number of cluster C1 suggests

varied conformations of the receptor and ligand can dock in this location, which increases the favorability of C1 compared to the other top clusters.

As noted in Table A-1 in Appendix A and Figure 1.1 footnote, the residues D190 and W153 were found in cluster C1 with the highest binding affinity (Figure 2.2). D190, which was found in every conforming member of the cluster, is known to play a critical role in H1N1 binding to human receptors.[94] As shown in Figure 2.1, the location of the C1 receptor-binding domain of ClO_2 was proximal to D225, which has also been shown to play an essential role in H1N1 binding to a host cell.[93,94]

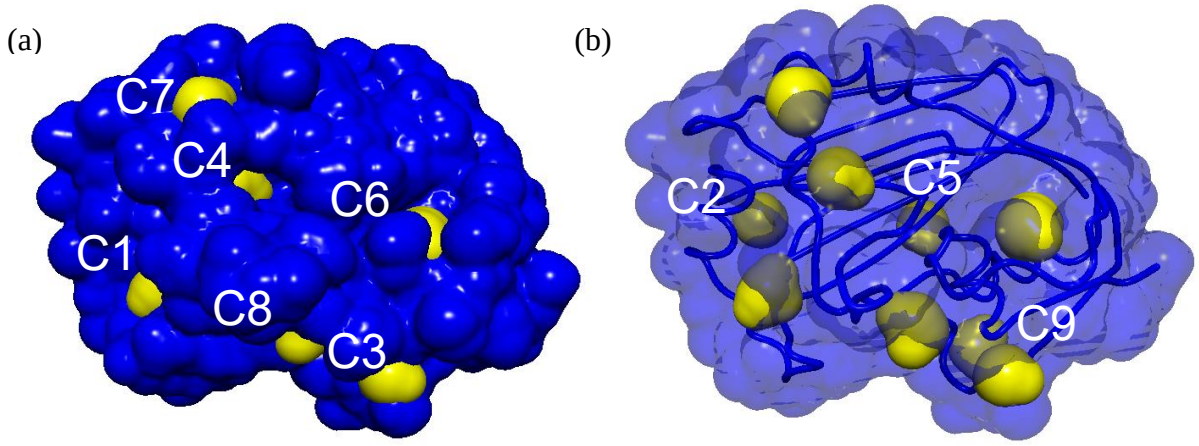

Cluster	C1*	C2	C3	C4	C5	C6	C7	C8	C9
Members	4	2	1	2	1	3	1	3	2
ΔG (kcal/mol)	-2.43 ± 0.04	-2.41	-2.40	-2.38	-2.30	-2.29 ±0.04	-2.29	-2.25 ± 0.03	-2.19
C1		0.120	—	—	—	—	—	—	—
C2			0.043	—	—	—	—	—	—
C3				—	—	—	—	—	—
C4					—	—	—	—	—
C5						0.700	0.934	—	—
C6							0.234	—	—
C7								—	—
C8									—

Figure 2.1 Solvent accessible surface of the H1N1 HA protein and nine docking conformations C1 through C9 for ClO2. The conformations are numbered in order of decreasing affinity between ClO2 and HA, and are listed as mean free energy of binding ± SD. The three docking locations obscured in the opaque protein structure (a) are visible in the transparent structure (b). P-values for the post-hoc Tukey's test are listed below the table. A P-value < 0.05 was considered significant. A dash indicates a P-value <0.0001. There was no statistical significance found between C1 and C2 (P-value 0.120) or C5 through C7 (P-value 0.934 for C5 versus C7). The footnote lists contacting residues for a given cluster.

* **C1** | Y98, W153, H183, S186, D190, L194, Q226, E227, G228
C2 | Q191, D199, A200, K214, P215, I217, N250
C3 | K63, T90, S90A, S91
C4 | S132, N133, K133A, G134, V135, F147, L151, I152, W153
C5 | I103, D104, Y209, Y233, W234
C6 | W69, E77, S78, T81
C7 | W127, H130, D131, S132, N133, K157
C8 | N73, E75, C97, C139, P140, R224
C9 | N65, I66, E89, S91, S92, D93, N94, Y105, R109

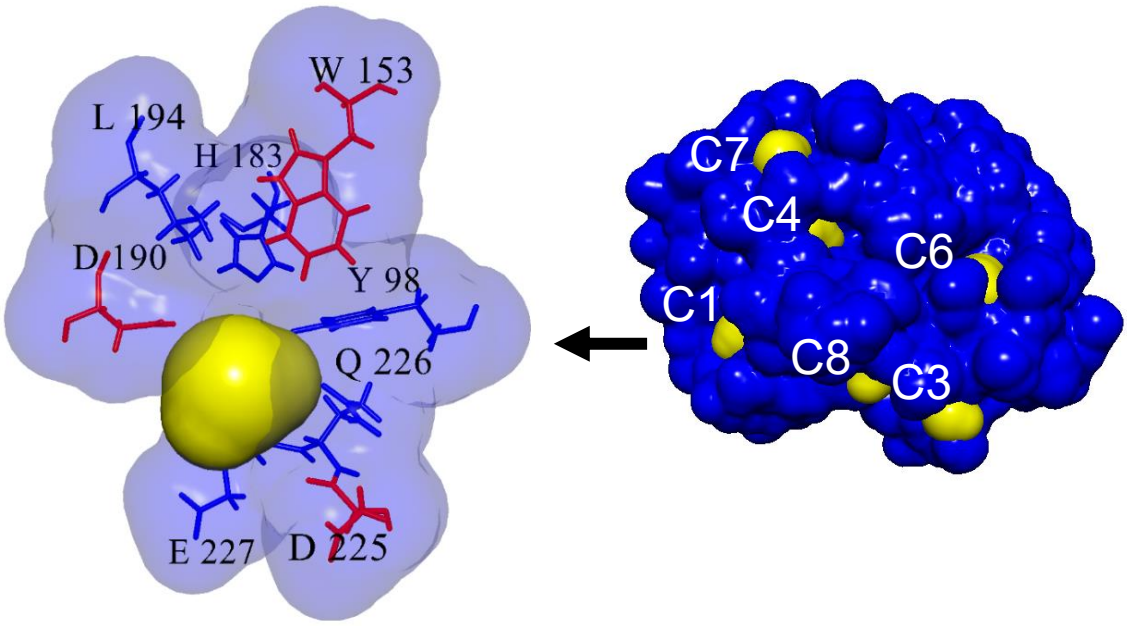

Figure 2.2 Receptor-binding domain of the docking conformation C1 with the highest ClO_2 binding affinity and cluster member number. Amino acids highlighted in red play a crucial role in H1N1 binding to host cells. The ClO_2 solvent-accessible surface area is visualized in yellow. HA protein contours are shown in transparent and opaque blue.

2.3.2 Protein receptor-binding domain with other molecules

Docking studies were also performed using *N*-bromosuccinimide (NBS) and hypochlorous acid (HOCl) in place of ClO_2 to assess the role of molecular size and disinfectant type on free energy of binding. NBS (Figure 2.3), containing eight more heavy atoms, is a larger molecule than ClO_2 and is known to oxidize tryptophan residues.[107,111] HOCl is a more commonly used disinfectant than ClO_2 and is less specific than ClO_2 in its oxidation of virus capsid proteins.[14] NBS was therefore expected to have a higher binding affinity and fewer binding sites than ClO_2 and to bind in the region of W153, whereas HOCl was expected to have similar ΔG values as ClO_2 but to form binding clusters in a greater number of locations. Larger molecules tend to have higher binding affinities as there is more area for ligand-receptor contact, if there are fewer than fifteen heavy atoms in the ligand.[112]

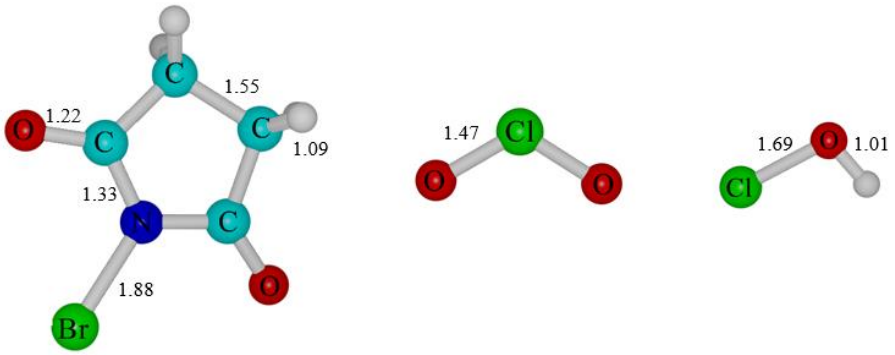

Figure 2.3 N-bromosuccinimide (NBS), chlorine dioxide (ClO2), and hypochlorous acid (HOCl) structures (reading left to right) used for computational modeling. Bond lengths, optimized in YASARA, are listed in Å.

Despite its chemical dissimilarities to ClO_2, NBS docked in the same region of the H1N1 receptor adjacent to W153, indicating the H1N1 HA protein might be more readily oxidized in this region. There were five binding locations for NBS on HA (Figure 2.4), which was fewer than that observed for ClO_2. This was expected, as NBS is larger than ClO_2, and it therefore has less capability to conform to the receptor surface. The NBS ΔG was also substantially more negative than the corresponding ClO_2 ΔG (P-value <0.001 for all NBS clusters compared to C1). NBS clusters N1 and N4 both contain W153 (Figure 2.4). Moreover, the N4 cluster is nearly identical in amino acid composition to the most strongly binding ClO_2 cluster C1 (Figure 2.2). Further statistical analysis showed the P-value for N1 versus N2 ΔG to be 0.047, and for N2 versus N5 P-value 0.556, indicating N1 to be significantly different from the other clusters.

HOCl had sixteen distinct binding locations, considerably more than either ClO_2 or NBS, and lower binding affinities (Table A-2). Two of the sixteen HOCl conformations, clusters H6 and H8, included W153. Only two HOCl clusters, H2 and H11, had more than one member. The most favorable ΔG for HOCl was -2.30 kcal/mol, which is more positive (i.e., less favorable) than the binding energies of the first five ClO_2 docking sites and all the NBS docking sites. Statistical

analysis of the HOCl clusters found there to be no significant difference between the means of the binding free energies of any of the clusters (one-way ANOVA P-value 0.199), supporting the hypothesis of a more randomized targeting of oxidation sites by HOCl in comparison to ClO_2 and NBS.

Given the comparable sizes of ClO_2 and HOCl, it was expected that their binding energies would be of similar magnitude, whereas the larger NBS was expected to have a correspondingly greater binding affinity. NBS, being larger has more surface area to bind with the receptor. The number of docking sites, and more positive ΔG for HOCl, suggest that this ligand (free chlorine) has a lower affinity for binding at a particular location on HA (i.e., that the binding is less specific). NBS had fewer docking clusters than ClO_2, which could also be explained by the difference in size. As a larger molecule, NBS is more conformationally limited in where it can bind compared to ClO_2.

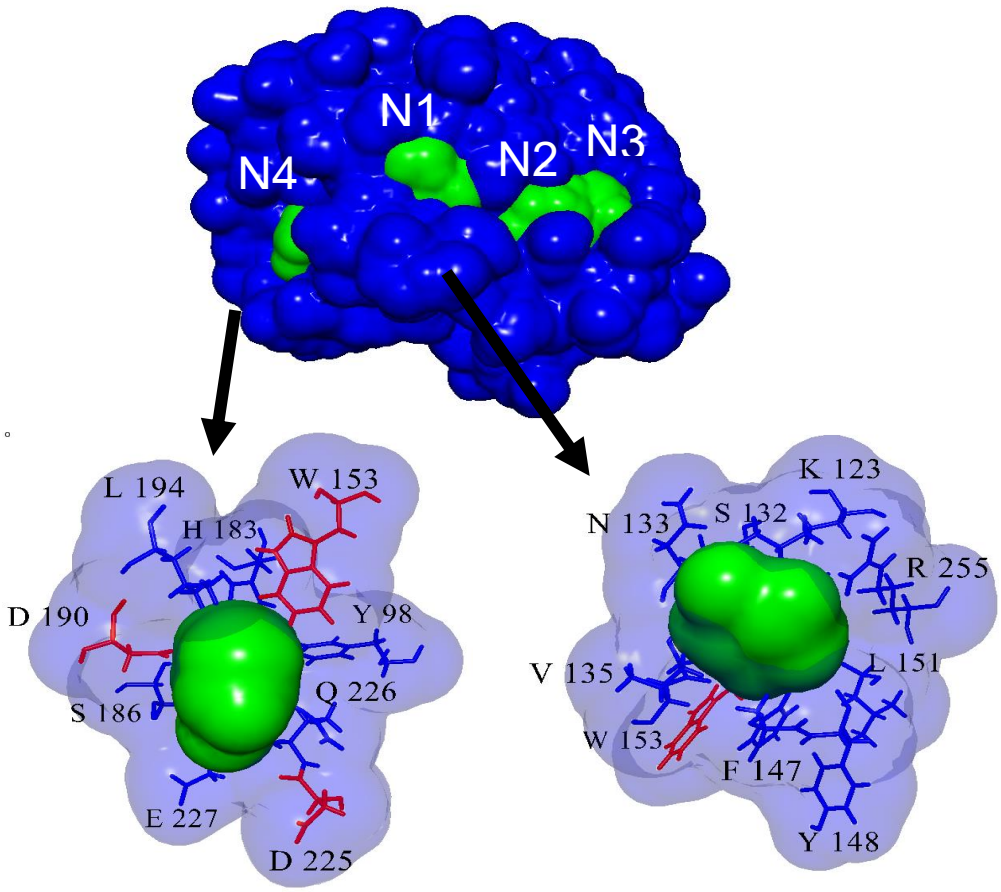

Cluster	N1†	N2	N3	N4	N5
Members	8	2	8	1	1
ΔG (kcal/mol)	-4.39 ± 0.23	-3.94 ± 0.06	-3.76 ± 0.13	-3.71	-3.58
N1		0.047	<0.0001	0.022	0.005
N2			0.757	0.858	0.556
N3				0.999	0.901
N4					0.989

Figure 2.4 Five docking conformations N1 through N5 for NBS and HA protein. The conformations are numbered in order of decreasing affinity between NBS and ClO_2, and are listed as mean free energy of binding ± SD. The fifth cluster, N5, on the backside of this image is not pictured. Amino acids key in H1N1 binding with host cells highlighted in red. Solvent accessible surface area of NBS in green. H1N1 protein solvent accessible surface area in opaque and translucent blue. P-values for the post-hoc Tukey's test are listed below the table. N1 was statistically different from all the clusters (P-value 0.047 for N1 versus N2), but N2-N5 were not statistically significant (P-value 0.556 for N2 versus N5). The footnote lists contacting residues for a given cluster.

† **N1** | K123, S132, N133, G134, V135, F147, Y148, K149, L151, I152, W153, R255
N2 | L59, W69, E77, S78, A82, S83, F116B, R117, F258
N3 | G68, W69, I70, G72, N73, P74, C76, E77, S78, T81, A82, F116B, R117, K149, N150, F258
N4 | Y98, W153, H183, S186, D190, L194, Q226, E227, G228
N5 | S126, W127, P128, N129, H130, L164, S165, K166

2.3.3 Mass Spectrometry

Oxidation of the H1N1 HA protein was examined by Orbitrap MS. After undergoing trypsin digestion, ClO_2-treated protein fragments were analyzed using LC-MS/MS. A total of 261 amino acids were recovered, comprising 46.3% of the HA sequence (Table A-3). The W153-containing fragment NLLWLLGK was found in both unmodified and modified forms. The change in mass can be explained by the addition of two oxygen atoms from protein oxidation by ClO_2. The MS/MS fragmentation spectra of the modified amino acid sequence (Figure A-1) further indicates that the tryptophan residue in the peptide NLLWLLGK was oxidized by ClO_2, with W153 in the oxidized peptide confirmed to be 31.990 mass units heavier than tryptophan in the unmodified peptide, consistent with the formation of *N*-formylkynurenine as an oxidation product (Figure 2.5), as reported previously.[20,100] Four additional protein modifications were detected in the MS experiments. They are listed in Table 1.1 and are addressed further in the discussion below

2.4 **DISCUSSION**

2.4.1 HA conserved region

During the initial stages of infection, the receptor-binding area allows transmission of the virus into the host cells. In the influenza virus, the HA protein mediates binding to the sialic acid receptor.[99] The membrane-distal end of the HA protein contains the receptor-binding regions.[113] At the base of the region are four conserved residues: Y98, W153, H183, and Y195.[99]

In this study, only the receptor-binding region was considered in the computational docking models. The full HA protein was analyzed in the experimental MS work. To confirm the results of Ogata, 2012,[20] the same strain of H1N1 was used in the Orbitrap mass spectrometry, A/New Caledonia/20/99 (H1N1). To choose the virus strain for the computational models, the resolution

of the crystal structure was given priority over exact matching of the strain. At the time of this study, the A/Mexico/4603/2009 (H1N1) strain receptor-binding region crystallography had the highest resolution, 2.09Å. W153 is conserved in both these strains and in nearly all subtypes of the influenza virus (Table A-4).[20]

2.4.2 Applying computational docking to virus inactivation

Docking calculations performed in this study suggest that computational work could be used in conjunction with experimental work to predict protein oxidation during disinfection thereby providing further insights into inactivation mechanisms. Molecular docking tools have been used to assess influenza A virus HA affinity for various sialic acid receptors.[114] Docking has also been used in conjunction with molecular dynamics to inspect the hydrogen bonding between H1N1 neuraminidase residues and inhibitors.[115] In these studies, computation docking focused on the infection cycle of influenza rather than the role of disinfectants in inactivation. Other computational methods, including QM/MM models, have been used to confirm reaction intermediates for UV irradiation protein damage.[16] Computational docking methods have looked at the binding of disinfection byproducts to estrogen receptors in humans.[116] This study suggests docking could be used to improve understanding of disinfectant-virus interactions.

Previous experimental work showed ClO_2 oxidizes W153 on the H1N1 binding protein.[20] It is likely that W153 is modified to *N*-formylkynurenine by the addition of two oxygen atoms (Figure 2.5).[100] From MALDI-TOF MS, it was suggested ClO_2 oxidizes W153 to *N*-formylkynurenine (NFK).[20,100] Experimental work using the Orbitrap MS also found W153 to be oxidized to NFK.

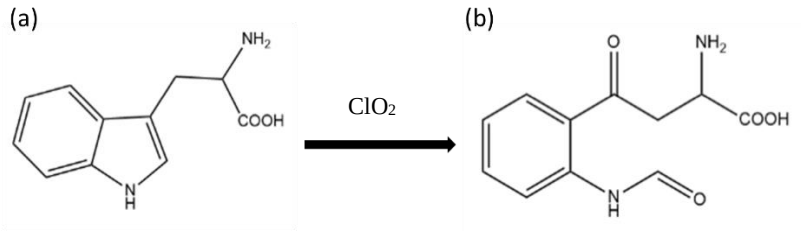

Figure 2.5 Tryptophan oxidation to N-formylkynurenine.

More interestingly, computational docking determined the region around W153 between D190 and D225 as the most energetically favorable binding location for ClO_2. This region had both the lowest free energy of binding and the highest member number, suggesting ClO_2 can bind to this location in more than one conformation. This region has also been cited as crucial in virus binding ability to a host cell due to the two aspartic acid residues 190 and 225.[93] Damage to the amino acids in this region could therefore impede the ability of the virus to bind to host cells, thus causing functional inactivation. Computational and experimental results both indicated the W153 residue in this region is susceptible to oxidation by ClO_2.

Computations were based only on the receptor-binding region of the HA protein in the H1N1 virus, whereas MS analysis was applied to the entire HA protein. Five protein modifications were identified from the MS analysis and were not found in the untreated protein (Table 2.1). Two of the five modified fragments that lie outside of the receptor-binding domain were noted, but these were considered unrelated to virus inactivation via HA oxidation, as they are not involved in the binding with the sialic acid residues in human receptors.[93] After receptor binding, membrane fusion occurs between the cell and virus, which is mediated by HA.[117] As binding precedes fusion, however, the receptor-binding domain was considered the focus of this study. The other fragments comprise tyrosine and tryptophan oxidation products, neither of which have been proposed as ClO_2 binding sites. Fragment 3 contains two tryptophan residues, but only had a mass shift of one

oxygen. This could be due to the tryptophan's location on the HA protein. W234 and W255 are both further embedded in the protein and their pyrrole ring structures could be less accessible for oxidation. Instead an oxygen atom is imparted onto the more accessible benzene ring during oxidation, forming hydroxy-tryptophan. Oxidations of the Table 1.1 fragments also appear in the docking calculations, specifically in C6 (Figure A-2), but because the MS fragments are much larger, it is difficult to associate them with only one binding cluster and a corresponding single oxidized residue.

Table 2.1 HA protein modifications found in MS results. The first three fragments are within the receptor-binding region that was also the focus of the computational modeling.

Fragment	Residue oxidized	Mass shift	Proposed modification
NLLWLTGK	W	+31.990	*N*-formylkynurenine[100,111,118]
ALYHTENAYVSVVSSHYSR	Y	+15.995	3,4-dihydroxyphenylalanine[17,118]
INYYWTLLEPGDTIIFEANGNL IAPWYAFALSR	W	+15.995	Hydroxy-tryptophan[17]
KVDDGFLDIWTYNAELLVLLE	Y	+15.995	3,4-dihydroxyphenylalanine[17,118]
NER	W	+31.990	*N*-formylkynurenine[100,111,118]
MNTQFTAVGK	M	+15.995	Methionine sulfoxides[17,118]

Docking results using the alternative ligands NBS and HOCl provided additional insight into virus inactivation. Despite clear differences in size, NBS and ClO_2 both appear to have an affinity for W153 according to the computational results. NBS has been shown to preferentially oxidize tryptophan residues,[111,119] and docking results corroborate this affinity. In contrast, HOCl has been shown to be more indiscriminate during inactivation, attacking many regions of the capsid and viral genetic material.[14] Computational docking again confirms these experimental observations, as the docking calculations reveal more potential binding sites for HOCl than for ClO_2.

Given the large quantities of data generated by mass spectrometry, computational docking can provide a means of winnowing MS datasets to find viral sites susceptible to oxidation or insights into the specificity of oxidation for a disinfectant. For unculturable or difficult-to-culture viruses in particular, docking calculations can be a crucial asset to determine the mechanisms of inactivation. Computational docking methods can also prospectively be used to predict the effects of virus mutations on their susceptibility to inactivation. Further work is needed to assess the transferability of this method to other disinfectants and viruses. This could include alternative disinfectants such as ozone, or capsid proteins in nonenveloped viruses.

Chapter 3. Lead Minerals Found in Drinking Water Distribution Systems Increase Chlorine Dioxide Decay to a Single Inorganic Byproduct

3.1 INTRODUCTION

Historically, the most commonly used disinfectant for drinking water treatment has been free chlorine due to its low cost.[5] Application of free chlorine however can exacerbate infrastructure corrosion[37] and induce the formation of toxic disinfection byproducts (DBPs).[5] The DBPs formed from the reactions of free chlorine with natural organic matter are strictly regulated by the United States Environmental Protection Agency (EPA) as they are nearly all carcinogenic and can damage essential bodily organs and functions.[120] Removal of DBPs and their organic precursors by the addition of chloride containing coagulants can also intensify the corrosion of infrastructure in water supply networks.[35,121] When selecting a disinfect for water treatment in a distribution system, the potential complications arising from corrosion scale and DBP formation must both be taken into consideration.

Water utilities now have recourse to consider disinfectants other than free chlorine to satisfy DBP regulation requirements.[6] Chlorine dioxide is comparable in power to free chlorine as an oxidant yet forms almost no organic DBPs. Moreover, unlike free chlorine, the disinfecting power of chlorine dioxide is insensitive to the pH of the treated water.[12,65] On account of these favorable attributes, utilities have used chlorine dioxide as a primary or secondary disinfectant in both Europe[12] and in the United States.[64] Chlorine dioxide can, however, undergo oxidation or reduction reactions to form the inorganic DBPs chlorite and chlorate, respectively. The EPA

regulates chlorite with a maximum contaminant level (MCL) of 1.0 mg L^{-1} and chlorine dioxide with a maximum residual disinfectant level (MRDL) of 0.8 mg L^{-1}. Although the World Health Organization recommends chlorate levels be limited to 0.7 mg L^{-1}, the EPA has no current MCLs for chlorate. In a typical drinking water disinfection system, 70% of the chlorine dioxide added is converted to chlorite and the rest (30%) forms chlorate, so if the proper concentration of chlorine dioxide is maintained, EPA regulations will be met.[41,74] Removal of chlorite in excess of the MCL can be accomplished as needed by the addition of sulfate or ferrous ions or by adsorption on granular activated carbon.[71]

Chlorine dioxide thus has the advantage of producing little if any organic DBPs regulated by the EPA, and its two primary inorganic byproducts can be removed post-disinfection. However, the disinfecting power of chlorine dioxide and the DBPs it forms can be altered by the presence of metals in and the mineral scales that form upon copper, nickel, and iron pipes and pipe connections of water supply infrastructure,[51] but this has not yet been investigate in lead-based systems. The type and extent of scale formation is strongly affected by pH, and hence treatment plants often adjust pH to control corrosion.[56] While the scale formed is itself not necessarily toxic, its dissolution can increase the concentrations of toxic metals in public drinking water.[58,122] Dissolution may be caused by switching between disinfectants, the misuse or neglect of passivating phosphate addition, or the addition of chemicals for mitigation of DBPs, which were all causes of the water crises that occurred in Flint, Michigan, beginning in 2014, and Washington DC, in 2001.[37,45,47,48]

For the research presented herein, the lead and copper minerals most commonly occurring in water supply systems were considered. Material characterization of lead supply lines where free chlorine was used as a disinfectant revealed lead oxide as the principal scale mineral.[53,59] Chlorine

dioxide has an oxidation-reduction potential equal to or greater than that of free chlorine; thus, its use as a disinfectant is likely to produce as similar lead oxide scale, but there are few studies that directly investigate lead-based scale formation in the presence of chlorine dioxide. Lead carbonate was also considered in this study as a scale mineral that is likely to form at lower pH regimes.[55,57] For a copper supply system, cupric oxide is the most prevalent scale mineral at free chlorine oxidation-reduction potentials.[51]

Previous work has shown that copper, nickel, and iron corrosion minerals react with chlorine dioxide to produce chlorate and chlorite.[51] In basic solutions absent of minerals, metallic or otherwise, chlorine dioxide decays along three possible pathways to form either chlorite or a combination of chlorite and chlorate.[123] Reaction rates and mechanisms chlorine dioxide interactions with lead corrosion minerals have not been reported. The goals of this study were therefore to compare chlorine dioxide decay and byproduct formation in the presence of different lead and copper corrosion scale minerals, and to investigate the effects of pH on these reactions. The data uncovered from these aims will help the design of lead-based water treatment distribution systems, by providing insight into the affect corrosion minerals have on disinfection kinetics and the type of byproducts they produce. This will aid water utilities in maintaining a disinfectant residual and mitigating byproduct production depending on the metallic composition of their distribution pipes.

3.2 MATERIALS AND METHODS

3.2.1 Standards and reagents

Reagent-grade scale minerals and buffer compounds were purchased from Fisher Scientific Company, Acros Organics, and Sigma Aldrich.

Chlorine dioxide stock solution was prepared by mixing aqueous solutions of potassium peroxodisulfate ($K_2S_2O_8$) and sodium chlorite ($NaClO_2$).[51] All solutions were prepared in deionized water (18.2 MΩ cm, Milli-Q). The stock solution was stored between 1 and 5°C in the dark. During production, the gaseous chlorine dioxide was dissolved into deionized water via a stream of nitrogen gas. The stream was passed through a sodium chlorite scrubber to remove impurities including chlorine. As it is non-volatile, limited amounts of chlorite could have entered the final stock solution.

3.2.2 Batch reaction setup

The effects of scale mineral type, initial chlorine dioxide concentration, pH, and the presence of phosphate or carbonate on the rate of chlorine dioxide decay and byproduct formation were investigated. Batch experiments were conducted in 4.5 L flasks, as shown in Figure B-1 illustration. Chlorine dioxide was diluted to a concentration between 29 and 94 μM (2.0 and 6.3 mg L^{-1}), and 2.5 mM tetraborate buffer with nitric acid was used to adjust the pH to 8.3. For all experiments in which the pH was varied, either nitric acid or sodium hydroxide was added to adjust pH to between 6.0 and 10.6.

The mineral concentrations were normalized based on their BET surface area measurements (Table B-1) to yield a mineral surface area per unit solution volume of 3.6 m^2/L for cupric oxide (initial CuO concentration of 0.96 g/L) and or 1.8 m^2/L for lead oxide and lead carbonate (initial concentrations of 3.4 and 2.2 g/L respectively). The surface areas for the lead compounds were halved to slow the chlorine dioxide decay reaction to a measurable rate. Otherwise, chlorine dioxide concentrations in the batch reactors were depleted within minutes of the reaction onset.

Reactions were initiated by addition of either cupric oxide, lead oxide, or lead carbonate. For batch experiments investigating the effect of anion concentration, 1 mM of phosphate or 63 mM of carbonate salts was added prior to introduction of the mineral. During the experimental measurements, the reactor was kept in the dark and continuously mixed by a stir plate at 350 rpm. Samples were withdrawn with a syringe and then filtered through a 0.22 μm syringe filter, which was pretreated with chlorine dioxide solution. The filtered solution was analyzed for chlorine dioxide and the remaining sample was purged with nitrogen gas for at least 10 minutes to remove any residual chlorine dioxide.

Batch experiments were carried out using powdered minerals that have higher active surface areas than the corrosion scale on actual water supply lines. This work, nonetheless, enables measurements of intrinsic rate constants for chlorine dioxide decay and byproduct formation in the presence of these minerals.

3.2.3 Analytical methods

Chlorine dioxide concentrations were determined using spectrophotometrically (ε_{359nm} = 1230 M^{-1} cm^{-1}).[101] 4 mL aliquots from the filtered batch reactor sample were placed in a quartz cuvette and analyzed in triplicate. Chlorite, chlorate, and chloride concentrations were all quantified using a Dionex ion chromatograph with an AS9 column and Na_2CO_3 eluent. Three injection volume samples of 25 μL each were taken from 1.8 mL aliquots of nitrogen purged batch reaction samples. Five standards for chlorite, chlorate, and chloride were used at 1.0, 1.5, 2.0, 4.0, and 8.0 mg/L. The detection limit was found to be 0.5 mg/L. X-ray powder diffraction analysis was done with a Rigaku Ultima IV with Cu Kα radiations and analyzed using ReX 0.8.3 software. Samples that were exposed to chlorine dioxide solution were oven-dried to recover the mineral

powder. BET surface area measurements were obtained in liquid nitrogen at 77 K using Micromeritcs ASAP 2050 gas adsorption analyzer. Particle size measurements were done using a Malvern Zetasizer.

3.3 RESULTS AND DISCUSSION

3.3.1 Effect of initial chlorine dioxide concentration on chlorine dioxide decay

Figure 3.1 shows chlorine dioxide decay and the formation of chlorite in the presence of lead oxide for initial chlorine dioxide concentrations ranging from 30 to 90 μM. Chlorine dioxide decay was accelerated regardless of initial chlorine dioxide concentration. Previous studies of chlorine dioxide decay in the presence of cupric oxide showed the initial concentration of chlorine dioxide influenced the concentration ratio of chlorite and chlorate formed during the reaction.[51] At high initial chlorine dioxide concentrations, the ratio was closest to 50:50, and the amount of chlorite produced increased as initial concentration decreased.[51] For the lead oxide and carbonate minerals, chlorite is produced as the sole decay product, regardless of initial chlorine dioxide concentration. At an initial concentration of 28.9 μM, decay was so rapid that no amount of chlorine dioxide was measurable one minute after the lead oxide was added to the batch reactor. At 48.6, 62.7, and 93.5 μM, pseudo-second order rate constants for chlorine dioxide decay are 290.4±0.1, 253.6±0.4, and 87.0±0.3 M^{-1} s^{-1} (R^2 values 0.999, 0.986, and 0.991) respectively. Rate constants and models are discussed further in Appendix B and were based on the adsorption limited pseudo-second order rate model.[124]

The accelerated decay of chlorine dioxide at lower concentrations presents a potential challenge for its used as a disinfectant. A concentration of 30 μM is equivalent to 2.0 mg/L which is well over the 0.8 mg/L MRDL standard set by the EPA. Also of concern, the complete chlorine

dioxide decomposition in the presence of lead oxide yields chlorite at a molar concentration essentially equal to that of the initial chlorine dioxide concentration. To implement chlorine dioxide disinfection in a lead-based distribution system, treatment plants might therefore need a mechanism for chlorite removal to achieve compliance with the chlorine MCL and a high enough initial concentration of chlorine dioxide to maintain a suitable residual. Chlorite removal processes have been implemented in previous systems employing chlorine dioxide disinfection.[71] Alternatively, corrosion control compounds, such as orthophosphate, can be added to the system to slow the rate of decay of chlorine dioxide.[49]

Chlorate was absent from all the byproduct analyses of chlorine dioxide reactions with lead oxide, even at high initial chlorine dioxide concentrations. Previous studies of chlorine dioxide decay kinetics on cupric oxide have shown, at lower initial chlorine dioxide concentrations, chlorite is the favored byproduct.[51,123] Reaction on lead oxide produces only chlorite as a decay product regardless of initial chlorine dioxide concentration. The chlorine balance in Figure 3.1 confirms that the chlorite concentration in the batch reactor closely matches the amount of chlorine dioxide consumed. The mechanisms of chlorine dioxide decay in the presence of copper as opposed to lead corrosion scale minerals must therefore differ.

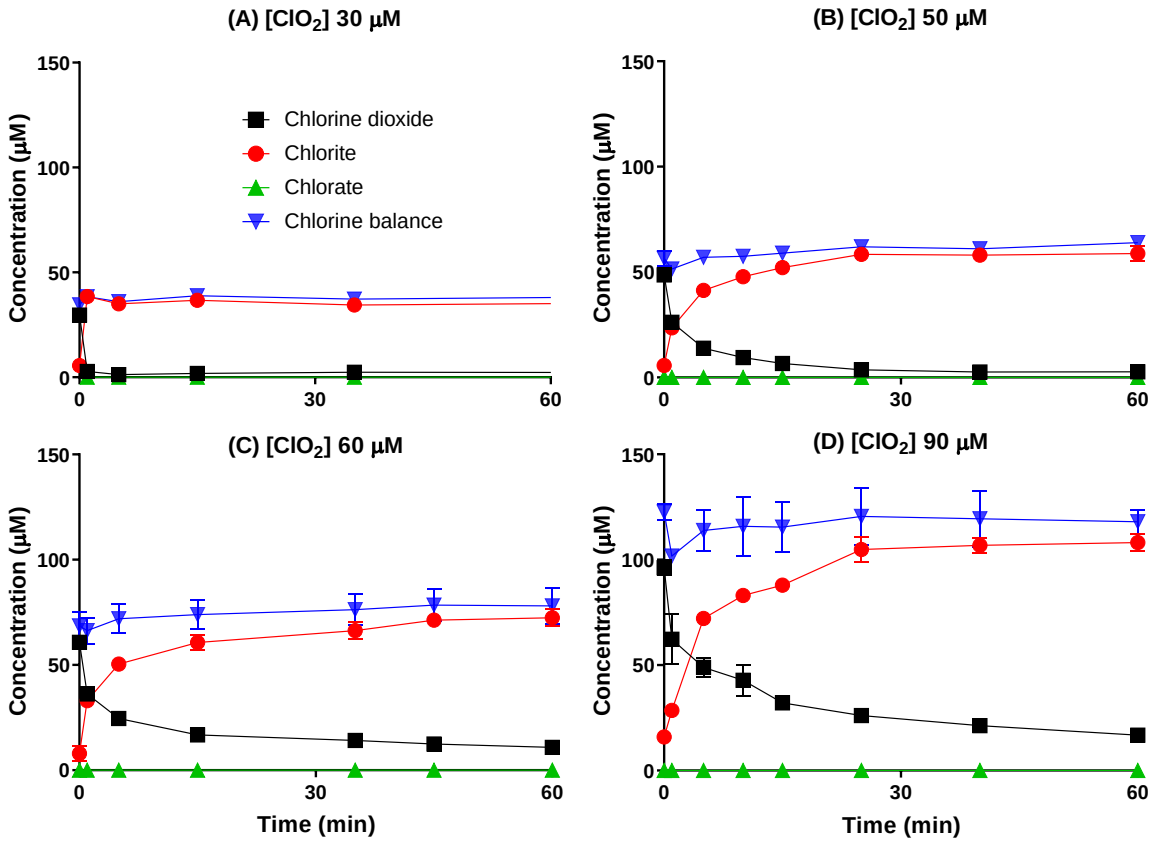

Figure 3.1 Chlorine dioxide decay, chlorite formation, chlorate formation, and chlorine balance equal to the sum of chlorine dioxide, chlorite, and chlorate in batch reactions containing different initial chlorine dioxide concentrations and lead oxide. Each data point represents the mean and standard deviation of duplicate experiments. If error bars were shorter than the symbol, they were removed.

3.3.2 Corrosion and Mineral Type

Figure 3.2 shows chlorine dioxide decay in the presence of the corrosion scale minerals lead oxide, lead carbonate, and cupric oxide. When compared against the "blank" reaction, containing only chlorine dioxide in solution, the scale-forming minerals are clearly observed to accelerate the decay of chlorine dioxide. The 5% chlorine dioxide loss over 4 hours in the batch reactor with no mineral present, can be attributed to volatilization when the reactor lid was removed. The reactor top was removed and exposed to the air to take samples at specific time

intervals but was otherwise kept closed to the atmosphere. In contrast to the blank, addition of lead oxide, lead carbonate, and cupric oxide to the batch reactor resulted in markedly faster chlorine dioxide decay causing 95%, 100%, and 42% loss of chlorine dioxide respectively after 1 hour.

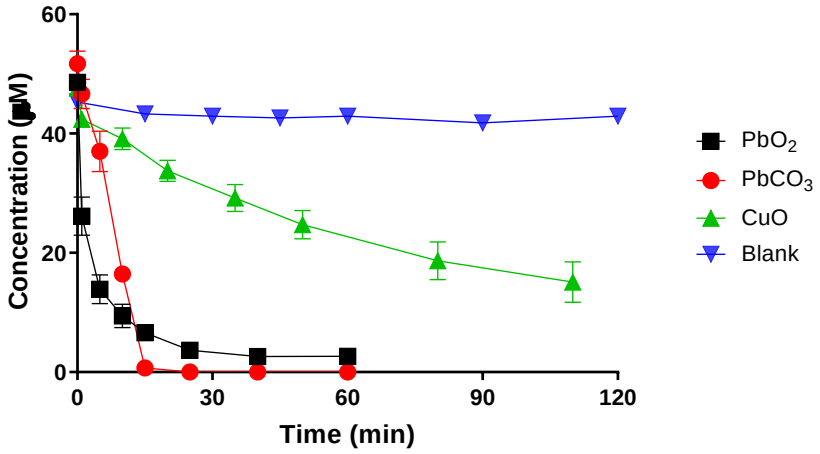

Figure 3.2 Chlorine dioxide decay in batch reactions containing chlorine dioxide and three different corrosion scale minerals: lead oxide, lead carbonate, and cupric oxide. Each data point represents the mean and standard deviation of duplicate experiments. If error bars were shorter than the symbol, they were removed.

For the lead minerals, the decay rates of chlorine dioxide followed an adsorption based pseudo-second order model,[124] with rate constants equal to 290.4±0.1 and 42.1±0.6 M s^{-1} (R^2 values of 0.998 and 0.947) for lead oxide and lead carbonate, respectively. The loss to volatilization in the batch reaction with no added mineral, labeled Blank, when fit to a second order model had a rate constant of 0.06±0.04 M s^{-1}. The cupric oxide-catalyzed chlorine dioxide decay data was fit to a second-order kinetics model with a rate constant of 6.4±0.5 M s^{-1} (R^2 value 0.967), in agreement with previously reported results.[51] The rates of chlorine dioxide decomposition on lead minerals are pointedly higher (more than 40 and 5 times faster on lead oxide and lead

carbonate, respectively) than the copper compound. Addition information on the rate models and equations used can be found in Appendix B.

Even more intriguing, the lead mineral reactions produce only chlorite as a byproduct of chlorine dioxide decay (Figure 3.3), unlike cupric oxide which produces both chlorite and chlorate. The production of chlorite is more rapid for the lead minerals, and the initial chlorine dioxide concentration is converted to chlorite byproduct. Cupric oxide produces both chlorite and chlorate in comparable amounts. At 110 minutes, chlorite and chlorate levels are 17.5 and 15.4 μM, while the loss of chlorine dioxide is 32.5 μM. Previous studies have hypothesized the production of chlorite and chlorate comes from a disproportionation reaction using the two byproducts (Equation 1).[51]

$$2ClO_2 + 2H_2O \xrightarrow{\text{Mineral}} ClO_2^- + ClO_3^- + 2H^+ \quad (1)$$

In the case of the lead minerals the disproportionation is clearly disfavored due to the absence of chlorate in byproduct analysis. The electrons must then be supplied by water (Equation 2), which is favorable in basic systems due to the high oxidation-reduction potential of chlorine dioxide.[52,55] The oxidation of water was further confirmed by the drop in pH of an buffered chlorine dioxide decay reaction in Milli-Q water (see Appendix B for calculation and Figure B-2).

$$4ClO_2 + 4OH^- \xrightarrow{\text{Mineral}} 4ClO_2^- + O_2 + 2H_2O \quad (2)$$

It has also been noted that chlorite can be the sole byproduct of first-order decay reactions in basic solutions.[123] At low initial concentrations of chlorine dioxide, it has been shown that alternative pathways to disproportionation can lead to higher levels of chlorite.[51] In the presence

of lead minerals, however, the reaction appears to be pseudo-second order and at any initial concentration of chlorine dioxide, only chlorite is produced (Figure 3.1).

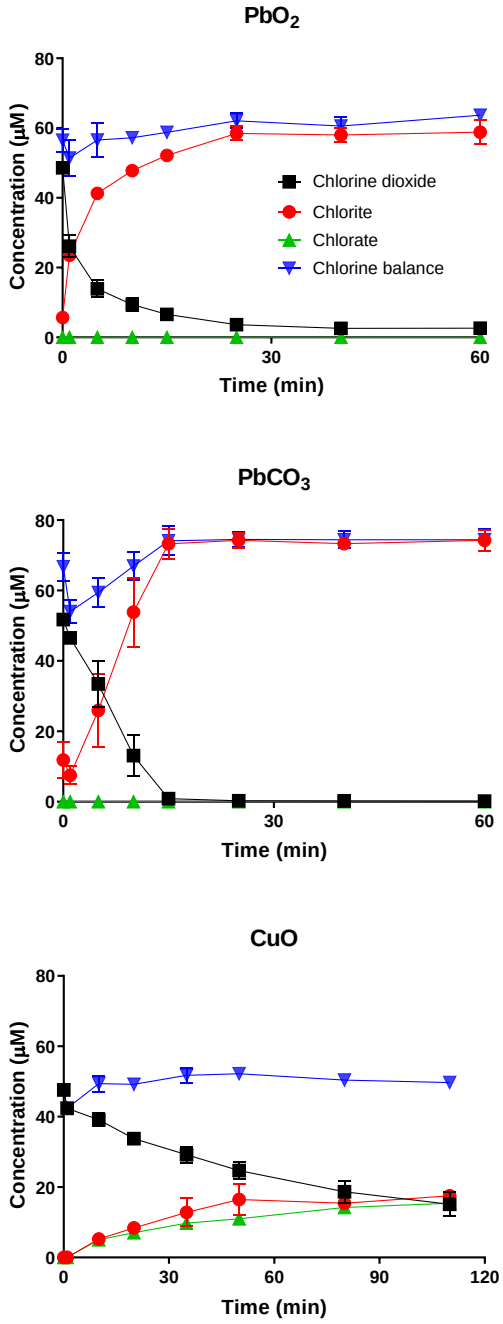

Figure 3.3 Chlorine dioxide decay, chlorite formation, chlorate formation, and chlorine balance for three separate batch reactions containing chlorine dioxide and different corrosion scale minerals: (A) lead oxide, (B) lead carbonate, and (C) cupric oxide. Each data point represents the mean and standard deviation of duplicate experiments. If error bars were shorter than the symbol, they were removed.

In lead carbonate reactions, the electron transfer could come from the mineral itself. The lead (II) carbonate mineral is oxidized to lead (IV) oxide. This reaction has been shown to occur in systems with high oxidation-reduction potential, i.e. systems disinfecting with free chlorine or chlorine dioxide.[53,56,125,126] The mineral also changes in color from white to pink during the course of the reaction, which could indicate lead carbonate being partially oxidized to lead (II, IV) oxide, which is distinctly red in color, unlike lead (IV) oxide which is black (Figure B-3). The variability in the lead carbonate reactions is higher, possibly due to the nonuniform oxidation of the surface to lead oxide. Partial oxidation could lead to faster rates on some surface locations, increasing the variability of the overall reaction. The oxidation mechanism and change in composition of lead carbonate could account for the increasing chlorine dioxide rate of decay and higher variability between batch reactions.

Chlorine dioxide rates of decay and chlorite rates of formation are higher in the presence of lead minerals compared to copper minerals. Chlorite and chlorate are both byproducts of the cupric oxide reaction, whereas chlorite is the only byproduct of both lead minerals, suggesting different mechanisms are occurring.

3.3.3 Notes on the Chlorine Balance

The actual chlorine balanced varied in the batch reactions due to initial chlorite concentrations that could not be controlled for and ranged from 0 to 9 µM. Most notably in the lead carbonate reaction, which had an initial chlorite concentration in one duplicate reaction and can be seen in the standard deviation of the time zero minutes. The initial starting concentration of chlorine dioxide was measured and adjusted to a target of 50 µM. While the initial starting point

for total chlorine in the system is not uniform, the chlorine balance is closed. Chloride was also measured during the batch reactions, but concentrations remained inert in all cases.

Initial chlorite concentrations in the batch reaction could be due to chlorite concentrations in the stock solution. While a scrubber solution is used to remove as much chlorite as possible during the generation of chlorine dioxide, there may still be some chlorite residual left in solution. Chlorite can also form in the batch reactor prior to the addition of mineral while the chlorine dioxide concentration is being calibrated. Although without a mineral catalyst, chlorine dioxide decay is relatively slow (Figure 3.2, Blank). The variation in the chlorine balance could also be due to inadequate sparging of chlorine dioxide before ion chromatography samples were taken. Sparging with nitrogen gas was performed for 10 minutes, but trace amounts of chlorine dioxide in the samples could form chlorite while waiting for analysis. Other sources of experimental errors were evaluated, including chlorine dioxide loss during filtration and chlorite formation while samples waited to be sparged. Chloride concentrations in all reactions were insignificant, and the chlorine balance accounts for most of the chlorine atoms in the system.

A second consideration is the abrupt drop in the chlorine balance when the mineral is added to the batch reactor, more notably in the lead than copper mineral reactions. This could be due to a reaction or complexation with the mineral that is unaccounted for due to the speed of the reaction. Notably, the drop chlorine balance does not occur during the reactions with copper mineral. The kinetics of the cupric oxide reaction are significantly slower, more than forty times below those of the lead oxide reaction. During the slower reaction, there may be fewer surface complexes forming.

Previous studies show surface adsorption binding energy correlates to valence of the adsorbate and coordination number at the adsorption site.[127,128] Complexation on the lead versus copper mineral surface could vary due to the different electronic d-orbital configurations.[128]

Copper has one electron in its valence shell, while lead has four. In the oxide form, copper is coordinated with four oxygens and lead is coordinated with six. Chlorine dioxide could complex more strongly with copper than lead, resulting in the retention of chlorine on the metal surface and slower reactions times.

3.3.4 Influence of pH

The effect of pH on chlorine dioxide decay and byproduct formation was explored from 5.9 to 10.6 and results are summarized in Figure 3.3. Drinking water pH is commonly between 6.5 and 8.5, but utilities sometimes increase pH above this range to prevent corrosion. The pH increments were chosen to be above and below the zero point pH of lead oxide with lies around 8.3[129] and previously published data on cupric oxide studies.[51] There was some variation at pH 5.9 (0.5) and pH 7.4, but at or above pH 8.3 and above there was minimal change (less than 0.03; Figure B-4). A tetraborate buffer with the addition of either nitric acid or sodium hydroxide was chosen to have minimal impact on reaction kinetics.

Cupric oxide-catalyzed reactions show a clear trend of increasing decay rates and chlorite formation as pH increases (Figure B-5). This is supported by previous work proposing the dependence of the cupric oxide-catalyzed reaction on hydroxide.[51] Second order rate constants 2.6±0.4, 6.4±0.5, and 71.9±5.7 M^{-1} s^{-1} were observed for pH 6.9, 8.3, and 10.4 respectively. Lead oxide reactions followed the same trend with rates increasing as pH increased from 5.9 to 8.3. However, above a pH of 8.3, the rate of chlorine dioxide decay decreased (Table 3.1).

Table 3.1. Pseudo-second order rate constants listed in increasing order at their corresponding pH values.

pH	Rate Constant (M^{-1} s^{-1})
10.6	87.8±0.7
9.7	156.0±0.9
7.4	166.3±0.4
5.9	267.6±0.7
8.3	290.4±0.1

As chlorite is the sole decay product formed due to the decay of chlorine dioxide in the presence of lead oxide, disproportionation cannot be occurring. Since chlorine dioxide and lead oxide are already in their most oxidized forms, water must supply the electron for chlorine dioxide reduction to chlorite, as previously discussed. Instead, surface interactions must be considered to provide a possible explanation of rate variations in the lead oxide reactions.

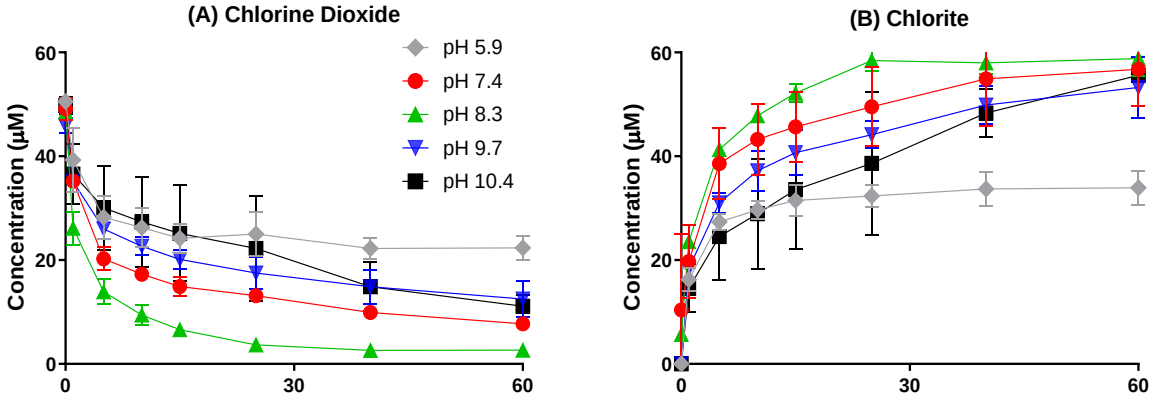

Figure 3.4 Chlorine dioxide decay and chlorite formation in batch reactions at different pH and in the presence of lead oxide. Each data point represents the mean and standard deviation of duplicate experiments. If error bars were shorter than the symbol, they were removed.

3.3.5 Influence of surface interactions

It seems likely adsorption on the surface of lead oxide is occurring. Phosphates are routinely added to drinking water to prevent corrosion by adsorbing to the surface of lead pipes.[60,130] Free chlorine has been shown to adsorb to the surface of lead oxide.[130] The adsorption can enhance the reactivity of free chlorine on the surfaces of cupric oxide, and promotes the formation of chlorite over chlorate.[51,131] Instead of inducing a disproportionation reaction (Equation 1), lead oxide surfaces could adsorb chlorine dioxide. The resulting complex could polarize the chlorine atom, increasing its electrophilicity and tendency to form chlorite. Metal are known to complex with ligands due to Lewis acid-base reactions.[51,132] In this case, the ligands are chlorine dioxide and water. A previous proposed pathway for cupric oxide posits the dimerization of chlorine dioxide, shown to occur in basic solutions,[123] and complexation of the dimer with hydroxide on the metal oxide surface (Scheme 1).[51]

Scheme 1. Proposed surface mediated mechanism for the decay of chlorine dioxide in solution with lead oxide.

$$ClO_2 + ClO_2 \overset{>PbO_2}{\rightleftharpoons} >PbO_2Cl_2O_4$$

$$>PbO_2Cl_2O_4 \xrightarrow{OH^-} >PbO_2HOClO_2 + ClO_2^-$$

$$>PbO_2HOClO_2 \xrightarrow{OH^-} >PbO_2 + ClO_2^- + 0.5O_2$$

Incorporation of surface interactions could explain the variation in rates at different pH points, which could be to be due to Coulombic interactions at the surface of lead oxide. The point

of zero charge for lead oxide, as reported in the literature, is in the range of 8.2-8.4 when using the isoelectric point method.[129,133] X-ray powder diffraction analysis of the pure lead oxide revealed the compound to be plattnerite rather than scrutinyite. Plattnerite tends to have higher point of zero charge values, which fits with the maximum rate occurring around pH 8.3.[130] Previous studies of adsorption of free chlorine on the surface of lead oxide showed a similar trend of maximum adsorption at the zero-point pH.[130] Above and below this point of zero charge, there is an increase in either negative or positive ions on the surface. With these charged species there is higher coulombic repulsion. This slows surface assisted reactions taking place. Minimum electrostatic repulsion exists at pH 8.3.

Lead oxide has been shown to speciate into three different surfaces, which vary depending on pH: >Pb(IV)OH, >Pb(IV)O^-, and >Pb(IV)OH_2^+.[125,130] The surface is deprotonated at pH above the pH_{pzc} and protonated at pH below the pH_{pzc}. Modifying a pathway proposed by Odeh et al.[123] could give a possible mechanism for the reaction of the neutral lead oxide surface and chlorine dioxide (Scheme 2). This proposed reaction is pseudo second-order in chlorine dioxide, which will be discussed later.

Scheme 2. Proposed surface mediated mechanism for the decay of chlorine dioxide in solution with lead oxide.

$$>Pb^{IV}OH + 2ClO_2 \rightleftharpoons >Pb^{IV}OHCl_2O_4$$

$$>Pb^{IV}OHCl_2O_4 + OH^- \rightarrow >Pb^{IV}OH_2OClO(O) + ClO_2^-$$

$$>Pb^{IV}OH_2OClO(O) \rightarrow >Pb^{IV}OH + ClO_2^- + OH^-$$

Speciation on the surface of the lead oxide was also considered to explain both reactions below pH 8. At lower pH, lead carbonate is favored to form over lead oxide, despite the high oxidation-reduction potential of chlorine dioxide. This could cause dissolution of the lead (IV) oxide to lead (II) compounds (Equation 4) and slow the rate of chlorine dioxide decay.

$$PbO_{2(s)} + 2H^{+} \leftrightarrow Pb^{2+} + 2H_2O \qquad (4)$$

Dissolution of lead oxide was significant at pH's below 5.7, and in the presence of free chlorine dissolution was inhibited.[125] X-ray powder diffraction analysis showed some evidence of reduction but X-ray photoelectron spectroscopy was inconclusive, due to the unusual presentation of lead oxidation states, suggesting reduction was too slow to be observed. There was however, visual evidence of lead carbonate as discussed in Corrosion and Mineral Type 3.3.2 (Figure B-3). Lead oxide at low pH could also be changing to a lead (II, IV) oxide, slowing the kinetics, but there is no visual evidence of this since lead oxide is a black powder. At low pH, electrons could be consumed by reducing lead (IV) to lead (II) rather than chlorine (IV) dioxide to chlorite (III), thus slowing down the chlorine dioxide decay reaction.

3.3.6 Impact on water treatment

While chlorine dioxide is not the most common disinfectant, it has been used in drinking water systems in Europe, Asia, and the USA. Lead oxide, lead carbonate, and cupric oxide are pervasive in distribution systems containing copper and/or lead due to corrosion. This study points to some key concerns for the use of chlorine dioxide in these systems: maintaining a disinfectant residual, inorganic byproduct formation, and how the operational pH influences both the residual

and byproducts. These batch reactions with powdered mineral have accelerated kinetics due to the increased available surface area of the metals. The mineral concentrations used here likely allow for higher exposure levels than those present with scale contained on a pipe surface. These data can still provide insight into the mechanisms and characteristics of chlorine dioxide decay and byproduct formation in the presence of lead minerals. In the environment, including distribution systems, metal oxides can be a porous matrix.[132] Although a powered mineral still presents more surface area, it could be considered more similar to the porous scale found in distribution systems.

If used for disinfection, the presence of corrosion scale minerals will enhance the decay of chlorine dioxide, possibly below the effective concentration needed to disinfect. The EPA limits the concentration of chlorine dioxide that can be applied to drinking water (MRDL = 0.8 mg L^{-1}) and the concentration of chlorite produced (MCL = 1.0 mg L^{-1}). At 30 µM initial concentration of chlorine dioxide, the presence of lead oxide will enhance the kinetics enough to consume all the disinfectant. To combat decay, the initial concentration of chlorine dioxide could be increased, but this could lead to excessive inorganic byproduct formation. Chlorine dioxide decay in the presence of lead minerals, however, only produces chlorite. Thus, treatment facilities could focus resources on chlorite removal. There have been precedents for chlorite removal using sulfate ions, granular activated carbon, or ferrous ions.[71–73]

Maintaining a basic pH (above 7.4) has been shown to be an effective corrosion control method for lead-containing distribution systems.[54,63,134] At high pH (8-10 range), calcium carbonate can form and block pipe flow or precipitate,[54,63] and there is evidence of diminishing returns above pH 9.2 for corrosion control.[134] If using a phosphate inhibitor for corrosion control, a pH between 7.0-8.0 is recommended.[134] These data suggest operating above or below the zero point pH of the distribution system lead could help maintain a disinfectant residual and decrease

the amount of chlorite produced. Combining previous published recommendations, pH 7.4 would be optimal for lead oxide/chlorine dioxide system with regards to corrosion and byproduct formation.

Operating treatment systems at pH above or below point of zero charge, could inhibit the decay of chlorine dioxide and decrease chlorite production. Treatment systems already prefer to maintain at least slightly basic pH to prevent corrosion.[61] If utilities are able to meet the criteria of (1) operating below or above the point of zero charge and (2) maintaining a basic pH, they could combat byproduct formation and corrosion while still maintaining a disinfection residual.

Chapter 4. Computational Modeling Predictions of Chlorine Dioxide Adsorption on Metal Oxide Surfaces Aid the Interpretation of Experimental Kinetic Data

4.1 INTRODUCTION

Copper and lead are common metals used for piping in drinking water distribution systems, and their concentration in drinking water has been limited by the US Environmental Protection Agency (EPA) Lead Copper Rule since 1991.[44] These metals naturally undergo corrosion which forms layers of corrosion minerals, commonly oxides or carbonates on the metal surface.[49,53,57,61] The type of corrosion layer formed depends most heavily on the oxidation-reduction potential of the water flowing through the pipes, which in turn is primarily controlled by the disinfectant present in the water.[55] Lead (IV) oxide and copper (II) oxide are the two most commonly formed layers in the presence of free chlorine, the most commonly employed disinfectant.[51,52,55,135]

In recent decades, there has been a push to find alternatives to free chlorine, due to the number of toxic byproducts it produces, namely trihalomethanes (THMs) and haloacetic acids (HAAs), both of which are strictly regulated by the EPA.[5,6] One such alternative is chlorine dioxide, which has equivalent if not higher disinfecting power, produces little to no THMs or HAAs, and maintains its disinfecting power under variable pH conditions.[10,12,65] It does, however, produce two inorganic and hazardous byproducts, chlorite and chlorate.[72] The formation of these byproducts and the interactions of disinfectants with corrosion minerals is important work in establishing safe alternatives to free chlorine.

Chapter 3 of this dissertation investigated chlorine dioxide decay reactions with copper and lead corrosion scale mineral. Three key differences in the reactions have been identified: (1) the rate of chlorine dioxide decomposition is an order of magnitude higher in the lead-catalyzed system; (2) the cupric oxide-catalyzed reaction produces both chlorite and chlorate, while the lead oxide- or carbonate-catalyzed reaction produces only chlorite; (3) reaction rates increased with increasing pH in the cupric oxide system, but peaked at the zero-point pH in the lead oxide system. The decay data appear to fit a second-order for cupric oxide or adsorption pseudo-second-order for lead oxide.[51]

In basic solutions free of metal oxides or other constituents, chlorine dioxide decays in a second-order reaction, putatively involving the dimerization of chlorine dioxide and subsequent formation of chlorite and chlorate.[123,136] For chlorine dioxide decay in the presence of lead oxide, the reaction mechanism is unknown. This chapter aims to determine if dimerization is a precursor step to decay on the lead oxide surface, and if so, why does chlorine dioxide decay only to chlorite rather than disproportionating into both chlorite and chlorate. Moreover, the role of hydroxide in these reactions is poorly understood. This work aims to investigate some of the reasons behind the kinetic rate disparity in chlorine dioxide reactions on cupric oxide and lead oxide surfaces and assess in particular the role that dimerization might serve in the chemisorption of chlorine dioxide on these mineral surfaces.

4.2 METHODS

4.2.1 Surface calculations

First principles calculations were done using spin-polarized Density Functional Theory (DFT) in CASTEP from BIOVIA Materials Studio 2019.[137] CASTEP implements the plane-wave

pseudopotential method. The exchange-correlation functionals were calculated using the Perdew, Burke and Ernzerhof method of generalized gradient approximation.[138] For these calculations utrasoft pseudopotentials and energy cutoff of 340 eV for lead oxide or 400 eV for cupric oxide were used. Geometry optimization were performed using the Broyden-Fletcher-Goldfarb-Shanno (BFGS) optimization method.[139] The convergence criteria for the basis set considering the plane-wave cutoff energy for pseudopotentials was set to 0.1 eV/atom. The energy and maximum force tolerances were 0.00001 eV/atom and 0.03 eV/Å. The k-points separation for metals was set at 0.04 $Å^{-1}$.

4.2.2 Crystal surfaces

The adsorption of chlorine dioxide monomer and dimer on the surface of either tenorite or plattnerite was simulated using DFT methods. Cleavage planes were chosen at (-110) and (111). Lead oxide does not have a known common cleavage plane but is very similar in structure to rutile compounds. Rutile structures, titanium oxide, are commonly modeled to cleave at (110), thus this same cleavage plane was used for platternite.[88,89,140,141] (-110) was chosen to keep an appropriate ratio of lead to oxygen atoms on the surface. (111) is the most prevalent cleavage plane for cupric oxide.[142]

Lead (IV) oxide and copper (II) oxide surfaces were constructed in CASTEP from plattnerite and tenorite the American Mineralogist Crystal Structure Database.[143] The oxides were cleaved at (-110) and (111) respectively. Two different sized vacuum slabs were used. The first, smaller slab, consisted of six layers and twenty-four atoms. The bottom three layers were kept fixed to simulate the bulk crystal. The second, larger slab, consisted of four layers and sixty atoms. The bottom two layers were kept fixed. 10 Å of vacuum thickness above and 5 Å below was

established to prevent erroneous interactions between periodic structures. The crystal and unit cell were relaxed prior to adsorption calculations. The smaller slab was originally used to keep computational time low, but the larger slab was used once larger and more species were introduced on the surface, i.e. the chlorine dioxide dimer and hydroxide. Adsorption energy was calculated using Equation 1 below.[142]

$$E_{adsorption} = E_{ClO_2 + \text{ metal oxide}} - E_{\text{metal oxide}} - E_{ClO_2} \qquad (1)$$

Equation 1 shows the adsorption energy is equal to the energy of the optimized adsorption conformation of chlorine dioxide on the metal oxide surface, either lead or cupric oxide, minus the relaxed energy of the metal oxide lattice, minus the energy of the optimized chlorine dioxide molecule.

Charge density differences were calculated by subtracting the unperturbed chlorine dioxide and metal oxide surface electron densities from the adsorbed system density (Equation 2).[137]

$$\Delta\rho = \rho_{system} - \rho_{ClO_2} - \rho_{\text{metal oxide}} \qquad (2)$$

Following previously published experimental work, hydroxide was incorporated into the adsorption simulations either already present and relaxed on the surface or in solution. Hydroxide appears to be a key component of the chlorine dioxide decay to chlorite and chlorate. It was added to the adsorption studies to assess its influence on the adsorption of the chlorine dioxide monomer or dimer on the metal oxides' surfaces.

4.2.3 Reaction pathway calculations

Reaction pathway analysis was preformed used GAUSSIAN 16 program to find optimized structures for reactants, products, intermediates, and transition states of the chlorine dioxide dimer reaction with hydroxide.[144] Calculations using the Becke three-parameter hybrid functional with the Lee, Yang, and Parr correlation (B3LYP) DFT method produced equilibrium geometries. The 6-311++G(3df,3pd) basis set was used for all optimizations except the transition state.[145] The transition state was optimized at a lower level 6-311G(d) basis set. The energies were corrected for zero-point energies from frequency calculations and the appropriate negative frequencies accounted for depending on the structure analyzed.

4.3 RESULTS AND DISCUSSION

4.3.1 PbO_2 and CuO surfaces

Two crystals were chosen to model lead oxide and cupric oxide surfaces. The lead oxide surface was cleaved from plattnerite, the most common lead oxide compound found in distribution systems, to a (-110) surface, similar to rutile compounds. The surface was relaxed, keeping the bottom layers of the slab fixed. The surface oxygens relax upward, distorting the planar surface, while the lead atoms remained close to their original placement (Figure 4.1). The cupric oxide crystal was cleaved to from tenorite to a (111) surface, the most common cleavage plane.[142] The bond distances between layers increased and the cupric oxide atoms relaxed inward (Figure 4.2).

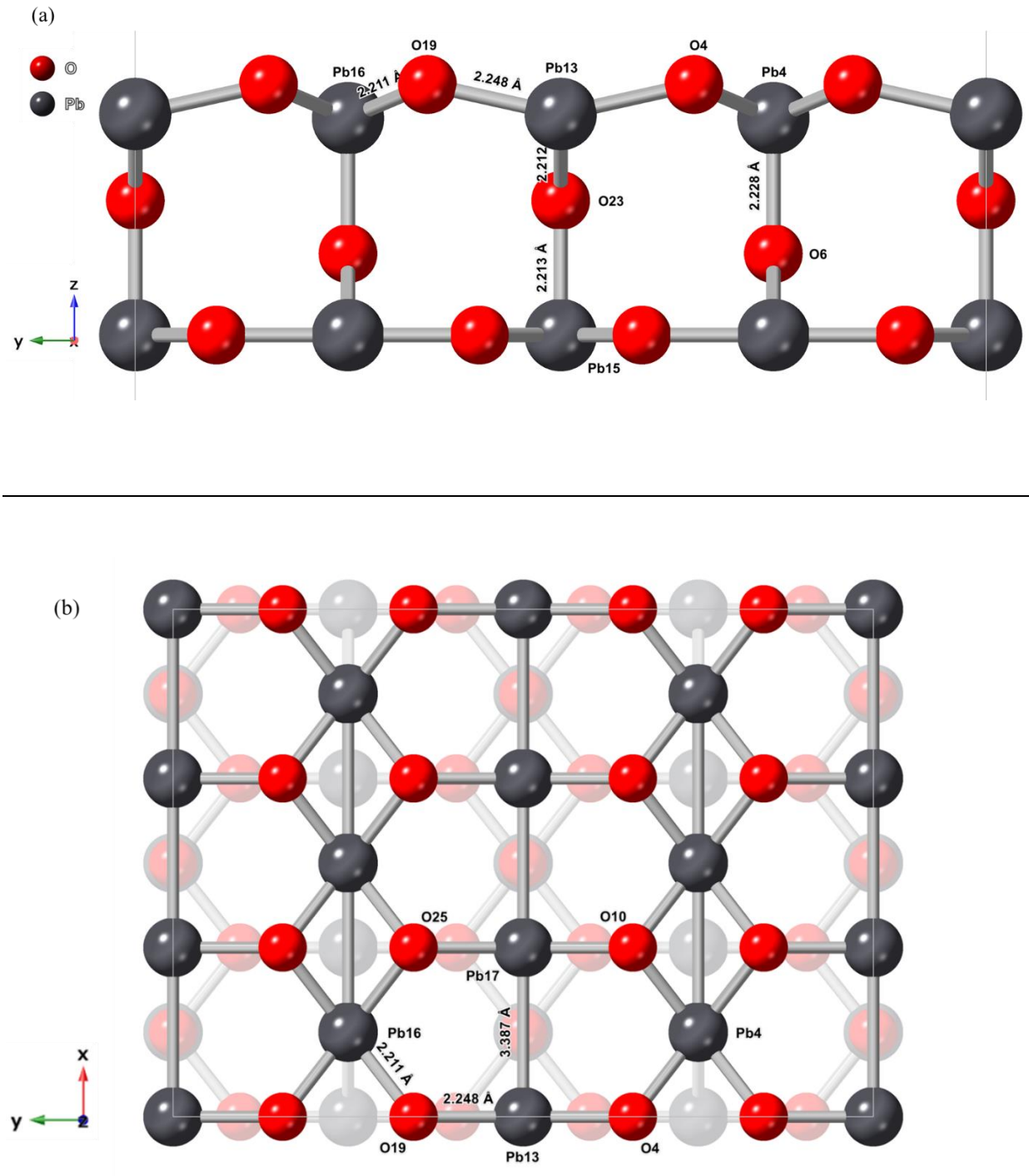

Figure 4.1 (a) Side view and (b) top view of the relaxed plattnerite (-1 1 0) surface. Red and grey spheres represent oxygen and lead atoms respectively.

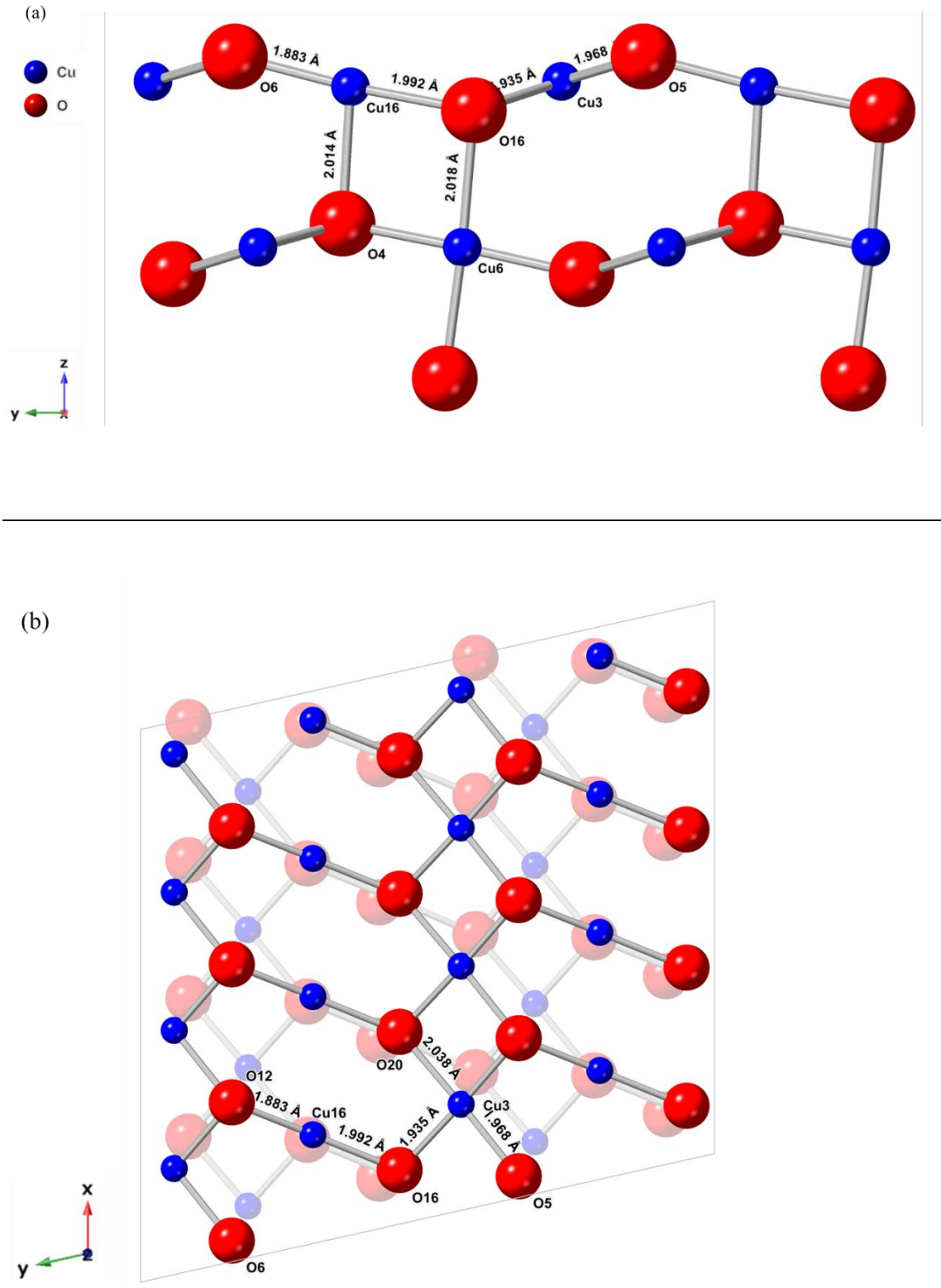

Figure 4.2 (a) Side view and (b) top view of the relaxed tenorite (1 1 1) surface. Red and blue spheres represent oxygen and cupric oxide atoms respectively.

To simulate a negatively charged surface, a hydroxide molecule was placed near the optimized surface, and the resulting configuration was relaxed before the chlorine dioxide was added to the system. The hydroxide anion orients its oxygen atom above the nearest surface lead, and the bond with hydrogen points towards the nearest surface oxygen. Adsorption of the hydroxide anion does alter the lattice structure, pulling the lead atom towards the hydroxide and away from the surface oxygens. On the cupric oxide surface, the hydroxide oxygen also orients above the nearest surface cupric oxide and the hydrogen orients towards the nearest oxygen. The cupric oxide in the lattice does not get pulled toward the surface, like the surface lead. Instead, bond distances in the vicinity of the hydroxide anion, in the lateral surface directions, are altered.

4.3.2 Adsorption of chlorine dioxide on lead oxide surface

As chlorine dioxide approaches the lead oxide surface it becomes increasingly more favorable to adsorb to the surface (Figure C-1). The chlorine dioxide molecular geometry remains constant but orients with the chlorine atom further from the surface than the two oxygen atoms. Closer to the surface, in its most stable conformation the chlorine atom situates directly above the nearest surface oxygen and the oxygen atoms above the two nearest surface lead atoms, which follows chemical intuition as it positions oppositely charged atoms near each other.

Of interest is the position of the chlorine atom on the surface (Figure 4.3). Previous studies have shown cupric oxide to polarize chlorine through complexation, making the atom more electrophilic, and catalyzing chlorine dioxide decay to its byproducts.[51,131,146] The adsorption conformation of chlorine dioxide on the lead oxide surface seems to corroborate this theory. Complexation of lead oxide, a Lewis acid, and chlorine dioxide leaves the chlorine atom sterically exposed to reactions with compounds near the lead oxide surface. The surface oxygen and

coordinated oxygens increase the positive charge of the chlorine atom, and the surface lead atoms increase the oxygens' ability to polarize the chlorine atom.

Charge density analysis shows depletion of charge on the chlorine atom in the plane of the chlorine dioxide molecule (Figure 4.3d), but enrichment above and below the slice of depletion (Figure 4.3e). This could lend evidence in support of the pseudo-second-order and second-order reaction rate models identified from the experimental studies reported in Chapter 3. The interaction of a second chlorine dioxide or hydroxide molecule creates a more electrophilic chlorine atom than the chlorine atom of an adsorbed chlorine dioxide monomer.

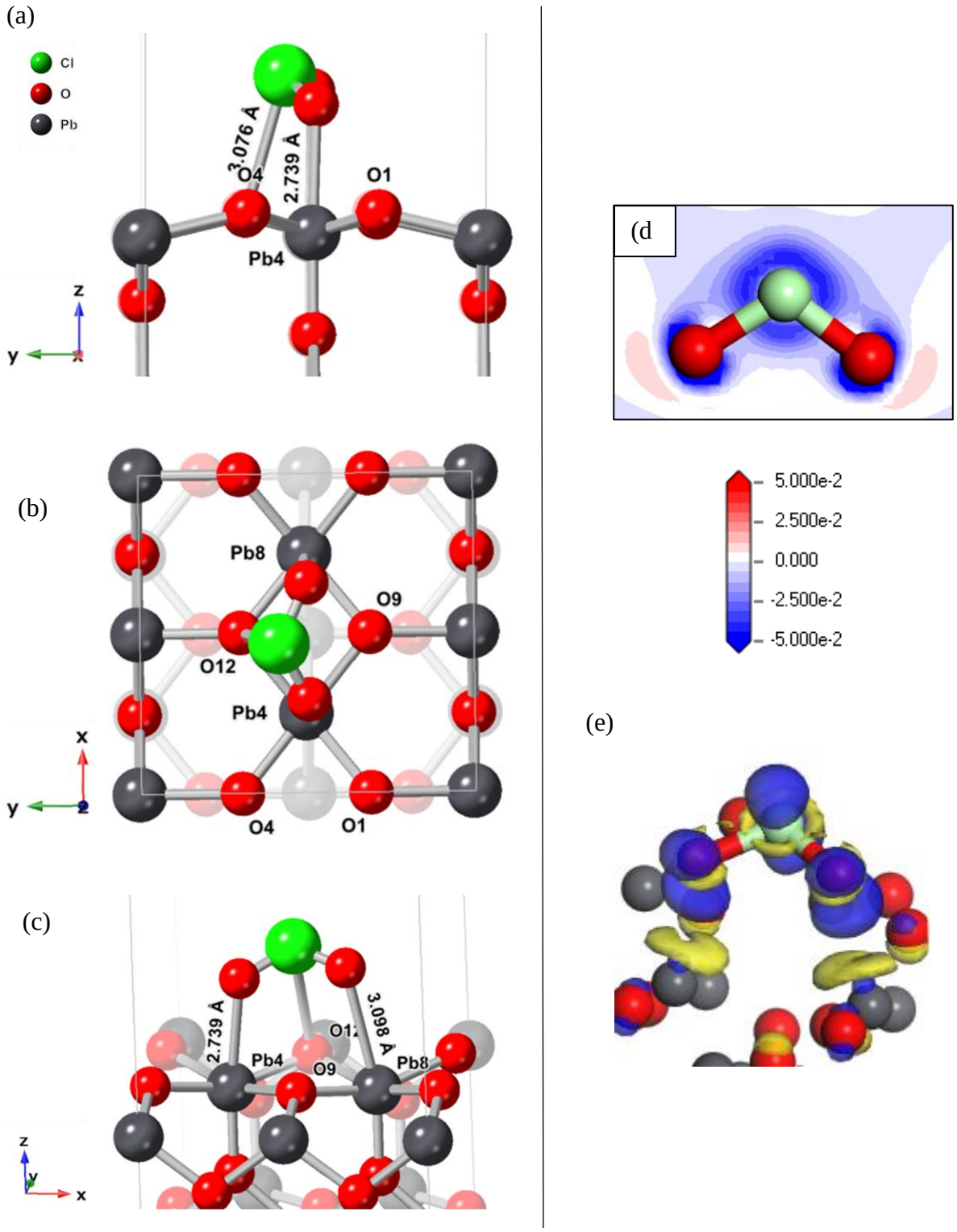

Figure 4.3 Optimized conformation of chlorine dioxide monomer adsorbed to the lead oxide surface from three different angles (a-c). (d) Slice of the charge density difference calculation in the plane of chlorine dioxide adsorption angle. Darker blue indicates a loss of electrons. (e) Isosurface of the adsorbed chlorine dioxide. Yellow indicates a depletion of electrons, 0.03 electrons/Å^3.

4.3.3 Adsorption of chlorine dioxide dimer and monomer on a larger lead oxide surface

A larger surface area, larger in the XY-plane, slab was constructed to better observe the adsorption of chlorine dioxide dimer, monomer, and both molecules in the presence of hydroxide anions. The primary proposed pathway for chlorine dioxide reactions in solution and metal oxide-catalyzed begin with chlorine dioxide dimerization.[51,123,136] Therefore the adsorption of this dimer on the surface of lead and cupric oxides was considered. Gas phase DFT calculations for the dimer were performed and compared to literature and are discussed in a later section of this chapter. Hydroxide has been shown to affect the rate of these reactions[51,123] and thus was also added into larger simulations either as present already on the surface or in solution with the monomer or dimer, which will be discussed further later. The adsorption of the monomer was observed on the larger surface to check for additional stable configurations.

Two stable configurations of chlorine dioxide monomer were found on the larger lead oxide surface, one matching the smaller surface and the other oriented with the chlorine dioxide molecule positioned with the chlorine above a subsurface oxygen and the oxygens directly above surface lead atoms (Figure C-2). Both configurations push the chlorine atom in the Z-direction away from the lead oxide surface, lending credence to the idea that the chlorine is sterically enhanced to react with other molecules in solution. The adsorption energies of each configuration are comparable, the second configuration on the larger surface being slightly lower, -0.92 eV to -1.09 eV. The larger adsorption energies compared to the smaller surface correspond to the increased number of atoms in the system. This was confirmed via simulations with varying atom amounts (Table B-1).

The dimer adsorption energy on the lead oxide surface was -0.98 eV, which is as favorable as either of the two monomer configurations, indicating the dimer is no more favorable than the

monomer. Considering the geometry of the system, the monomer adsorbs closer to the surface than the dimer, 3.076 versus 3.184 Å between the chlorine atom and nearest surface oxygen atom (Figure 4.4). The chlorine dioxide molecule in the dimer closest to the surface is skewed in orientation compared to the chlorine dioxide monomer. The charge density difference shows very little charge depletion or enrichment on the dimer or lead oxide surface at the 0.03 electrons/ $Å^3$ level. This will be discussed more compared to the cupric oxide surface dimer adsorption but seems to indicate adsorption of the dimer does not create an electrophilic chlorine atom that is needed for a catalyzed reaction. These results cast doubt on the chlorine dioxide lead oxide reaction following the same pathway as the cupric oxide reaction, i.e. dimerization leading to disproportionation. Experimental results that show only the formation of chlorite and pseudo-second-order analysis corroborate this.

(a)

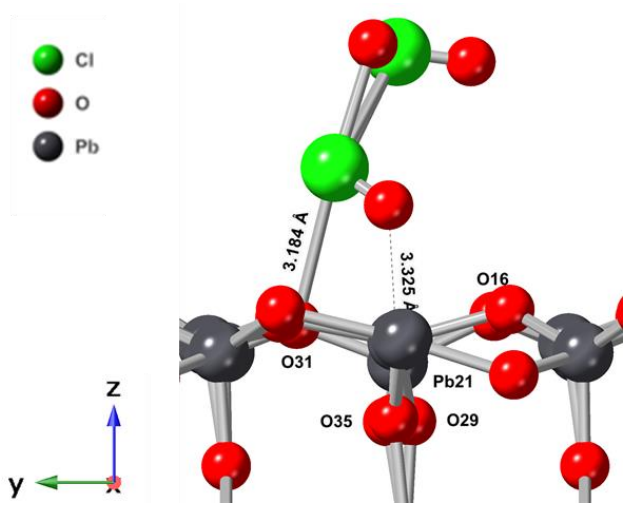

(b)

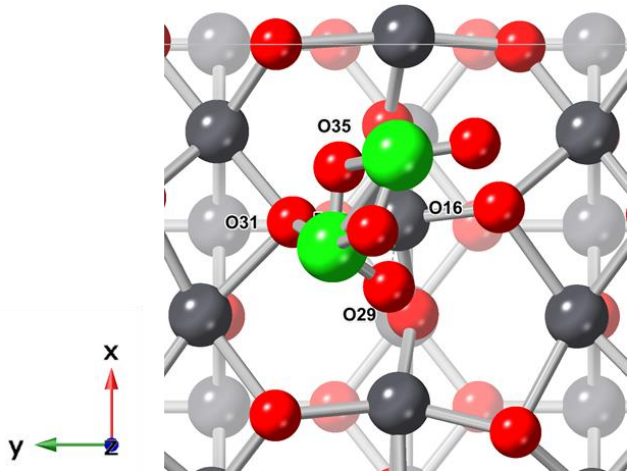

(c)

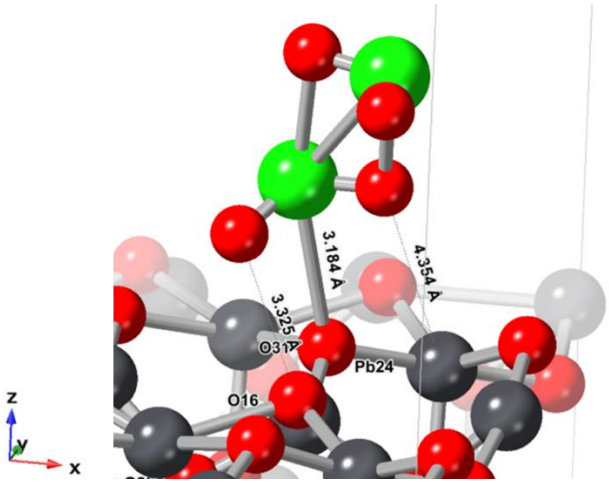

Figure 4.4 Optimized conformation of chlorine dioxide dimer adsorbed to the lead oxide surface from three different angles (a-c).

4.3.4 Adsorption of chlorine dioxide monomer and dimer on cupric oxide surface

The chlorine dioxide molecule adsorbs to the surface of cupric oxide in a similar conformation as on the lead oxide surface. The oxygen atoms alight closer to the surface copper atoms than surface lead atoms (Figure 4.5). Considering only the distance, the chlorine atom rests close to 3.0 Å from the surface oxygens in either mineral, 2.996 Å and 3.076 Å from the surface oxygens in the cupric oxide and lead oxide minerals respectively. The adsorption energy, however, is higher for the cupric oxide conformation than the lead oxide conformation, -1.74 eV versus -0.92 or -1.09 eV.

The orientation of the molecules adsorbed to both surfaces leaves the chlorine atom sterically exposed to chemical reactions with other molecules, notably hydroxide ions, and creates a more electrophilic halogen atom. Adsorption on the surface is favorable for both minerals and appears to increase the electrophilic nature of chlorine. These corroborate previously published experimental results that show higher kinetic rates of decay of chlorine dioxide in the presence of lead and cupric oxide minerals compared to chlorine dioxide in solution.[51,123]

In studies of transition-metal and transition-metal compound catalysts, adsorption energy must be considered in the kinetics of the reactions, in order to fulfill the Sabatier principle.[127,128,147,148] The best catalytic activity occurs when interactions between the catalyst and substrate are strong enough to bind, but weak enough to then dissociate. The strength of adsorption can be related to the structure of the catalyst, and its coordination number with the substrate.[127,149] Compared with each other, rates are significantly higher for lead than copper. The lead oxide surfaces have a lower adsorption energy than the cupric oxide surface, which could mean the cupric oxide surface retains the chlorine dioxide more strongly than the lead oxide surface. The lead oxide

surface increases the electrophilicity of the chlorine atom, but more readily releases the chlorine dioxide molecule to surface or in solution reactions, thus satisfying the Sabatier principle.

Considering the charge density difference, especially the isosurface analysis, the cupric oxide mineral appears to increase the electrophilicity of the chlorine atom more than the lead oxide surface. This could be due to the ratio of cupric oxide to oxygen atoms is higher than lead to oxygen atoms in the lead oxide crystal, and the corresponding differences in coordination number.[127,149] There are more cupric oxide atoms to pull electrons away from the chlorine. Considering the Cu^{2+} orbitals, [Ar] $3d^9$, and Pb^{4+}, [Xe] $4f^{14}$ $5d^{10}$, it seems further likely that the cupric oxide would enhance the electrophilicity of the chlorine atom more than the lead atom.

The highly electrophilic chlorine then readily reacts with the negatively charged hydroxides in the system, explaining the increases rates that occur when the pH is increased in the cupric oxide-catalyzed reaction. The lead oxide reaction, in contrast, shows a decrease in rate when pH and hydroxide concentration increase.

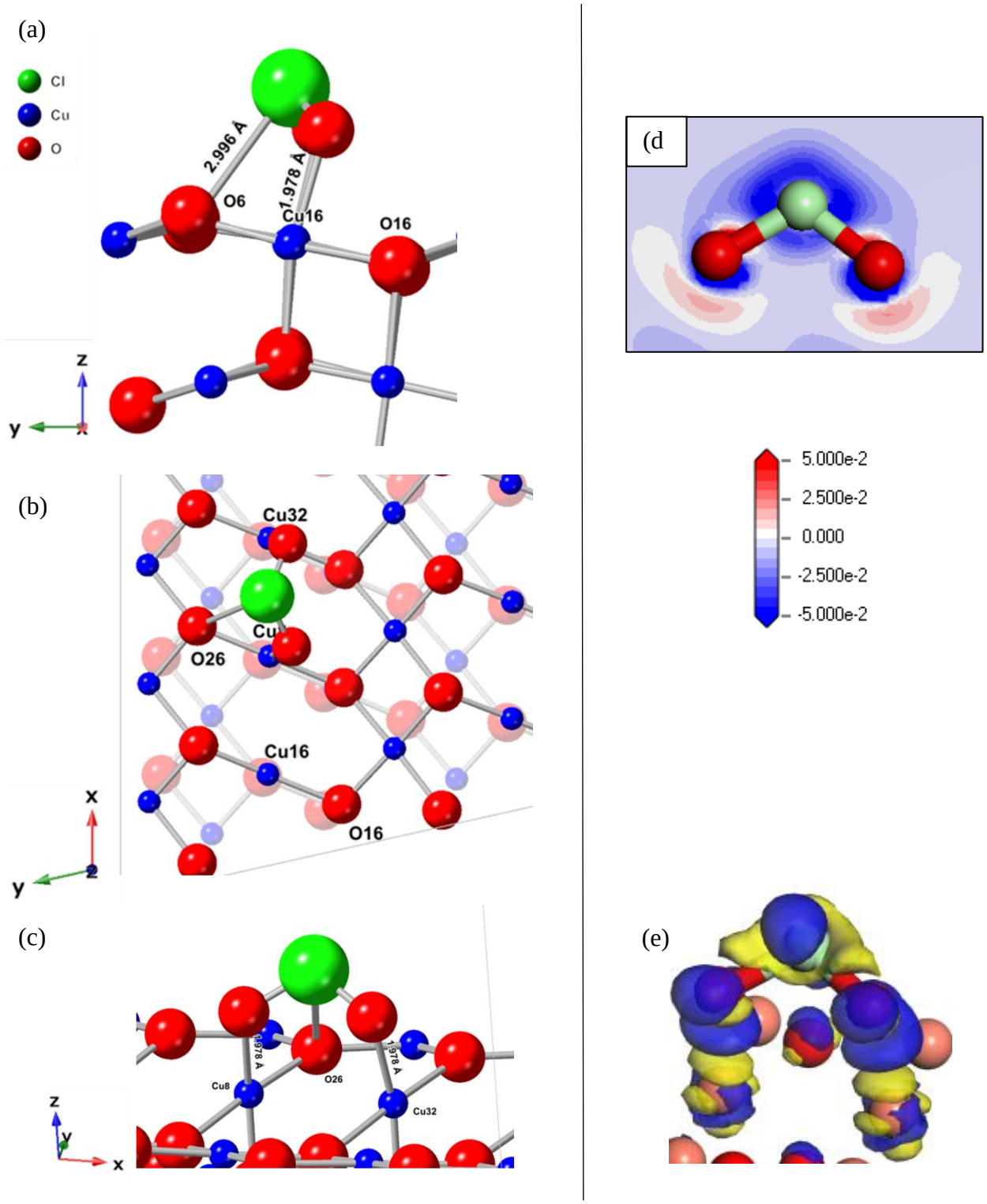

Figure 4.5 Optimized conformation of chlorine dioxide monomer adsorbed to the cupric oxide surface from three different angles (a-c). (d) Slice of the charge density difference calculation in the plane of chlorine dioxide adsorption angle. Darker blue indicates a loss of electrons. (e) Isosurface of the adsorbed chlorine dioxide. Yellow indicates a depletion of electrons, 0.03 electrons/Å^3.

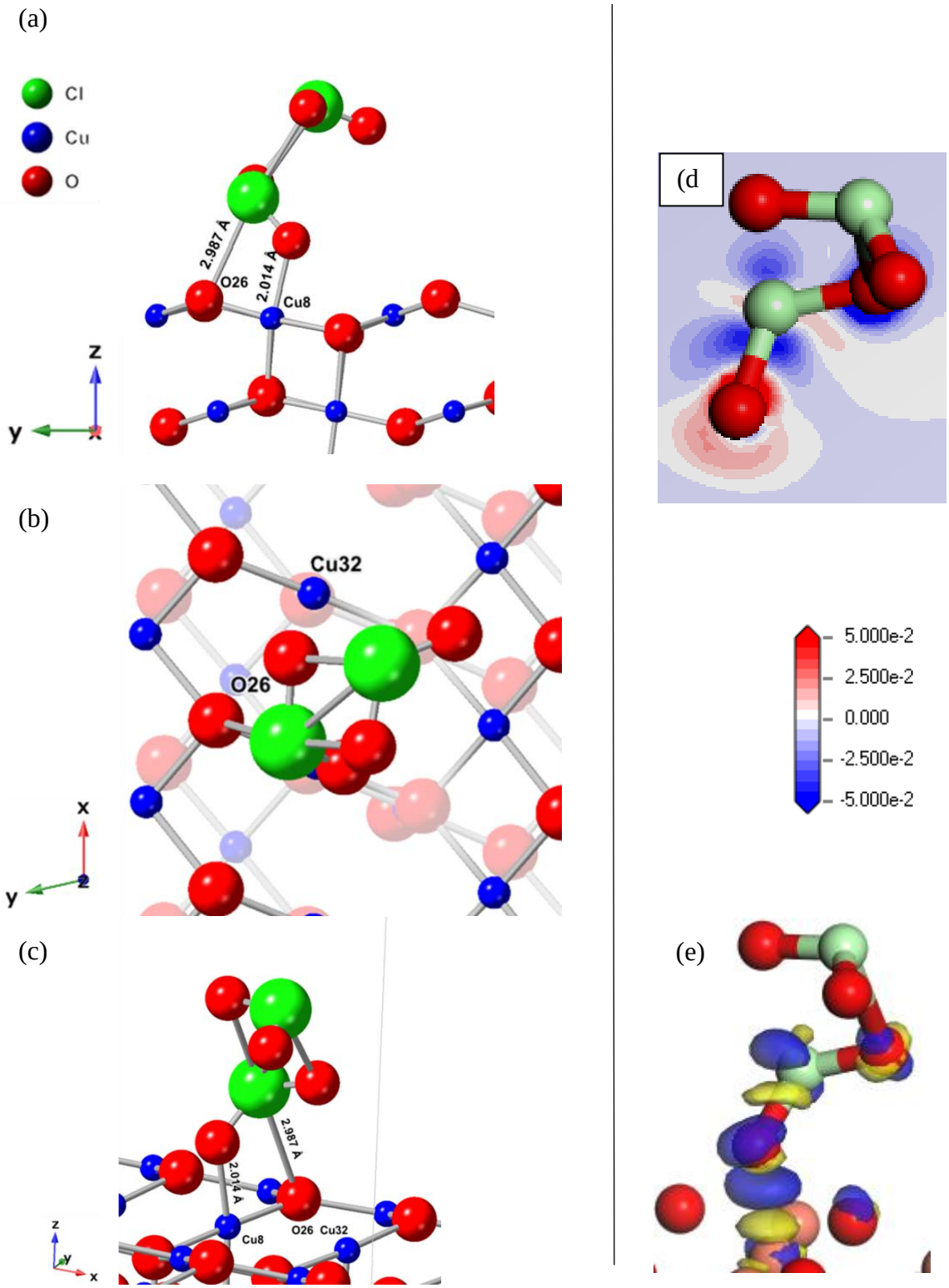

Figure 4.6 Optimized conformation of chlorine dioxide dimer adsorbed to the cupric oxide surface from three different angles (a-c). (d) Slice of the charge density difference calculation in the plane of the lower chlorine dioxide angle. Darker blue indicates a loss of electrons. (e) Isosurface of the adsorbed chlorine dioxide. Yellow indicates a depletion of electrons, 0.01 electrons/Å^3.

Compared to the chlorine dioxide monomer on the cupric oxide surface, adsorption energy is lower for the dimer, -1.74 eV versus -1.01 eV, but both are favorable. The monomer and dimer also adsorb at a similar distance from the surface, 2.996 versus 2.987 Å from the lower chlorine atom to the nearest surface oxygen (Figure 4.6). More interestingly, there is a starker charge density difference in the dimer than the monomer. The upper chlorine atom in the dimer appears to have more pronounced regions of electron depletion and little or no enrichment. It seems cupric oxide surface reactions with chlorine dioxide create a more electrophilic chlorine atom when a dimer rather than a monomer is adsorbed. This contrasts with the lead oxide surface, which adsorbs monomer and dimer equally favorably, and, more notably perhaps, has enrichment rather than depletion of charge on the chlorine dimer (Figure 4.7). To note, this is at 0.005 versus 0.03 electrons/Å^3 isosurface, thus the enrichment is not as large as the monomer, but the lack of enrichment is notable.

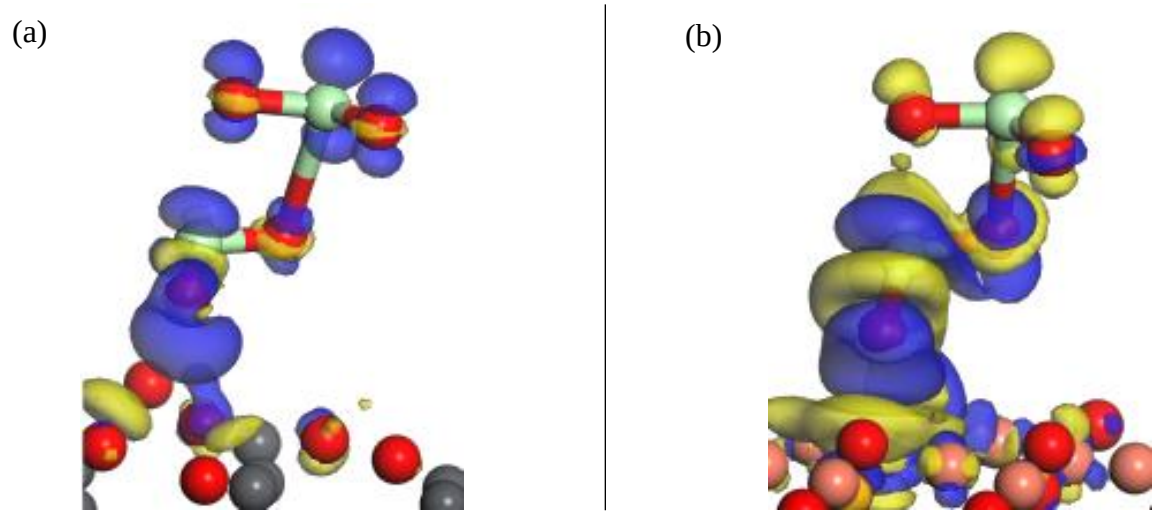

Figure 4.7 Isosurface of the adsorbed chlorine dioxide dimer on (a) lead oxide and (b) cupric oxide surfaces. Yellow indicates a depletion of electrons, 0.005 electrons/Å^3.

4.3.5 Reaction kinetics and chemisorption

The surface cupric oxide reaction is second-order catalyzed by the adsorption.[51] The metal oxide-catalyzed rate of chlorine dioxide decay seems due to the electrophilicity of the chlorine atom being increased by adsorption. The electrophilicity appears to increase when a dimer rather than a monomer is involved, hence the second-order dependence in chlorine dioxide. At higher chlorine dioxide concentrations the ratio of chlorite to chlorate produced becomes increasingly equivalent.[51] The dimerization of chlorine dioxide is more likely at higher concentrations, and the disproportionation reaction requires the formation of said dimer.

The lead adsorption data does not seem to favor a dimer over a monomer in terms of both adsorption energy and electron density difference. Considering the increased rate of decay in the lead versus cupric oxide reaction and the absence of chlorate byproduct, it seems more likely that a dimer is not needed for the lead oxide surface reactions. Instead the decay could be limited by chemisorption and exchange of valence electrons between the chlorine dioxide, water, and lead oxide surface. Dependence on chemisorption could also explain the kinetic rate dependence on pH for the lead oxide surfaces. Above and below the zero-point pH, charged particles accumulate on the surface, possibly hindering the adsorption of chlorine dioxide and thus limiting its adsorption to the surface. Pseudo-second-order rate models have been developed for adsorption and employed in many studies since.[124,150,151] From Chapter 3 of this work, chlorine dioxide decay appears to fit this model. The physical meaning of the pseudo-second-order likely correspond to chemisorption being the rate-limiting step.[124,150,152]

In the presence of lead, perhaps direct electron transfer from water to chlorine dioxide to form chlorite is more favorable than dimerization and subsequent disproportionation to chlorite and chlorate. The reaction is limited by adsorption on the surface. The adsorption energies are

favorable for chlorine dioxide monomer, but perhaps weak enough for desorption to easy occur after the electron transfer reaction.

4.3.6 Equilibrium geometries of intermediates from Gaussian

Previous experimental work of chlorine dioxide decay in basic solution and in the presence of metal oxides, including cupric oxide, suggest three key reaction pathways.[51,123] The first pathway being first order and a disproportionation reaction was not considered for this study since the lead oxide pathway produces only chlorite and is pseudo-second-order, and the cupric oxide pathway is second-order. The other two pathways were considered, with a focus on the rate limiting step of each reaction. Both reactions guided the adsorption studies, thus the chlorine monomer, chlorine dimer, and presence of hydroxide were all considered in the adsorption analyses.

Scheme 1. First and second order decay reactions of chlorine dioxide to its byproducts chlorite and chlorate in solution.

(a) First-order pathway in chlorine dioxide

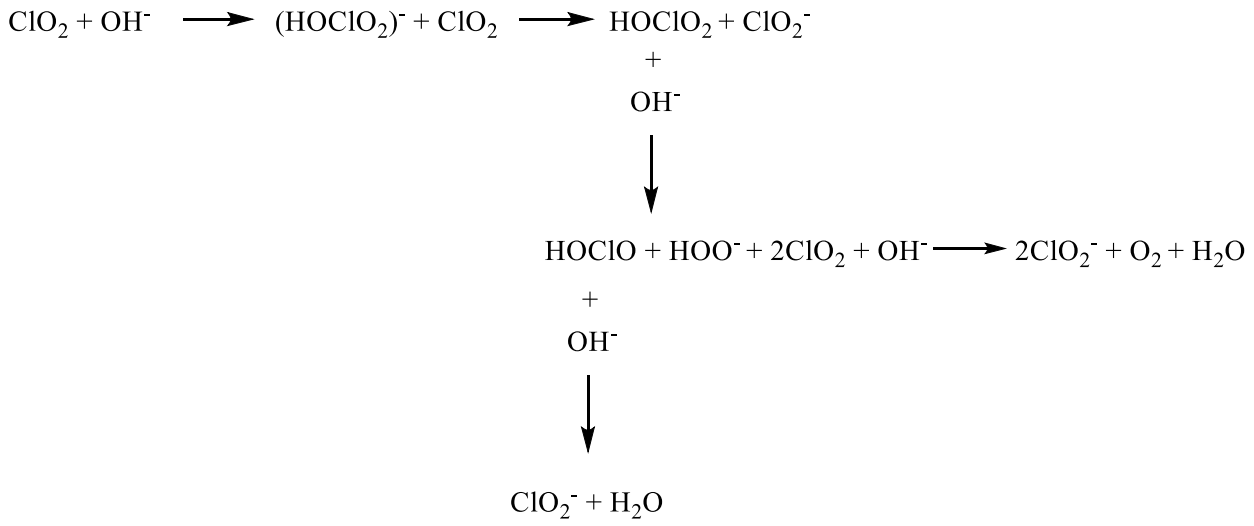

(b) Second-order pathway in chlorine dioxide

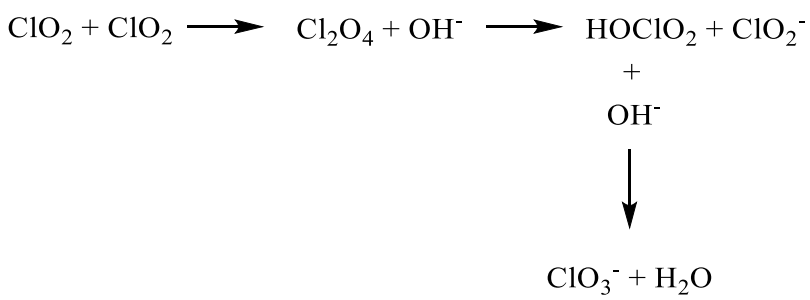

The optimized geometries of reactants, products, and intermediates of these two reactions were calculated using DFT methods (Table B-2). Using these energies, the reaction enthalpies of the chlorine monomer (first-order pathway) and dimer (second-order pathway) reactions were calculated, considering the rate limiting step of each reaction. The dimer pathway is more favorable from an energetic standpoint (Table 4.1). The dimer reaction also seems more likely to be occurring, given the reaction order of the reactions on the lead and copper surfaces. Thus, the transition state of the dimer pathway was also calculated (Figure 4.8).

Ideally these calculations would be performed on the metal oxide surface, which could be considered for future work. As stands, these calculations provide some support of the dimer pathway and guided the adsorption studies. They also highlight the importance of hydroxide in these reactions, which led to the final analysis of this study.

Table 4.1 Relative enthalpies of formation for the rate limiting step in a chlorine dioxide dimer or monomer reaction with hydroxide anion.

Rate limiting step	ClO_2 form	ΔH° (eV)
$Cl_2O_4 + OH^- \longrightarrow HOClO_2 + ClO_2^-$	Dimer	-1.75
$ClO_2 + OH^- \longrightarrow (HOClO_2)^- + ClO_2$	Monomer	-1.15

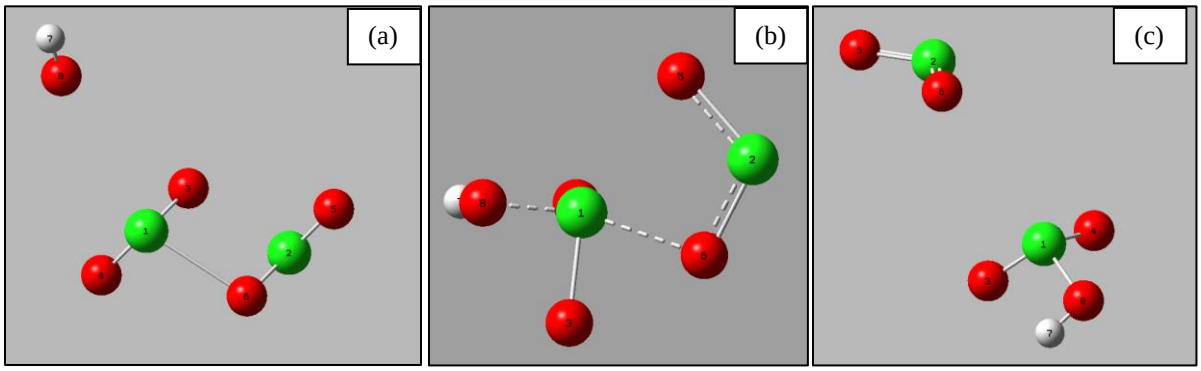

Figure 4.8 (a) Reactants, (b) transition state, and (c) intermediates of the rate limiting step in the chlorine dioxide dimer reaction with hydroxide anion. Chlorine, oxygen, and hydrogen atoms are represented by green, red, and white spheres respectively.

4.3.7 Influence of hydroxide on chlorine dioxide dimer and monomer adsorption

Hydroxide appears to have a strong influence on the cupric oxide surface reactions, as pH increased the rate of chlorine dioxide decay increased.[51] The effect of hydroxide on the lead oxide reactions is more nebulous. Clearly water is being oxidized to supply electrons for the formation of chlorite, but increasing pH decreases the rate of chlorine dioxide decay. The reaction pathways in Scheme 1 seem inadequate in describing the lead oxide surface reaction. Nevertheless, the influence on hydroxide on adsorption was considered. Two scenarios were run for both the chlorine dioxide monomer and dimer: the hydroxide already adsorbed to the metal oxide surface

and the hydroxide in solution equal distance from the metal oxide surface as the chlorine dioxide sorbate.

Adsorption energies suggest that the presence of hydroxide either on the surface or in solution inhibits adsorption of chlorine dioxide (Table 4.2). The less favorable adsorption could lead to reduced kinetic rates of decay, which adds to the theory of chemisorption being the rate limiting step of the pseudo-second-order reaction on the lead oxide surface.

Table 4.2 Energy of adsorption for chlorine dioxide monomer or dimer on the surface of lead oxide in the presence of hydroxide anion either previously adsorbed to the surface or in solution with the sorbate.

	ClO_2 only	**ClO_2 + surface OH^-**	**ClO_2 + OH^- in solution**
Monomer E_{ads} (eV)	-0.92	-0.17	-0.04
Dimer E_{ads} (eV)	-0.98	0.01	0.26

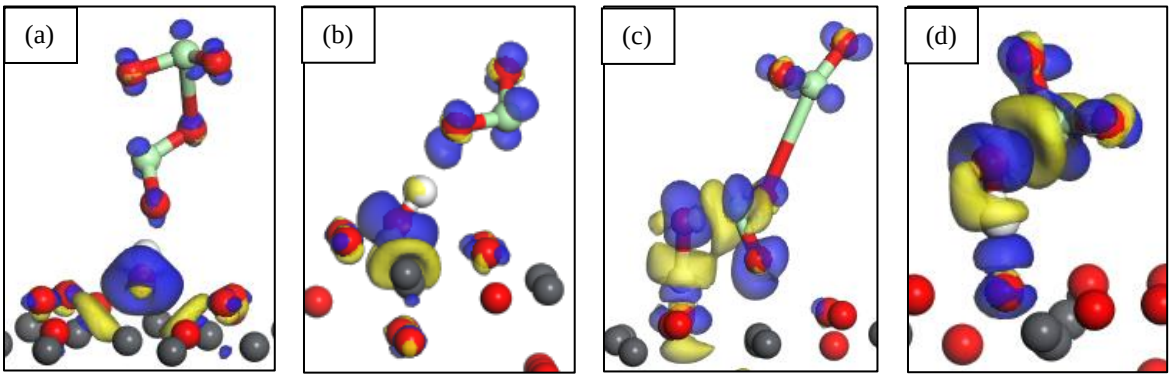

Figure 4.9 Charge density differences of chlorine dioxide dimer (a, c) and monomer (b, d) adsorption on the surface of lead oxide in the presence of hydroxide anion either previously adsorbed to the surface (a, b) or in solution with the sorbate (c, d). The yellow isosurface indicates charge depletion, 0.03 electrons/$Å^3$.

When assessing the influence of hydroxide on the charge density differences, the chlorine dioxide monomer and dimer both become more electrophilic when the hydroxide was present in

solution rather than starting on the surface (Figure 4.9). This corroborates the theory that the zero-point pH plays a role in lead oxide surface reactions. Above the zero-point pH there will be an excess of negatively charged species already on the surface, and in this simple system, primarily hydroxide. The presence of these ions will both prevent chemisorption and decrease the effect on the chlorine atom electrophilicity.

From computational adsorption data, it seems the cupric oxide surface is well suited for the adsorption of monomer and dimer chlorine dioxide. Adsorption increases the electrophilic nature of the chlorine atom in either case, but especially on the dimer. The adsorption energy of the monomer is stronger, but in this system, could be too strong for desorption of the reaction products leading to slower reaction rates. All this supports the theory of chlorine dioxide dimerization and decay to chlorite and chlorate proposed by previous work. Adsorption on the lead oxide surface is still favorable for either a chlorine dioxide monomer or dimer, but less favorable than the cupric oxide surface, supporting the experimental data that shows higher kinetic rates of decay on the lead oxide surface. The adsorption energy strikes a balance that allow the chlorine dioxide to adsorb, but also react and desorb, which has been shown to be key in developing useful catalysts.

Chapter 5. Conclusions and Future Work

5.1 Overview

Balancing the risks of waterborne disease, toxic byproduct formation, and pipe corrosion, associated with drinking water distribution systems remains a concern of water utilities tasked with providing potable water to modern society. The goal of the work reported in this dissertation is to assess the interplay of these three issues in the context of a particular drinking water disinfectant, chlorine dioxide. Despite the prevalence of free chlorine usage as a disinfectant in drinking water treatment over the last several decades, knowledge gaps remain in free chlorine disinfection mechanisms, byproduct formation, and corrosion. These literature gaps are even larger for free chlorine alternatives including chlorine dioxide. Drinking water treatment plants have considered chlorine dioxide as a free chlorine replacement in their disinfection processes primarily because chlorine dioxide produces almost no THMs or HAAs. However, little is known about how chlorine dioxide inactivates pathogens, forms inorganic byproducts, or impacts corrosion; thus, this dissertation aimed to fill some of those knowledge gaps using both computational and experimental methods. Computational methods from molecular scale models, not typically employed by environmental engineers, offer a new way to analyze these mechanisms and add insight to macroscale phenomena observed by experimental measurements in the laboratory,

Each chapter of this dissertation advances the current understanding of chlorine dioxide disinfection chemistry from the complementary perspectives of pathogen disinfection, byproduct formation, and corrosion. From the work presented in Chapter 2, chlorine dioxide appears to have an unusually specific method of inactivating the H1N1 influenza virus, oxidizing the tryptophan

153 residue, thereby disrupting the virus's ability to bind to its host. More significantly, molecular modeling was used to predict the location of this oxidation site on the protein, which was then confirmed via mass spectrometry measurements of the oxidized protein. Expansion of these results to more pathogens and oxidants could lead to more efficient disinfection systems and safeguards against viral mutations that impact the efficacy of disinfection. Chapter 3 provides insight into byproduct formation and the reaction kinetics of chlorine dioxide decay in the presence of corrosion minerals. Notable differences between lead and copper minerals were discovered including a lack of chlorate formation, higher reaction rates, and zero-point pH dependence in the lead mineral-catalyzed decay. These findings motivated the adsorption studies reported in Chapter 4, which employed DFT methods to examine the molecular-scale interactions that govern the experimental results described in Chapter 3. Adsorption energies, geometries, and charge density differences support the hypothesized mechanism of chlorine dioxide dimerization and subsequent disproportionation for the cupric oxide-catalyzed reaction pathway, but not for the lead oxide-catalyzed reaction pathway, which appears instead to be limited by chemisorption.

There are implications and limitations to each of these studies that will be discussed in more detail along with suggestions for future work to extend this research.

5.2 Computational modeling and virus inactivation mechanisms

Using molecular docking methods, it was shown that the target of chlorine dioxide oxidation on the H1N1 influenza virus was tryptophan 153, and moreover, this target could be predicted by both mass spectrometry and molecular modeling. Admittedly, a main limitation of this study is its lack of breath in terms of both number of viruses and oxidants tested using the molecular docking methodology. Ideally, future work would include a range of representative

viruses and commonly used water disinfectants i.e. chloramines. Additional data would help to show patterns in protein susceptibility thus aiding water treatment efficiency and efficacy. Disinfection systems could become more tailored to the types of pathogens present in the source water they treat. This could be of value for hospitals concerned with opportunistic pathogens not typically monitored by standard water treatment facilities. Having a more efficient disinfection system also reduces the amount of disinfectant that needs to be added to drinking water, thereby reducing the formation of DBPs, coagulants added for DBP removal, and issues related to corrosion.

Beyond matching computational to experimental data, molecular modeling could be used to better explain why particular protein oxidations cause inactivation, by examining molecular-scale changes in protein structure and folding. Insight into protein modifications could unlock patterns that help describe pathogen disinfection mechanisms and promote better treatment practices. Knowledge of protein oxidation, in general, could also have further implications in the public health realm specifically for aging and disease. Data could be gathered through molecular docking calculations and molecular dynamics simulations.

Of growing concern in drinking water treatment is also the ability of viruses to mutate and thereby decrease the disinfecting power of the chemical oxidants presently used to treat drinking water. Molecular modeling seems an ideal realm to explore the implications of viral mutations. Numerous sequences of potential mutations could be screened, and the potentially dangerous mutations further explored. Armed with more knowledge, treatment systems could adjust their disinfection techniques to maintain the efficacy of their disinfection process. Computational work could furthermore provide insight into the structural and chemical changes that occur after a

mutation to assess the susceptibility of the mutated virus to various oxidants. This could help to determine which oxidants would still be effective against mutated viruses.

5.3 Relationship between disinfection, corrosion, and toxic byproducts

Chapters 3 and 4 of this dissertation have shown that there are clear differences in water supply systems that contain lead versus copper scale minerals. Lead-catalyzed reactions occur at higher kinetic rates and produce only chlorite as a byproduct. The lead oxide-assisted decay reaction also appears to be dependent on surface charge, with the chlorine dioxide decay rates peaking at the zero-point pH, whereas in the cupric oxide reaction, as the pH increases, the chlorine dioxide decay rate also increases. Lead and copper, possibly due to their orbital structures and coordination numbers, promote different reaction pathways, with chemisorption and direct electron transfer in the case of the former and dimerization to disproportionation favored on the latter.

For drinking water plants considering chlorine dioxide as a disinfectant, there are key recommendations that can be taken from this dissertation's findings. Drinking water treatment plants often increase pH to mitigate corrosion effects, which will enhance the decay of disinfectants, in the case of a copper-based system. In a lead pipe system, it seems more important to increase the pH above or below the zero-point if chlorine dioxide is used as a disinfectant. Distribution systems comprised primarily of lead infrastructure could focus efforts on removing chlorite, since it seems unlikely any chlorate would be produced.

Future work for these chapters could benefit from additional computational and experimental investigations. The primarily limitation of Chapter 3 lies in the use of batch reaction and powdered minerals to determine decay kinetics. Future work could include first laboratory

grown scale and then true scale samples taken from actual water supply networks, rather than synthesized powdered minerals. These samples could give more realistic kinetic rates and perhaps include the effects of flow. The effects of corrosion inhibitors, namely orthophosphate, and natural organic matter should also be considered as both constituents are often present in treated drinking water. Future computational adsorption studies could include the effects of solvation and look at reaction pathways on the corrosion mineral surfaces rather than in a vacuum.

Overall, this dissertation provides insights into chlorine dioxide chemistry through experimental and computational methods and was motivated by the intriguing relationships between disinfection, byproduct formation, and corrosion.

Appendices

Appendix A. Supplementary Information for Chapter 2

Table A-1 The chlorine dioxide conformations with the free energies of binding, C1, contains four indistinct members, listed below. D190 and W153 are highlighted in bold where present in the cluster members.

ΔG (kcal/mole)	**Amino acid residues**								
-2.471	Y 98	S 186	**D 190**	Q 226	E 227	G 228			
-2.470	Y 98	S 186	**D 190**	Q 226	E 227	G 228			
-2.385	Y 98	**W 153**	H 183	**D 190**	L 194	Q 226	E 227	G 228	
-2.382	Y 98	**W 153**	H 183	S 186	**D 190**	L 194	Q 226	E 227	G 228

Table A-2 The sixteen conformations with the free energy of binding calculated for the global docking of HA with hypochlorous acid. The conformations are numbered in order of decreasing affinity between HOCl and HA, and are listed as mean free energy of binding ± SD. In the statistical analysis, one-way ANOVA showed none of the mean free energies of binding were significantly different (P-value 0.199). The footnote lists contacting residues for a given cluster.

Cluster	Members	ΔG (kcal/mol)
H1[††]	1	-2.30
H2	1	-2.17
H3	1	-2.00
H4	2	-1.99±0.27
H5	2	-1.99±0.07
H6	1	-1.94
H7	2	-1.88±0.25
H8	1	-1.88
H9	1	-1.83
H10	1	-1.76
H11	1	-1.73
H12	2	-1.71±0.03
H13	1	-1.71
H14	1	-1.65
H15	1	-1.56
H16	1	-1.51

[††]**H1** | D93, N94, G95, T96
H2 | L71, N150, L151, V178, L179, P254, R255, Y256, A257, F258
H3 | G62, K63, E75, C76, E77
H4 | S132, N133, K133A, G134, V135, F147, I152, W153
H5 | I103, D104, Y209, Y233, W234
H6 | L59, W69, S78, S80, T81, A82
H7 | Q191, A198, D199, A200, K214, P215, I217, N250
H8 | Y98, W153, H183, P185, S186, D190, L194, G228
H9 | E119, P122, K123, T124, S125, R255
H10 | F147, Y148, K149, L151, I152, R255
H11 | S167, G205, S206, K242, I243, T244
H12 | L123, W127, P128, H130, D131, S132, N133, K157
H13 | I66, T86, I87, R109, L112, S113
H14 | I182, H184, F213, P215, N231, Y233
H15 | Q111, E175, M260, E261, R262
H16 | H184, R220, R229

Table A-3 H1N1 hemagglutinin capsid protein sequence. Orbitrap MS detected the underlined fragments. 261 amino acids, or 46.3% of the total, were recovered.

MKAKLLVLLC[10] TFTATYADTI[20] CIGYHANNST[30] DTVDTVLEKN[40] VTVTHSVNLL[50] EDSHNGKLCL[60] LKGIAPLQLG[70] NCSVAGWILG[80] NPECELLISK[90] ESWSYIVETP[100] NPENGTCYPG[110] YFADYEELRE[120] QLSSVSSFER[130] FEIFPKESSW[140] PNHTVTGVSA[150] SCSHNGKSSF[160] YRNLLWLTGK[170] NGLYPNLSKS[180] YVNNKEKEVL[190] VLWGVHHPPN[200] IGDQRALYHT[210] ENAYVSVVSS[220] HYSRRFTPEI[230] AKRPKVRDQE[240] GRINYYWTLL[250] EPGDTIIFEA[260] NGNLIAPWYA[270] FALSRGFGSG[280] IITSNAPMDE[290] CDAKCQTPQG[300] AINSSLPFQN[310] VHPVTIGECP[320] KYVRSAKLRM[330] VTGLRNIPSI[340] QSRGLFGAIA[350] GFIEGGWTGM[360] VDGWYGYHHQ[370] NEQGSGYAAD[380] QKSTQNAING[390] ITNKVNSVIE[400] KMNTQFTAVG[410] KEFNKLERRM[420] ENLNKKVDDG[430] FLDIWTYNAE[440] LLVLLENERT[450] LDFHDSNVKN[460] LYEKVKSQLK[470] NNAKEIGNGC[480] FEFYHKCNNE[490] CMESVKNGTY[500] DYPKYSEESK[510] LNREKIDGVK[520] LESMGVYQIL[530] AIYSTVASSL[540] VLLVSLGAIS[550] FWMCSNGSLQ[560] CRIC

Table A-4 Hemagglutinin protein amino acid sequences of A/New Caledonia/20/99, used for experimental work, and A/Mexico/4603/2009, used in the computational modeling. The third sequence contains the most commonly occurring residues in human strains of H1N1 hemagglutinin.

```
NewCal  MKAKLLVLLCTFTATYADTICIGYHANNSTDTVDTVLEKNVTVTHSVNLLEDSHNGKLCLLKGIAPLQL
Mex     MKAILVVLLYTFATANADTLCIGYHANNSTDTVDTVLEKNVTVTHSVNLLEDKHNGKLCKLRGVAPLHL
Human   MKVKLLVLLCTFTATYADTICIGYHANNSTDTVDTVLEKNVTVTHSVNLLEDSHNGKLCLLKGIAPLQL

NewCal  GNCSVAGWILGNPECELLISKESWSYIVETPNPENGTCYPGYFADYEELREQLSSVSSFERFEIFPKES
Mex     GKCNIAGWILGNPECESLSTASSWSYIVETSSSDNGTCYPGDFIDYEELREQLSSVSSFERFEIFPKTS
Human   GNCSVAGWILGNPECELLISKESWSYIVETPNPENGTCYPGYFADYEELREQLSSVSSFERFEIFPKES

NewCal  SWPNHTVT-GVSASCSHNGKSSFYRNLLWLTGKNGLYPNLSKSYVNNKEKEVLVLWGVHHPPNIGDQRA
Mex     SWPNHDSNKGVTAACPHAGAKSFYKNLIWLVKKGNSYPKLSKSYINDKGKEVLVLWGIHHPSTSADQQS
Human   SWPNHTVTKGVSASCSHNGKSSFYRNLLWLTGKNGLYPNLSKSYANNKEKEVLVLWGVHHPPNIGDQRA

NewCal  LYHTENAYVSVVSSHYSRRFTPEIAKRPKVRDQEGRINYYWTLLEPGDTIIFEANGNLIAPWYAFALSR
Mex     LYQNADAYVFVGSSRYSKKFKPEIAIRPKVRDQEGRMNYYWTLVEPGDKITFEATGNLVVPRYAFAMER
Human   KCQTPQGAINSSLPFQNVHPVTIGECPKYVRSAKLRMVTGLRNIPSIQSRGLFGAIAGFIEGGWTGMVD

NewCal  GFGSGIITSNAPMDECDAKCQTPQGAINSSLPFQNVHPVTIGECPKYVRSAKLRMVTGLRNIPSIQSRG
Mex     NAGSGIIISDTPVHDCNTTCQTPKGAINTSLPFQNIHPITIGKCPKYVKSTKLRLATGLRNVPSIQSRG
Human   GWYGYHHQNEQGSGYAADQKSTQNAINGILYHTENAYVSVVSSHYSRRFTPEIAKRPKVRDQEGRINYY

NewCal  LFGAIAGFIEGGWTGMVDGWYGYHHQNEQGSGYAADQKSTQNAINGITNKVNSVIEKMNTQFTAVGKEF
Mex     LFGAIAGFIEGGWTGMVDGWYGYHHQNEQGSGYAADLKSTQNAIDEITNKVNSVIEKMNTQFTAVGKEF
Human   WTLLEPGDTIIFEANGNLIAPRYAFALSRGFGSGIITSNAPMDECDATNKVNSVIEKMNTQFTAVGKEF

NewCal  NKLERRMENLNKKVDDGFLDIWTYNAELLVLLENERTLDFHDSNVKNLYEKVKSQLKNNAKEIGNGCFE
Mex     NHLEKRIENLNKKVDDGFLDIWTYNAELLVLLENERTLDYHDSNVKNLYEKVRSQLKNNAKEIGNGCFE
Human   NKLERRMENLNKKVDDGFLDIWTYNAELLVLLENERTLDFHDSNVKNLYEKVKSQLKNNAKEIGNGCFE

NewCal  FYHKCNNECMESVKNGTYDYPKYSEESKLNREKIDGVKLESMGVYQILAIYSTVASSLVLLVSLGAISF
Mex     FYHKCDNTCMESVKNGTYDYPKYSEEAKLNREEIDGVKLESTRIYQILAIYSTVASSLVLVVSLGAISF
Human   FYHKCNDECMESVKNGTYDYPKYSEESKLNREKIDGVKLESMGVYQILAIYSTVASSLVLLVSLGAISF

NewCal  WMCSNGSLQCRIC-
Mex     WMCSNGSLQCRICI
Human   WMCSNGSLQCRICI
```

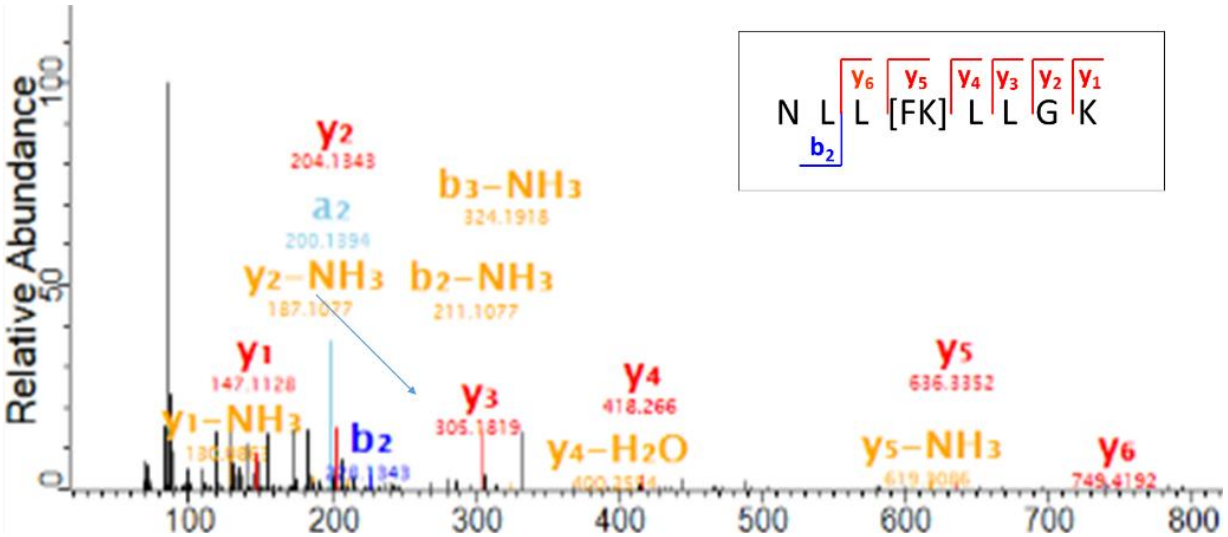

Figure A-1 MS/MS analysis of Orbitrap MS peak. The inset shows the amino acid residues, indicating NLLWLLGK was oxidized to NLL[FK]LLGK, tryptophan oxidized to N-formylkynurenine.

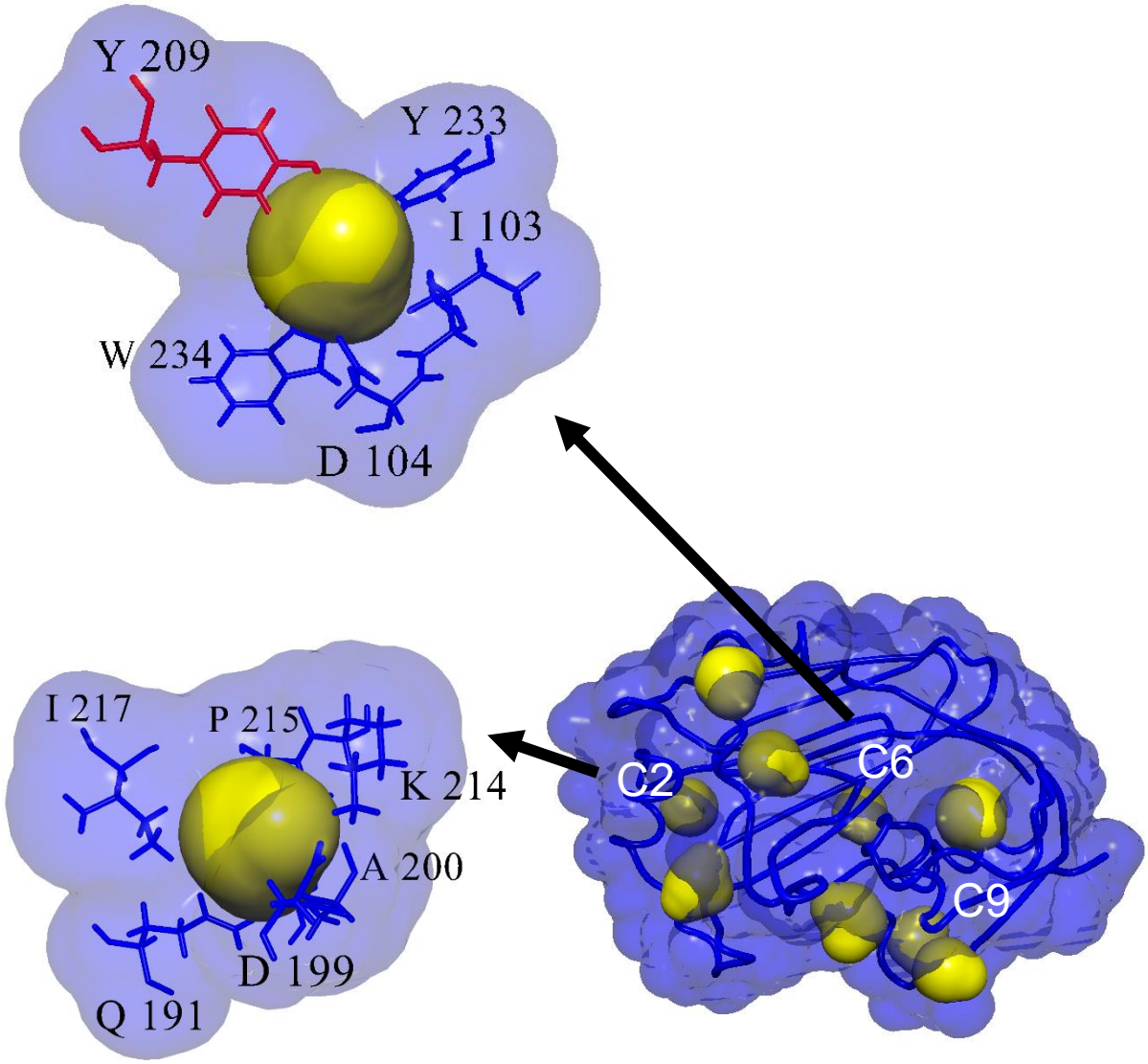

Figure A-2 Amino acids of the chlorine dioxide docking conformation with the second highest binding energy. The tyrosine highlighted in red was identified as modified in the experimental MS analysis. The chlorine dioxide solvent accessible surface area is depicted in yellow. The HA protein is shown in transparent blue.

Appendix B. Supplementary Information for Chapter 3

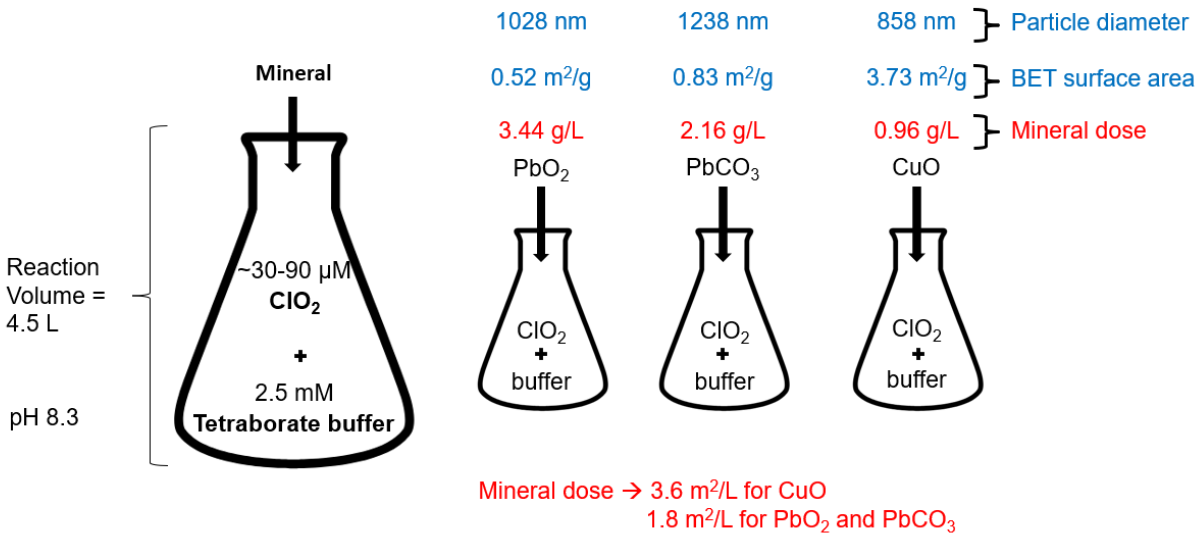

Figure B-1 Graphic illustration of batch reactions and experimental parameters.

Table B-1 Characteristics and concentrations of scale minerals used in batch reactions.

Compound	BET surface area ($m^2 g^{-1}$)	Particle diameter (nm)	Reaction surface area ($m^2 L^{-1}$)	Mass concentration ($g L^{-1}$)
PbO_2	0.52	1028	1.8	3.4
$PbCO_3$	0.83	1238	1.8	2.2
CuO	3.73	858	3.6	0.96

Rate models

Six different rate models were considered for the analysis of chlorine dioxide decay: first-order, second-order, mixed-order (simultaneous first and second order reactions), and two-phase (two simultaneous first-order reactions), and pseudo-first and pseudo-second order adsorption models. Despite matching the proposed reaction mechanism, first-order models were significantly worse than any of the other models. When fitted to a two-phase model, the R^2 values improve over a second-order or mixed-order model (Table B-2). P-values for both models indicated evidence of an inadequate model for the second and mixed order decay, but an adequate model for two phase decay.

The mixed-order model was used in previous studies observing chlorine dioxide decomposition in basic solutions.[123] The rate constants essentially followed a second order decay, with the first order rate constant essential equal to zero. A second order model fit the pH 8.3 data best. At phases above and below the zero-point pH there is an initial phase of lead oxide surface reacting with chlorine dioxide. As the experiment progresses the lead surface becomes populated with charged ions, positive or negative depending on whether the experiment was conducted above or below the point of zero charge. The kinetic rates slow as the surface becomes blocked for chlorine dioxide adsorption. Perhaps these surface interactions are incorporated into the two-phase model, where the phases represent (1) the first-order reaction of chlorine dioxide on the lead surface, and (2) the reduction of surface sites for the reaction to take place.

The final two rate models considered, pseudo-first (Equation 5) and pseudo-second order (Equation 6), were chosen to incorporate adsorption into the chlorine dioxide decay rate constants. The rate laws are based on adsorption kinetics and the capacity of the sorbent.[124,130] These models have been used in the adsorption of free chlorine adsorption on lead (IV) oxide at different pH

values. For the chlorine dioxide model, adsorbed chlorine dioxide was taken to be the difference between initial chlorine dioxide concentration and the concentration at time t.

$$log(q_e - q_t) = \log q_e - \frac{k_1}{2.303} t \qquad (5)$$

$$\frac{t}{q_t} = \frac{1}{k_2 q_e^2} + \frac{1}{q_e} t \qquad (6)$$

Chlorine dioxide adsorption follows the pseudo-second order adsorption based on the R^2 values. These results suggest that hydroxide ions are in excess and then the reaction is dependent on chlorine dioxide concentration. Previously published work demonstrated copper, nickel, and iron enhancement of chlorine dioxide decay followed a second-order dependence on chlorine dioxide.[51]

A secondary consideration is the phase of the lead mineral itself. The oxidation-reduction potential for chlorine dioxide is high,[55] and for pH levels relevant to drinking water, lead (IV) oxide is favored to form.[52,53] At lower pH, the mineral surface could be changing composition to lead carbonate, which has a slower reaction rate with chlorine dioxide than lead oxide. The phase shift from lead (IV) oxide to lead (II) carbonate could also point to why a second order model is statistically unfavorable at pH less than 7. In this case the first phase rate constant corresponds to the presence of lead oxide and is more rapid than the second phase rate constant, corresponding to a new surface of lead carbonate.

Table B-2 Rate constants and R^2 values for three different exponential decay models fit to chlorine dioxide decay in the presence of lead oxide at varying pH values.

pH	Mixed order decay			Second order decay		Pseudo-second order adsorption	
	Rate		R^2	Rate	R^2	Rate	R^2
	First (s^{-1})	Second (M^{-1} s^{-1})		(M^{-1} s^{-1})		(M^{-1} s^{-1})	
5.9	0.0001±1.4	11.7±3.5	0.58	14.1±3.4	0.58	267.6±0.7	0.994
7.4	0.0006±27	61.1±9.0	0.92	58.5±8.2	0.92	166.3±0.4	0.988
8.3	0.0020±189	217±46	0.98	203.0±22	0.98	290.4±0.1	0.999
9.7	0.0003±9.8	25.8±4.2	0.87	25.6±3.9	0.87	156.0±0.9	0.968
10.4	0.0011±557	20.9±5.0	0.76	19.7±4.4	0.76	87.8±0.7	0.965

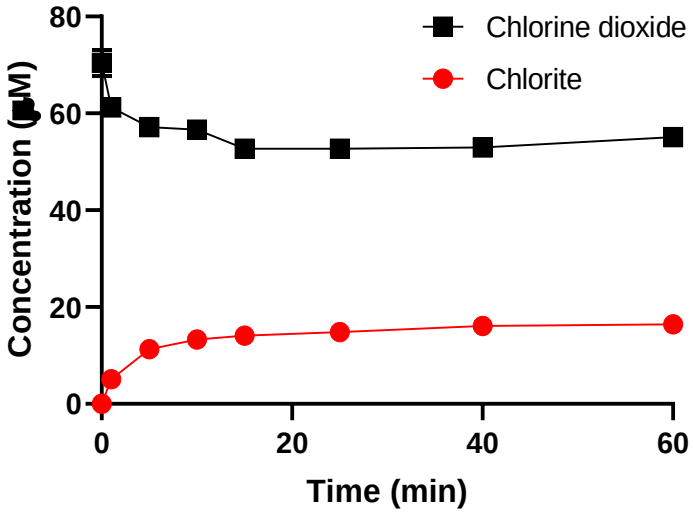

Figure B-2 Chlorine dioxide decay and chlorite formation in an unbuffered batch reaction with PbO_2. Each data point represents the mean and standard deviation of duplicate experiments. If error bars were shorter than the symbol, they were removed.

Electron supply

The two unbuffered batch reactions were done in Milli-Q water, a starting chlorine dioxide concentration of about 70 μM, and the same PbO_2 concentration as the buffered reactions. They were performed to confirm the oxidation of water via pH measurements.

Chlorine dioxide oxidizes water (eq 1).

$$ClO_2 + \frac{1}{2}H_2O = \frac{1}{4}O_2 + ClO_2^- + H^+ \quad (1)$$

In an unbuffered system this corresponds to a drop in pH (eq 2 and 3):

$$\Delta ClO_2 \text{ moles} = H^+ \text{ moles} \quad (2)$$

$$pH = -\log [H^+] \quad (3)$$

The change in chlorine dioxide concentration in both replicates of the unbuffered batch reaction had a theoretical pH of 4.76 and 4.79, and measured pH of 5.1 and 4.8 respectively.

Figure B-3 Lead carbonate batch reaction over the course of one hour. Image 1 was taken immediately upon the addition of lead carbonate. Images 2 and 3 are taken after late batch reaction samples.

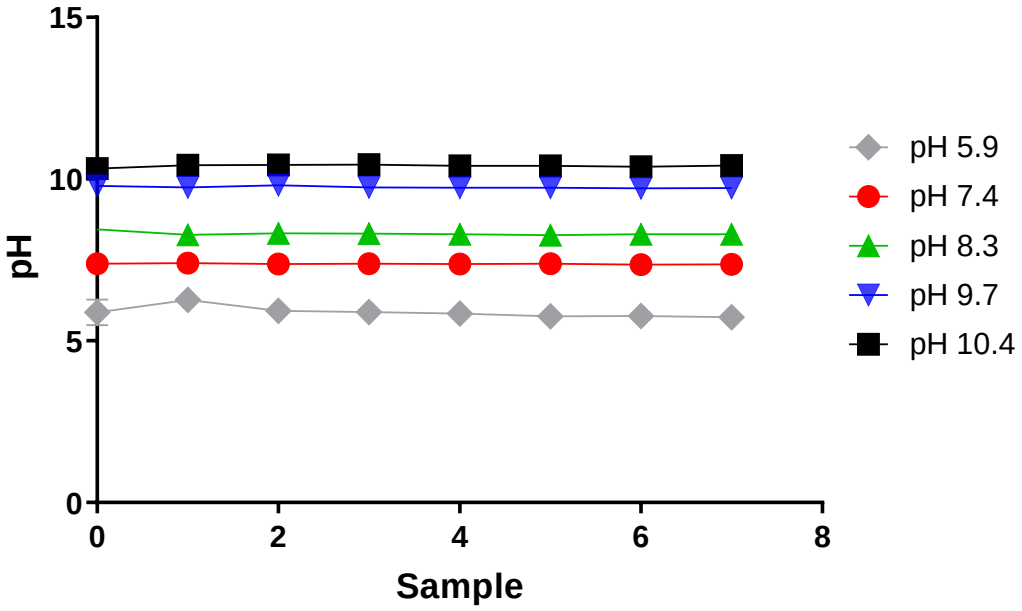

Figure B-4 Variation in pH during pH batch experiments corresponding to Figure 3. At pH 5.9 and pH 7.4 the variation was 0.5. Above pH 8.3 there was less than 0.03 change in pH.

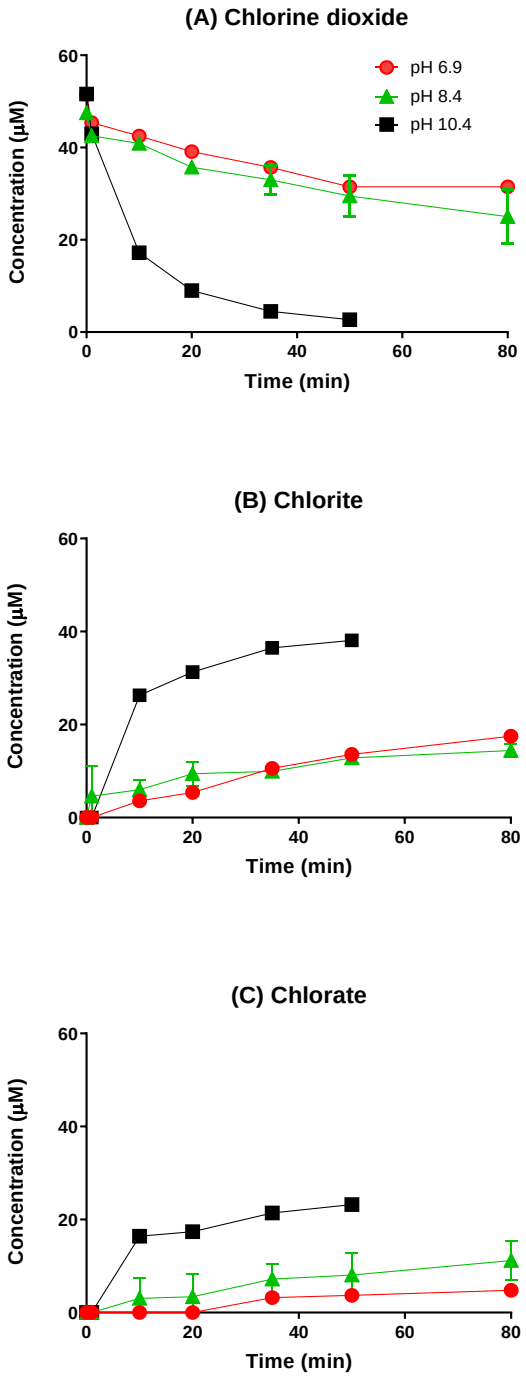

Figure B-5 (A) Chlorine dioxide decay, (B) chlorite formation, and (C) chlorate formation in batch reactions containing chlorine dioxide and cupric oxide at three different pH values. Each data point represents the mean and standard deviation of duplicate experiments. If error bars were shorter than the symbol, they were removed.

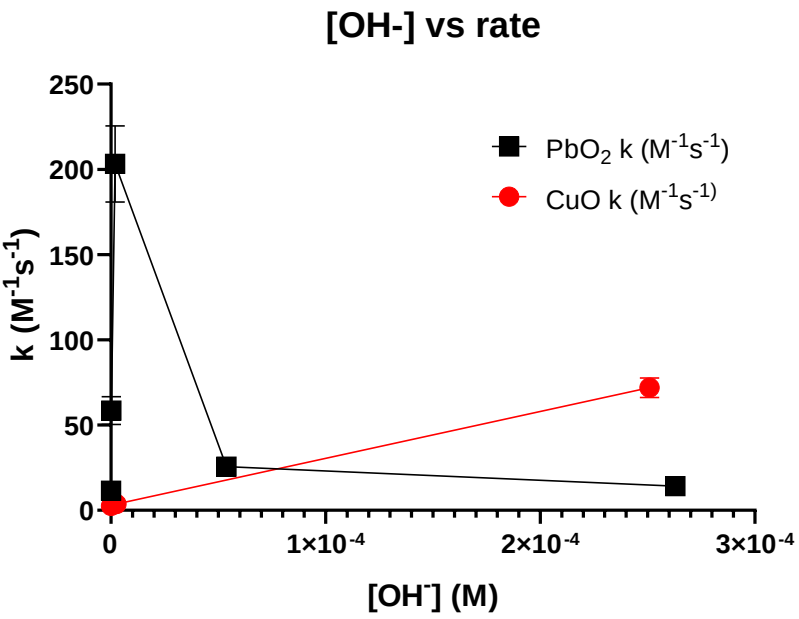

Figure B-6 Relationship between measured second-order rate constants and hydroxide concentration. Batch experiments with CuO showed a linear dependence on [OH-], while PbO_2 showed no dependence and a maximal rate at pOH 5.7 (pH 8.3).

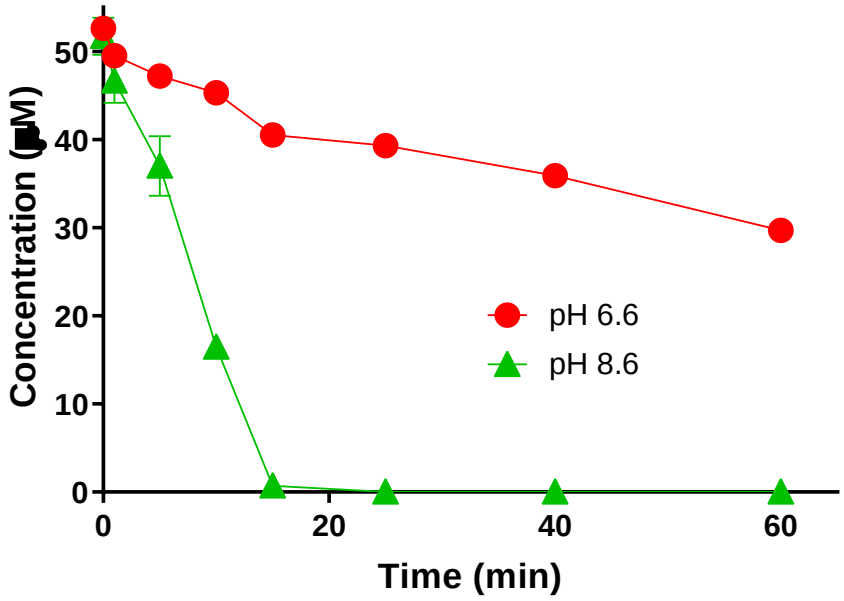

Figure B-7 Chlorine dioxide decay in batch reactions at different pH and in the presence of lead carbonate. Each data point represents the mean and standard deviation of duplicate experiments. If error bars were shorter than the symbol, they were removed.

Appendix C. Supplementary Information for Chapter 4

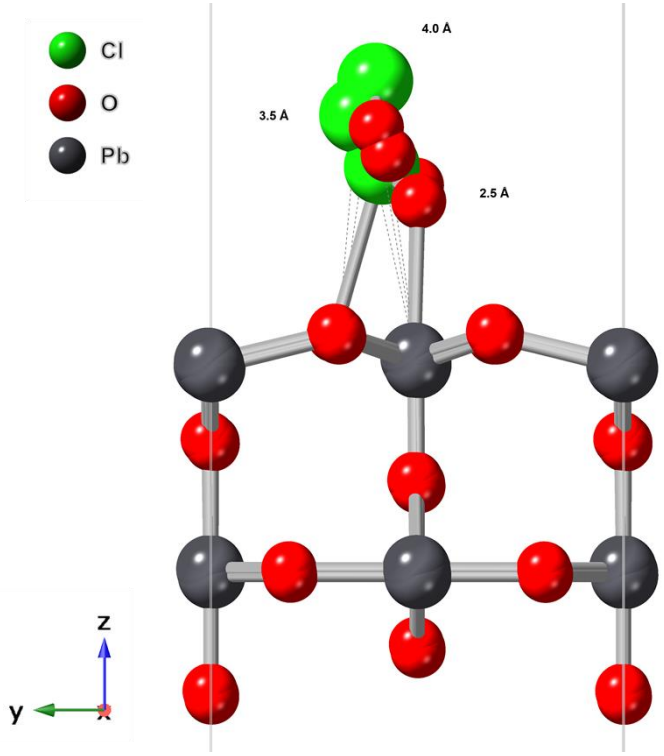

Figure C-1 Side view of the optimized configurations of adsorbed chlorine dioxide on lead oxide surface. The distances in angstroms represent the initial distance of the chlorine atom from the nearest surface oxygen atom. Chlorine, oxygen, and lead atoms are represented by green, red, and grey spheres respectively.

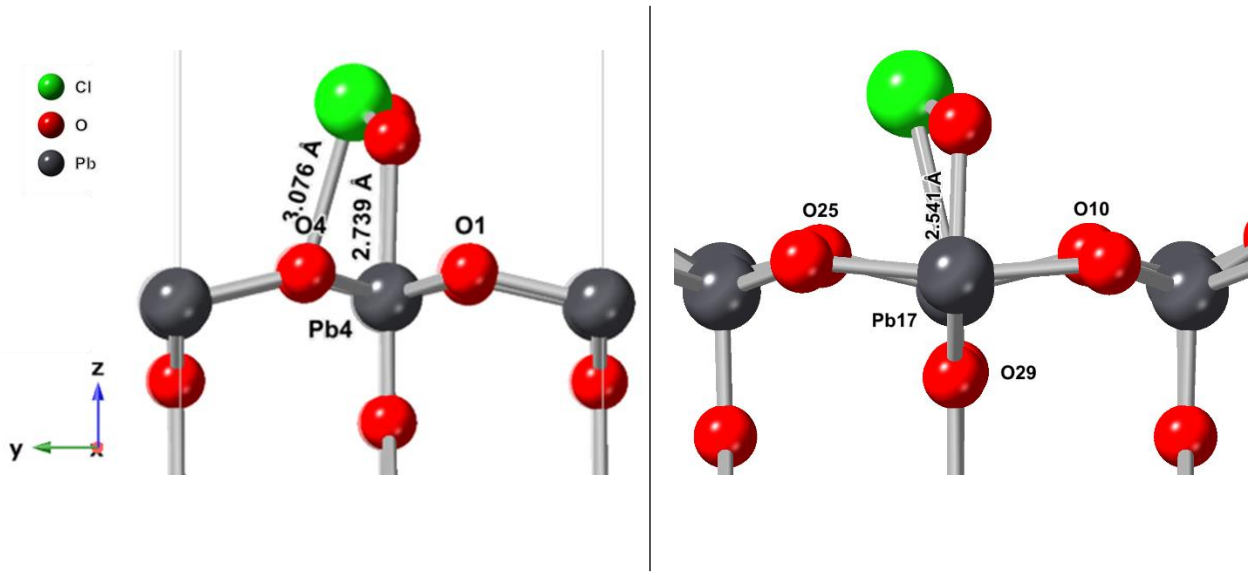

Figure C-2 Two configurations found on the 60-atom lead oxide surface. The configuration on the left is slightly more favorable in terms of adsorption energy.

Table C-1 Variation in adsorption energy of chlorine dioxide on the lead oxide surface depending on number of atoms in the system. The total energy and energy normalized by atom number are shown.

Atoms	Energy (eV)	Energy (eV/atom)
20	-0.359	-0.016
40	-0.871	-0.020
60	-0.977	-0.016
80	-1.243	-0.015

Table C-2 Total energies and zero-point energy correction calculated in Gaussian of species in the two pathways presented in Scheme 1. Literature values are shown for comparison.[123,136]

Molecule	**Calculated**		**Literature**	
	6-311++g(3df,3pd) (Hartrees)	**ZPE (kcal/mol)**	**6-311++g(3df,3pd) (Hartrees)**	**ZPE (kcal/mol)**
ClO_2	-610.5493027	3.62	-610.549303	3.6
ClO_2^-	-610.622099	2.86	-610.626663	2.9
H_2O	-76.443196	13.38	-76.464512	13.4
OH^-	-75.8309271	5.38	-75.830927	5.4
ClO_2ClO_2	-1221.091561	9.03	-1221.0901446	8.6
$OHClO_2$	-686.341628	13.14	-686.362561	13.1
OClOOH-	-686.4246207	10.32	-686.414346	11.2
TS: $OHClO_3ClO$	-1293.087427	13.34		

Bibliography

1. Rodríguez-Lázaro, D. *et al.* Virus hazards from food, water and other contaminated environments. *FEMS Microbiol. Rev.* **36**, 786–814 (2012).

2. Morino, H., Fukuda, T., Miura, T. & Shibata, T. Effect of low-concentration chlorine dioxide gas against bacteria and viruses on a glass surface in wet environments. *Lett. Appl. Microbiol.* **53**, 628–634 (2011).

3. Greatorex, J. S. *et al.* Effectiveness of common household cleaning agents in reducing the viability of human influenza A/H1N1. *PLoS One* **5**, 1–5 (2010).

4. Ooi, B. G. & Branning, S. A. Correlation of Conformational Changes and Protein Degradation with Loss of Lysozyme Activity Due to Chlorine Dioxide Treatment. *Appl. Biochem. Biotechnol.* **182**, 782–791 (2017).

5. Deborde, M. & von Gunten, U. Reactions of chlorine with inorganic and organic compounds during water treatment-Kinetics and mechanisms: A critical review. *Water Res.* **42**, 13–51 (2008).

6. Edzwald, J. *Water Quality & Treatment: A Handbook on Drinking Water*. (McGraw-Hill, 2010).

7. Richardson, S. D. *et al.* Identification of new drinking water disinfection by-products from ozone, chlorine dioxide, chloramine, and chlorine. *Environ. Prot.* **123**, 95–102 (2000).

8. Charrois, J. W. A. & Hrudey, S. E. Breakpoint chlorination and free-chlorine contact time: Implications for drinking water N-nitrosodimethylamine concentrations. *Water Res.* **41**, 674–682 (2007).

9. Walker, J. T. *et al.* Control of Legionella pneumophila in a hospital water system by chlorine dioxide. 384–390 (1995).

10. Junli, H., Li, W., Nanqi, R. & Ma, F. Disinfection effect of chlorine dioxide on bacteria in water. *Water Res.* **31**, 607–613 (1997).

11. Aieta, M., Berg, J. D., Roberts, P. V. & Cooper, R. C. Comparison of Chlorine Dioxide and Chlorine in Wastewater Disinfection. *J. Water Pollut. Control Fed.* **52**, 810–822 (1980).

12. Gagnon, G. A. *et al.* Comparative analysis of chlorine dioxide, free chlorine and chloramines on bacterial water quality in model distribution systems. *J. Environ. Eng.* **130**, 1269–1279 (2004).

13. EPA. Drinking Water Treatment Plant Residuals Management. Technical Report: Summary of Residuals Generation, Treatment, and Disposal at Large Community Water Systems. (2011).

14. Wigginton, K. R., Pecson, B. M., Sigstam, T., Bosshard, F. & Kohn, T. Virus inactivation mechanisms: Impact of disinfectants on virus function and structural integrity. *Environ. Sci. Technol.* **46**, 12069–12078 (2012).

15. Sigstam, T. *et al.* Subtle differences in virus composition affect disinfection kinetics and mechanisms. *Appl. Environ. Microbiol.* **79**, 3455–3467 (2013).

16. Wigginton, K. R. *et al.* UV radiation induces genome-mediated, site-specific cleavage in viral proteins. *Chembiochem* **13**, 837–45 (2012).

17. Rule Wigginton, K., Menin, L., Montoya, J. P. & Kohn, T. Oxidation of virus proteins during UV254 and singlet oxygen mediated inactivation. *Environ. Sci. Technol.* **44**, 5437–5443 (2010).

18. Richardson, S. D. *et al.* Multispectral identification of chlorine dioxide disinfection byproducts in drinking water. *Environ. Sci. Technol.* **28**, 592–9 (1994).

19. Sigstam, T., Rohatschek, A., Zhong, Q., Brennecke, M. & Kohn, T. On the cause of the tailing phenomenon during virus disinfection by chlorine dioxide. *Water Res.* **48**, 82–9 (2014).

20. Ogata, N. Inactivation of influenza virus haemagglutinin by chlorine dioxide: Oxidation of the conserved tryptophan 153 residue in the receptor-binding site. *J. Gen. Virol.* **93**, 2558–2563 (2012).

21. Richardson, S. D., Plewa, M. J., Wagner, E. D., Schoeny, R. & DeMarini, D. M. Occurrence, genotoxicity, and carcinogenicity of regulated and emerging disinfection by-products in drinking water: A review and roadmap for research. *Mutat. Res. - Rev. Mutat. Res.* **636**, 178–242 (2007).

22. Davis, C. C. & Edwards, M. Coagulation With Hydrolyzing Metal Salts: Mechanisms and Water Quality Impacts. *Crit. Rev. Environ. Sci. Technol.* **44**, 303–347 (2014).

23. Shannon, M. a *et al.* Science and technology for water purification in the coming decades. *Nature* **452**, 301–10 (2008).

24. Richardson, S. Disinfection by-products and other emerging contaminants in drinking water. *TrAC Trends Anal. Chem.* **22**, 666–684 (2003).

25. Jeong, C. H. *et al.* Occurrence and toxicity of disinfection byproducts in European drinking waters in relation with the HIWATE epidemiology study. *Environ. Sci. Technol.* **46**, 12120–12128 (2012).

26. Sadiq, R. & Rodriguez, M. J. Disinfection by-products (DBPs) in drinking water and predictive models for their occurrence: a review. *Sci. Total Environ.* **321**, 21–46 (2004).

27. Rook, J. J. Haloforms in drinking water. *J. / Am. Water Work. Assoc.* **68**, 168–172 (1976).

28. Rook, J. J. Chlorination reactions of fulvic acids in natural waters. *Environ. Sci. Technol.* **2**, 478–482 (1975).

29. Shah, A. D. & Mitch, W. A. Halonitroalkanes, Halonitriles, Haloamides, and N-Nitrosamines: A Critical Review of Nitrogenous Disinfection Byproduct Formation Pathways. *Environ. Sci. Technol.* **46**, 119–131 (2012).

30. Hrudey, S. E. Chlorination disinfection by-products, public health risk tradeoffs and me. *Water Res.* **43**, 2057–2092 (2009).

31. Guo, Z. *et al.* Factors affecting THM , HAN and HNM formation during UV-chlor (am) ination of drinking water. (2016).

32. Gan, W., Bond, T., Yang, X. & Westerhoff, P. Role of Chlorine Dioxide in N - Nitrosodimethylamine Formation from Oxidation of Model Amines. *Environ. Sci. Technol.* 11429–11437 (2015).

33. Muellner, M. G. *et al.* Haloacetonitriles vs. regulated haloacetic acids: Are nitrogen-containing DBFs more toxic? *Environ. Sci. Technol.* **41**, 645–651 (2007).

34. EPA. National primary drinking water regulations: Long Term 1 Enhanced Surface Water Treatment Rule. Final rule. *Fed. Regist.* **67**, 1811–1844 (2002).

35. Edwards, M. & Triantafyllidou, S. Chloride-to-sulfate mass ratio and lead leaching to water. *J. / Am. Water Work. Assoc.* **99**, (2007).

36. Nguyen, C. K., Stone, K. R., Dudi, A. & Edwards, M. A. Corrosive microenvironments at lead solder surfaces arising from galvanic corrosion with copper pipe. *Environ. Sci. Technol.* **44**, 7076–7081 (2010).

37. Edwards, M. & Dudi, A. Role of chlorine and chloramine in corrosion of lead-bearing plumbing materials. *J. Am. Water Work. Assoc.* **96**, (2004).

38. Weinberg, H. S., Delcomyn, C. A. & Unnam, V. Bromate in Chlorinated Drinking Waters : Occurrence and Implications for Future Regulation Bromate in Chlorinated Drinking Waters : Occurrence and Implications for Future Regulation. **37**, 3104–3110 (2003).

39. Krasner, S. W. *et al.* The Occurrence of a New Generation of Disinfection By-Products S1 S2. *Environ. Sci. Technol.* **40**, 7175–7185 (2006).

40. Zhang, J. *et al.* Role of NOM molecular size on iodo-trihalomethane formation during chlorination and chloramination. *Water Res.* **102**, (2016).

41. Korn, C., Andrews, R. C. & Escobar, M. D. Development of chlorine dioxide-related by-product models for drinking water treatment. *Water Res.* **36**, 330–342 (2002).

42. WHO. Chemistry of Disinfectants and Disinfectant By-Products. in *Environmental Health Criteria 216: Disinfectants Disinfectant By- products* 27–109 (World Health Organization, 2000).

43. EPA. *U.S. Environmental Protection Agency 2009a National Primary Drinking Water Standards and National Secondary Drinking Water Standards.*

44. Agency, U. E. P. *National Primary Drinking Water Regulations: Control of Lead and Copper*. (56 FR 26548, June 7, 1991, 1991).

45. Guidotti, T. L. *et al.* Elevated lead in drinking water in Washington, DC, 2003-2004: The public health response. *Environ. Health Perspect.* **115**, 695–701 (2007).

46. Järup, L. Hazards of heavy metal contamination. *Br. Med. Bull.* **68**, 167–182 (2003).

47. Edwards, M., Triantafyllidou, S. & Best, D. Elevated Blood Lead in Young Children Due to Lead-Contaminated Drinking Water: Washington, DC, 2001-2004. *Environ. Sci. Technol.* **43**, 1618–1623 (2009).

48. Boyd, G. R. *et al.* Effects of Changing Disinfectants on Lead and Copper Release. *J. Am. Water Work. Assoc.* **100**, 75–87 (2009).

49. Cantor, A. F., Park, J. K. & Vaiyavatjamai, P. Effect of chlorine on corrosion in drinking water systems. *J. / Am. Water Work. Assoc.* **95**, 112–122 (2003).

50. Lin, N. H., Torrents, A., Davis, A. P., Zeinali, M. & Taylor, F. A. Lead corrosion control from lead, copper-lead solder, and brass coupons in drinking water employing free and combined chlorine. *J. Environ. Sci. Heal. Part A Environ. Sci. Eng. Toxicol.* **32**, 865–884 (1997).

51. Liu, C., Von Gunten, U. & Croue, J.-P. P. Enhanced chlorine dioxide decay in the presence of metal oxides: Relevance to drinking water distribution systems. *Environ. Sci. Technol.* **47**, 8365–8372 (2013).

52. Lytle, D. A., Schock, M. R. & Scheckel, K. The inhibition of Pb(IV) oxide formation in chlorinated water by orthophosphate. *Environ. Sci. Technol.* **43**, 6624–6631 (2009).

53. Lytle, D. A. & Schock, M. R. Formation of Pb(IV) oxides in chlorinated water. *J. / Am. Water Work. Assoc.* **97**, 102–114 (2005).

54. Schock, M. R. Understanding Corrosion Control Strategies for Lead. *Am. Water Work. Assoc.* **81**, 88–100 (1989).

55. James, C., Copeland, R. & Lytle, D. Relationships between oxidation-reduction potential, oxidant, and pH in drinking water. *Proc. AWWA Water Qual. Technol. Conf.* 1–13 (2004).

56. Xie, Y. Dissolution , Formation , and Transformation of the Lead Corrosion Product PbO 2 : Rates and Mechanisms of Reactions that Control Lead Release in Drinking Water Distribution Systems. *Diss. Washingt. Univ. Open Scholarsh.* (2010).

57. Kim, E. J. & Herrera, J. E. Characteristics of lead corrosion scales formed during drinking water distribution and their potential influence on the release of lead and other contaminants. *Environ. Sci. Technol.* **44**, 6054–6061 (2010).

58. Xie, Y. & Giammar, D. E. Effects of flow and water chemistry on lead release rates from pipe scales. *Water Res.* **45**, 6525–6534 (2011).

59. Lin, Y. & Valentine, R. L. The Release of Lead from the Reduction of Lead Oxide (PbO_2) by Natural Organic Matter. *Environ. Sci. Technol.* **42**, 760–765 (2008).

60. Noel, J. D., Wang, Y. & Giammar, D. E. Effect of water chemistry on the dissolution rate of the lead corrosion product hydrocerussite. *Water Res.* **54**, 237–46 (2014).

61. Xie, Y., Wang, Y., Singhal, V. & Giammar, D. E. Effects of pH and carbonate concentration on dissolution rates of the lead corrosion product PbO_2. *Environ. Sci. Technol.* **44**, 1093–1099 (2010).

62. Edwards, M. & McNeill, L. S. Effect of phosphate inhibitors on lead release from pipes. *J. / Am. Water Work. Assoc.* **94**, 79–90 (2002).

63. Dodrill, D. & Edwards, M. Corrosion control. *Am. Water Work. Assoc.* 74–85 (1995).

64. AWWA Disinfection Committee. Committee Report : Disinfection Survey , Part 2- Alternatives , experiences , and future plans. *J. AWWA* **100**, 110–124 (2008).

65. Junli, H. *et al.* Disinfection effect of chlorine dioxide on viruses, algae and animal planktons in water. *Water Res.* **31**, 455–460 (1997).

66. Wilczak, A. *et al.* Occurrence of nitrification in chloraminated distribution systems. *J. / Am. Water Work. Assoc.* **88**, 74–85 (1996).

67. USEPA. Comprehensive Disinfectants and Disinfection Byproducts Rules (Stage 1 and Stage 2): Quick Reference Guide Overview of the Rules. 2–5 (2010).

68. Reckhow, D. a, Singer, P. C. & Malcolm, R. L. Chlorination of humic materials: Byproduct formation and chemical interpretations. *Environ. Sci. Technol.* **24**, 1655–1664 (1990).

69. Yang, X., Guo, W. & Lee, W. Formation of disinfection byproducts upon chlorine dioxide preoxidation followed by chlorination or chloramination of natural organic matter. *Chemosphere* **91**, 1477–1485 (2013).

70. Sorlini, S., Gialdini, F., Biasibetti, M. & Collivignarelli, C. Influence of drinking water treatments on chlorine dioxide consumption and chlorite/chlorate formation. *Water Res.* **54**, 44–52 (2014).

71. Henderson, R., Carlson, K. & Gregory, D. The impact of ferrous ion reduction of chlorite ion on drinking water process performance. *Water Res.* **35**, 4464–4473 (2001).

72. Sorlini, S. & Collivignarelli, C. Chlorite removal with ferrous ions. *Desalination* **176**, 267–271 (2005).

73. Katz, A. & Narkis, N. Removal of chlorine dioxide disinfection by-products by ferrous salts. *Water Res.* **35**, 101–108 (2001).

74. Hoehn, R. C. *et al.* ClO_2 and By-Product Persistence in a Drinking Water System. *Awwa* **95**, 141–150 (2003).

75. Oleg, T. & Olson, A. J. AutoDock Vina: Improving the speed and accuracy of docking with a new scoring function, efficient optimization, and multithreading. *J. Comput. Chem.* **31**, 455–461 (2009).

76. Li, H., Leung, K. S., Wong, M. H. & Ballester, P. J. Improving autodock vina using random forest: The growing accuracy of binding affinity prediction by the effective exploitation of larger data sets. *Mol. Inform.* **34**, 115–126 (2015).

77. Forli, S. *et al.* Computational protein-ligand docking and virtual drug screening with the AutoDock suite. *Nat. Protoc.* **11**, 905–919 (2016).

78. Friesner, R. Ab initio quantum chemistry: methodology and applications. *Proc. Natl. Acad. Sci. U. S. A.* **102**, 6648–6653 (2005).

79. Allen, M. P., Attig, N., Binder, K., Grubm, H. & Eds, K. K. Introduction to Molecular Dynamics Simulation Introduction to Molecular Dynamics Simulation. **23**, (2004).

80. Cramer, C. J. & Truhlar, D. G. Density functional theory for transition metals and transition metal chemistry. *Phys. Chem. Chem. Phys.* **11**, 10757–10816 (2009).

81. Sholl, D. & Steckel, J. *Density functional theory: a practical introduction*. *Annual Review of Physical Chemistry* **7**, (John Wiley & Sons, Inc., 2011).

82. Cheng, G. J., Zhang, X., Chung, L. W., Xu, L. & Wu, Y. D. Computational organic chemistry: Bridging theory and experiment in establishing the mechanisms of chemical reactions. *J. Am. Chem. Soc.* **137**, 1706–1725 (2015).

83. Zhang, Y.-Q. *et al.* Homo-coupling of terminal alkynes on a noble metal surface. *Nat. Commun.* **3**, 1286 (2012).

84. Foti, M. C., Daquino, C., Mackie, I. D., DiLabio, G. A. & Ingold, K. U. Reaction of phenols with the 2,2-diphenyl-1-picrylhydrazyl radical. Kinetics and DFT calculations applied to determine ArO-H bond dissociation enthalpies and reaction mechanism. *J. Org. Chem.* **73**, 9270–9282 (2008).

85. Stirling, A. S., Nair, N. N., Lledó, A. & Ujaque, G. Challenges in modelling homogeneous catalysis: new answers from ab initio molecular dynamics to the controversy over the Wacker process. *Chem. Soc. Rev.* **43**, 4940–4952 (2014).

86. Yuan, C. *et al.* Metal-free oxidation of aromatic carbon–hydrogen bonds through a reverse-rebound mechanism. *Nature* **499**, 192–196 (2013).

87. Mu, R., Zhao, Z. J., Dohnálek, Z. & Gong, J. Structural motifs of water on metal oxide surfaces. *Chem. Soc. Rev.* **46**, 1785–1806 (2017).

88. Wu, X., Selloni, A. & Nayak, S. K. First principles study of CO oxidation on TiO 2(110): The role of surface oxygen vacancies. *J. Chem. Phys.* **120**, 4512–4516 (2004).

89. Sorescu, D. C. *et al.* Coadsorption properties of CO_2 and H_2O on TiO_2 rutile (110): A dispersion-corrected DFT study Coadsorption properties of CO_2 and H_2O on TiO_2 rutile (110): A dispersion-corrected DFT study. **074704**, (2017).

90. Matthiesen, J. *et al.* Formation and diffusion of water dimers on rutile TiO_2(110). *Phys. Rev. Lett.* **102**, 2–5 (2009).

91. Sieben, C. *et al.* Influenza virus binds its host cell using multiple dynamic interactions. *Proc. Natl. Acad. Sci. U. S. A.* **109**, 13626–31 (2012).

92. Childs, R. A. *et al.* Receptor-binding specificity of pandemic influenza A (H1N1) 2009 virus determined by carbohydrate microarray. *Nat. Biotechnol.* **27**, 797–9 (2009).

93. Xu, R., McBride, R., Nycholat, C. M., Paulson, J. C. & Wilson, I. A. Structural characterization of the hemagglutinin receptor specificity from the 2009 H1N1 influenza pandemic. *J. Virol.* **86**, 982–990 (2012).

94. Neumann, G., Noda, T. & Kawaoka, Y. Emergence and pandemic potential of swine-origin H1N1 influenza virus. *Nature* **459**, 931–9 (2009).

95. Lénès, D. *et al.* Assessment of the removal and inactivation of influenza viruses H5N1

and H1N1 by drinking water treatment. *Water Res.* **44**, 2473–2486 (2010).

96. Chan, M. C. W., Lee, N., Chan, P. K. S., Leung, T. F. & Sung, J. J. Y. Fecal detection of influenza A virus in patients with concurrent respiratory and gastrointestinal symptoms. *J. Clin. Virol.* **45**, 208–211 (2009).

97. Ogata, N. & Shibata, T. Protective effect of low-concentration chlorine dioxide gas against influenza A virus infection. *J. Gen. Virol.* **89**, 60–67 (2008).

98. Shibata, T. *et al.* Inactivation of Airborne Bacteria and Viruses Using Extremely Low Concentrations of Chlorine Dioxide Gas. *Pharmacology* **97**, 301–306 (2016).

99. Gamblin, S. *et al.* The structure and receptor binding properties of the 1918 influenza hemagglutinin. *Science* **303**, 1838–42 (2004).

100. Ogata, N. Denaturation of protein by chlorine dioxide: Oxidative modification of tryptophan and tyrosine residues. *Biochemistry* **46**, 4898–4911 (2007).

101. Furman, C. S. & Margerum, D. W. Mechanism of Chlorine Dioxide and Chlorate Ion Formation from the Reaction of Hypobromous Acid and Chlorite Ion. *Inorg. Chem.* **37**, 4321–4327 (1998).

102. Krieger, E. & Vriend, G. YASARA View molecular graphics for all devices from smartphones to workstations. *Bioinformatics* **30**, 2981–2982 (2014).

103. Garrett, M. M. *et al.* AutoDock4 and AutoDockTools4: Automated docking with selective receptor flexibility. *J. Comput. Chem.* **30**, 2785–2791 (2009).

104. DuBois, R. M. *et al.* The Receptor-Binding Domain of Influenza Virus Hemagglutinin Produced in Escherichia coli Folds into Its Native, Immunogenic Structure. *J. Virol.* **85**, 865–872 (2011).

105. Duan, Y. *et al.* A point-charge force field for molecular mechanics simulations of proteins based on condensed-phase quantum mechanical calculations. *J. Comput. Chem.* **24**, 1999–2012 (2013)

106. Spande, T. F., Green, N. M. & Witkop, B. The Reactivity toward N-Bromosuccinimide of Tryptophan in Enzymes, Zymogens, and Inhibited Enzymes. *Biochemistry* **5**, 1926–1933 (1966).

107. Spande, T. F. & Witkop, B. Determination of the tryptophan content of proteins with N-bromosuccinimide. *Methods Enzymol.* **11**, 498–506 (1967).

108. Pence, H. E. & Williams, A. Chemspider: An online chemical information resource. *J. Chem. Educ.* **87**, 1123–1124 (2010).

109. Skehel, J. J. & Wiley, D. C. Receptor Binding and Membrane Fusion in Virus Entry: The Influenza Hemagglutinin. *Annu. Rev. Biochem.* **69**, 531–569 (2000).

110. Matrosovich, M. *et al.* Early alterations of the receptor-binding properties of H1, H2, and H3 avian influenza virus hemagglutinins after their introduction into mammals. *J. Virol.* **74**, 8502–8512 (2000).

111. Ehrenshaft, M. *et al.* Immunological detection of N-formylkynurenine in oxidized proteins. *Free Radic. Biol. Med.* **46**, 1260–1266 (2009).

112. Kuntz, I. D., Chen, K., Sharp, K. A. & Kollman, P. A. The maximal affinity of ligands. *Proc. Natl. Acad. Sci. U. S. A.* **96**, 9997–10002 (1999).

113. Nicola, A. V., Aguilar, H. C., Mercer, J., Ryckman, B. & Wiethoff, C. M. Virus entry by endocytosis. *Advances in Virology* **2013**, 803–833 (2013).

114. Al-qattan, M. N. & Mordi, M. N. Docking of sialic acid analogues against influenza A hemagglutinin: a correlational study between experimentally measured and computationally estimated affinities. *J. Mol. Model.* **16**, 1047–1058 (2010).

115. Lu, S. J. & Chong, F. C. Combining molecular docking and molecular dynamics to predict the binding modes of flavonoid derivatives with the neuraminidase of the 2009 H1N1 influenza A virus. *Int. J. Mol. Sci.* **13**, 4496–4507 (2012).

116. Holmes, B. E., Smeester, L., Fry, R. C. & Weinberg, H. S. Disinfection By-Products Bind the Human Estrogen Receptor-Alpha. *Environ. Toxicol. Chem.* **38**, 956–964 (2019).

117. Flint, J., Racaniello, V. R., Rall, G. F., Skalka, A. M. & others. Principles of virology, Volume I: molecular biology. *Principles of virology, Volume I: molecular biology.* (ASM press, 2015).

118. Kotiaho, T., Eberlin, M. N., Vainiotalo, P. & Kostiainen, R. Electrospray mass and tandem mass spectrometry identification of ozone oxidation products of amino acids and small peptides. *J. Am. Soc. Mass Spectrom.* **11**, 526–35 (2000).

119. Triquigneaux, M. M. *et al.* Targeted oxidation of Torpedo californica acetylcholinesterase by singlet oxygen: identification of N-formylkynurenine tryptophan derivatives within the active-site gorge of its complex with the photosensitizer Methylene Blue. *Biochem. J.* **448**, 83–91 (2012).

120. USEPA. *Drinking Water Contaminants: National Primary Drinking Water Regulations. US EPA website http://water.epa.gov/drink/contaminants/index.cfm* (2015).

121. Knowles, A. D. *et al.* Role of iron and aluminum coagulant metal residuals and lead release from drinking water pipe materials. *J. Environ. Sci. Heal. Part A* **50**, 414–423 (2015).

122. Kim, E. J., Herrera, J. E., Huggins, D., Braam, J. & Koshowski, S. Effect of pH on the concentrations of lead and trace contaminants in drinking water: A combined batch, pipe loop and sentinel home study. *Water Res.* **45**, 2763–2774 (2011).

123. Odeh, I. N., Francisco, J. S. & Margerum, D. W. New pathways for chlorine dioxide decomposition in basic solution. *Inorg. Chem.* **41**, 6500–6506 (2002).

124. Ho, Y., S. & McKay, G. Pseudo-second order model for sorption processes. *Process Biochem.* **34**, 451–465 (1999).

125. Wang, Y., Wu, J., Wang, Z., Terenyi, A. & Giammar, D. E. Journal of Colloid and Interface Science Kinetics of lead (IV) oxide (PbO_2) reductive dissolution : Role of lead (II) adsorption and surface speciation. *J. Colloid Interface Sci.* **389**, 236–243 (2013).

126. Liu, H. *et al.* Investigation of the Kinetics and Mechanisms of the Oxidation of Cerussite and Hydrocerussite by Chlorine. *Environ. Sci. Technol.* **42**, 3241–3247 (2008).

127. Calle-Vallejo, F., Loffreda, D., Koper, M. T. M. & Sautet, P. Introducing structural sensitivity into adsorption-energy scaling relations by means of coordination numbers. *Nat. Chem.* **7**, 403–410 (2015).

128. Fernndez, E. M. *et al.* Scaling relationships for adsorption energies on transition metal oxide, sulfide, and nitride surfaces. *Angew. Chemie - Int. Ed.* **47**, 4683–4686 (2008).

129. Kosmulski, M. *Surface Charging and Points of Zero Charge*. (CRC Press, 2009).

130. Zhang, Y. & Lin, Y.-P. Adsorption of Free Chlorine on Tetravalent Lead Corrosion Product (PbO_2). *Environ. Eng. Sci.* **29**, 52–58 (2012).

131. Liu, C., Von Gunten, U. & Croué, J. P. Enhanced bromate formation during chlorination of bromide-containing waters in the presence of CuO: Catalytic disproportionation of hypobromous acid. *Environ. Sci. Technol.* **46**, 11054–11061 (2012).

132. Brown Jr, G. E. & ET AL., E. A. ChemInform Abstract: Metal Oxide Surfaces and Their Interactions with Aqueous Solutions and Microbial Organisms. *ChemInform* **30**, no-no (2010).

133. Kosmulski, M. The pH dependent surface charging and points of zero charge. VI. Update. *J. Colloid Interface Sci.* **426**, 209–212 (2014).

134. Edwards, M., Jacobs, S. & Dodrill, D. Desktop guidance for mitigating Pb and Cu corrosion by-products. *J. Am. Water Work.* **91**, 66–77 (1999).

135. Lin, Y. & Valentine, R. L. Release of Pb (II) from Reduction of Lead Oxide (PbO_2). *Environ. Sci. Technol.* **42**, 9137–9143 (2008).

136. Jia, Z., Margerum, D. W. & Francisco, J. S. General-acid-catalyzed reactions of hypochlorous acid and acetyl hypochlorite with chlorite ion. *Inorg. Chem.* **39**, 2614–2620 (2000).

137. Lark, S. J. *et al.* First principles methods using CASTEP. *Zeitschrift für Krist.* **220**, 567–570 (2005).

138. Perdew, J. P., Burke, K. & Ernzerhof, M. Generalized Gradient Approximation Made Simple. *Phys. Rev. Lett.* **77**, 3865–3868 (1996).

139. Pfrommer, B. G., Côté, M., Louie, S. G. & Cohen, M. L. Relaxation of Crystals with the Quasi-Newton Method. *J. Comput. Phys.* **131**, 233–240 (1997).

140. Bahri, S. *et al.* Adsorption and Surface Complexation Study of L-DOPA on Rutile (α-TiO 2) in NaCl Solutions Hazen Environ. Sci. Technol.pdf. 3959–3966 (2011).

141. Jonsson, C. M. *et al.* Adsorption of l-aspartate to rutile (α-TiO_2): Experimental and theoretical surface complexation studies. *Geochim. Cosmochim. Acta* **74**, 2356–2367 (2010).

142. Mishra, A. K., Roldan, A. & De Leeuw, N. H. CuO Surfaces and CO_2 Activation: A Dispersion-Corrected DFT+U Study. *J. Phys. Chem. C* **120**, 2198–2214 (2016).

143. Downs, R. T. & Hall-Wallace, M. The American Mineralogist crystal structure database. *Am. Mineral.* **88**, 247–250 (2003).

144. Frisch, M. J. *et al.* Gaussian16. (2016).

145. McLean, A. D. & Chandler, G. S. Contracted Gaussian basis sets for molecular calculations. I. Second row atoms, Z=11–18. *J. Chem. Phys.* **72**, 5639–5648 (1980).

146. Gallard, H., Allard, S., Nicolau, R., Von Gunten, U. & Croué, J. P. Formation of iodinated organic compounds by oxidation of iodide-containing waters with manganese dioxide. *Environ. Sci. Technol.* **43**, 7003–7009 (2009).

147. Calle-Vallejo, F., Martínez, J. I., García-Lastra, J. M., Sautet, P. & Loffreda, D. Fast prediction of adsorption properties for platinum nanocatalysts with generalized coordination numbers. *Angew. Chemie - Int. Ed.* **53**, 8316–8319 (2014).

148. T. Jiang, D. J. *et al.* Trends in CO oxidation rates for metal nanoparticles and close-packed, stepped, and kinked surfaces. *J. Phys. Chem. C* **113**, 10548–10553 (2009).

149. Ma, X. & Xin, H. Orbitalwise Coordination Number for Predicting Adsorption Properties of Metal Nanocatalysts. *Phys. Rev. Lett.* **118**, 1–5 (2017).

150. Boujelben, N., Bouzid, J. & Elouear, Z. Removal of Lead(II) Ions from Aqueous

Solutions Using Manganese Oxide-Coated Adsorbents: Characterization and Kinetic Study. *Adsorpt. Sci. Technol.* **27**, 177–191 (2009).

151. Azizian, S. Kinetic models of sorption: A theoretical analysis. *J. Colloid Interface Sci.* **276**, 47–52 (2004).

152. Robati, D. Pseudo-second-order kinetic equations for modeling adsorption systems for removal of lead ions using multi-walled carbon nanotube. *J. Nanostructure Chem.* **3**, 55 (2013).